NIST Center for Neutron Research

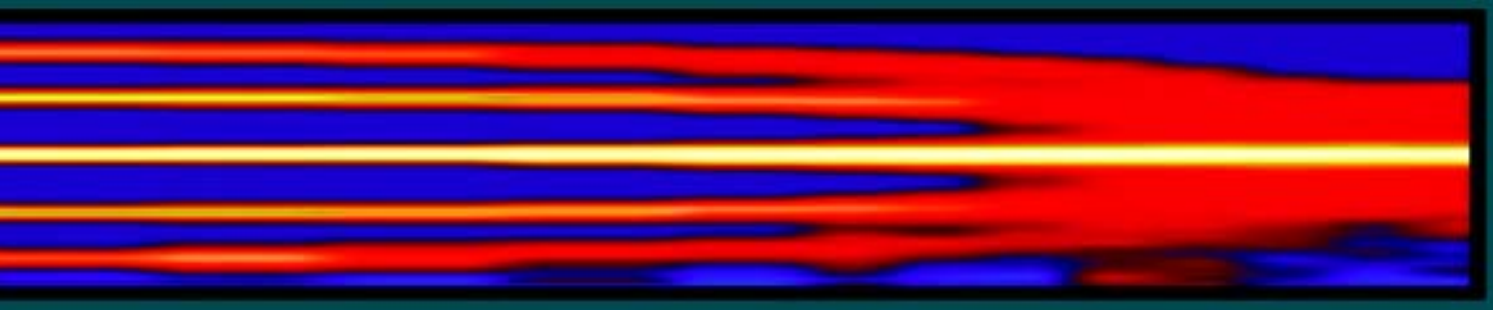

Materials Science and Engineering Laboratory

FY 2002 Programs and Accomplishments

NIST
National Institute of Standards and Technology
Technology Administration
U.S. Department of Commerce
NISTIR 6908
September 2002

On the Cover:

The graphic on the cover is a false-color image of the inelastic neutron scattering intensity for m-xylene ($(CH_3)_2C_6H_4$) as a function of energy transfer (-35 μeV to 35 μeV: y-axis) and temperature (7 K to 29 K: x-axis). At temperatures below 15 K (left) the CH_3 (methyl) groups undergo quantum rotational tunneling, resulting in sharp spectral features. As the temperature increases (right), the methyl motion becomes more classical, causing the tunneling peaks to merge into a single broadened central peak. The temperature-dependences of the widths and centers of the tunneling peaks are extremely sensitive to the potential energy experienced by the molecules, as well as to the interactions of the methyl groups with lattice vibrations.

The measurements were made using the NCNR High-Flux Backscattering Spectrometer: O.Kirstein, M.Prager (Forschungszentrum Juelich), and R.M.Dimeo (NCNR).

National Institute of Standards and Technology
Arden L. Bement, Jr.,
Director

Technology Administration
Phillip J. Bond,
Under Secretary for Technology

U.S. Department of Commerce
Donald L. Evans,
Secretary

Materials Science and Engineering Laboratory

FY 2002 Programs and Accomplishments

NIST Center for Neutron Research

J. Michael Rowe, Director

NISTIR 6908

September 2002

DISCLAIMER
Certain commercial entities, equipment, or materials may be identified in this document in order to describe an experimental procedure or concept adequately. Such identification is not intended to imply recommendation or endorsement by the National Institute of Standards and Technology, nor is it intended to imply that the entities, materials, or equipment are necessarily the best available for the purpose.

Contents

Foreword

Once again, it is a great pleasure to report on a year of accomplishments in all areas of the Center. Although the shutdown was prolonged by unforeseen problems in an auxiliary system, the results when we restarted were everything that we had hoped for. The new cooling tower is functioning well, reducing the visible plume during cold weather dramatically. This system is now well prepared for another twenty-plus years of operation. The work on relicensing is also on track — the new analyses are almost complete, and confirm the existing Safety Analysis Report. A new liquid hydrogen cold source of improved design was installed during the same shutdown. It is working well, producing nearly twice as many cold neutrons as its predecessor, exactly in agreement with the detailed MCNP predictions. In every respect, the future for neutron production at the NIST source looks excellent.

As always, we continue to improve existing instruments and work on new ideas. An optical filter was installed in the NG-3 30 m SANS instrument (a key part of the NIST/NSF Center for High Resolution Neutron Scattering), providing further gains of up to a factor of three at long wavelength. A modification to the guide that runs through the choppers of the Disk Chopper time-of-flight Spectrometer has given intensity increases of 2 to 3 over the whole wavelength range. So these two instruments have increased in performance by factors of between 3 and 5 over the past year, a direct result of our continuing investment in instrumentation. A consortium of researchers from five universities has been awarded a grant from the National Institutes of Health to begin development of a new Research Resource called Cold Neutrons for Biology and Technology, which includes construction of a new diffractometer/reflectometer for membrane and related structures. The National Science Foundation has increased its partnership with the NCNR, and now helps to support the high-resolution inelastic scattering instruments in the guide hall. These and other partnerships, such as the ones with Johns Hopkins University, the University of Maryland, and Brookhaven National Laboratory, are a key part of our plans to move forward, and have been an essential part of our past success.

And again, as always, the science being produced fully justifies the dedication and work of the people who provide the neutrons and instruments. While walking through the facility during operating cycles, I am always amazed at the breadth and depth of research now being done with neutrons, and delighted by the energy and intensity of the young people doing it. I derive great pleasure helping to choose scientific highlights, and then from reading the results of those choices. They form the greatest portion of this report, and I hope that you enjoy them as much as I do.

The NIST Center for Neutron Research (NCNR)

Neutrons are powerful probes of the structure and dynamics of materials ranging from molecules inserted into membranes mimicking cell walls to protons migrating through fuel cells. The unique properties of neutrons (see inset) can be exploited by a variety of measurement techniques to provide information not available by other means. They are particularly well suited to investigate all forms of magnetic materials such as those used in computer memory storage and retrieval. Atomic motion, especially that of hydrogen, can be measured and monitored, like that of water during the setting of cement. Residual stresses such as those inside stamped steel automobile parts can be mapped. Neutron-based research covers a broad spectrum of disciplines, including engineering, biology, materials science, polymers, chemistry, and physics.

The NCNR's neutron source provides the intense beams of neutrons required for these types of measurements. In addition to the thermal energy neutron beams from the heavy water or graphite moderators, the NCNR has a large area liquid hydrogen moderator, or cold source, that provides intense neutron beams for the only cold neutron facility presently operating in the United States.

There are currently 28 experiment stations: six provide high neutron flux positions for irradiation, and 22 are beam facilities most of which are used for neutron scattering research. The following pages show a schematic layout of the beam facilities. More complete descriptions of instruments can be found at www.ncnr.nist.gov.

The NCNR supports important NIST research needs, but is also operated as a major national user facility with merit-based access made available to the entire U.S. technological community. Each year, over 1700 research participants from all areas of the country, from industry, academia, and government use the facility for measurements. Beam time for research to be published in the open literature is without cost to the user, but full operating costs are recovered for proprietary research. Access is gained mainly through a peer-reviewed, web-based proposal system with beam time allocated by a Program Advisory Committee twice a year. For details see www.ncnr.nist.gov/beamtime.html. The National Science Foundation and NIST co-fund the Center for High Resolution Neutron Scattering (CHRNS) that operates six of the world's most advanced instruments. Time on CHRNS instruments is made available through the proposal system. Some access to beam time for collaborative measurements with the NIST science staff can also be arranged on other instruments.

Why Neutrons?

Neutrons at the NCNR reveal properties not available to other probes. They can behave like microscopic magnets, can diffract like waves, or set particles into motion as they recoil from them.

Wavelengths – range from 0.1 Å to 100 Å, allowing them to form observable ripple patterns from structures as small as atoms to as large as proteins.

Energies – of millielectronvolts, the same as that of motions of atoms in solids or liquids, waves in magnetic materials, or vibrations in molecules. Exchanges of energy between neutrons and matter as small as nanoelectronvolts and as large as tenths of electronvolts can be detected.

Selectivity – in scattering power varies from nucleus to nucleus almost randomly. Specific isotopes can stand out from other isotopes, even of the same kind of atom. Specific light atoms, difficult to observe with x-rays, are revealed by neutrons. Hydrogen, especially, can be distinguished from chemically equivalent deuterium.

Magnetism – makes the neutron sensitive to the magnetic spins of both nuclei and electrons, allowing the behavior of ordinary and exotic magnets to be detailed precisely.

Neutrality – of the uncharged neutrons allows them to penetrate deeply without destroying samples, and pass through walls controlling a sample's environment allowing measurements under extreme conditions. Properties ranging from the residual stresses in steel girders to the unfolding motions of proteins are amenable to measurement by neutrons.

Capture – characteristic radiation emanating from specific nuclei capturing incident neutrons can be used to identify and quantify minute amounts of material in pollutants or ancient pottery shards.

Instruments in the cold neutron guide hall.

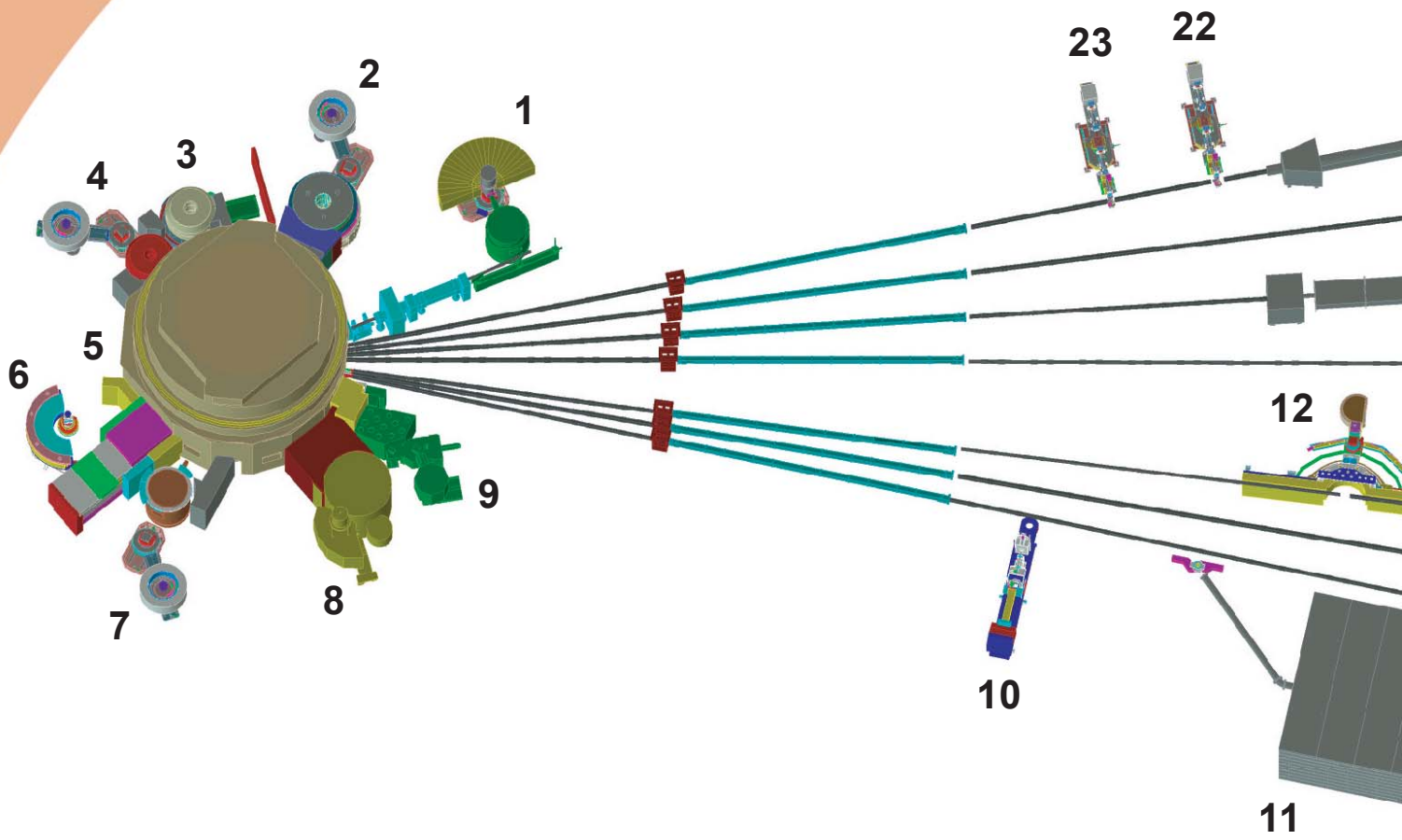

1 **A Cold Neutron Depth Profiling** instrument (not shown) for quantitative profiling of subsurface impurities currently at this site will be moved to another position. Shown is MACS, a triple axis cold neutron crystal spectrometer under construction with double focusing monochromator and multiple crystal analyzer/detectors that can be flexibly configured for several energies simultaneously or for high throughput at one energy.

2 **BT-7 Triple Axis Spectrometer** with fixed incident energy for measurements of excitations and structure.

3 **BT-8 Residual Stress Diffractometer** optimized for depth profiling of residual stress in large components.

4 **BT-9 Triple Axis Crystal Spectrometer** for measurements of excitations and structure.

5 **Thermal Column** a very well-thermalized beam of neutrons used for radiography, tomography, dosimetry and other experiments.

6 **BT-1 Powder Diffractometer** with 32 detectors; incident wavelengths of 0.208 nm, 0.154 nm, and 0.159 nm, with highest resolution of $\delta d/d = 8 \times 10^{-4}$.

7 **BT-2 Triple Axis Crystal Spectrometer** with polarized beam capability for measurement of magnetic dynamics and structure.

8 **BT-4 Filter Analyzer Neutron Spectrometer** with cooled Be/Graphite filter analyzer for chemical spectroscopy.

9 **BT-5 Perfect Crystal Diffractometer SANS** small angle neutron scattering instrument for microstructure on the 10^4 nm length scale, sponsored by the National Science Foundation and NIST, part of the Center for High Resolution Neutron Scattering (CHRNS).

10 **NG-7 Horizontal Sample Reflectometer** allows reflectivity measurements of free surfaces, liquid vapor interfaces, as well as polymer coatings.

11 **Neutron Interferometry and Optics Station** with perfect silicon interferometer; vibration isolation system provides exceptional phase stability and fringe visibility.

12 **Spin Polarized Triple Axis Spectrometer (SPINS)** using cold neutrons with position sensitive detector capability for high resolution studies — part of CHRNS.

NIST Center for Neutron Research Layout

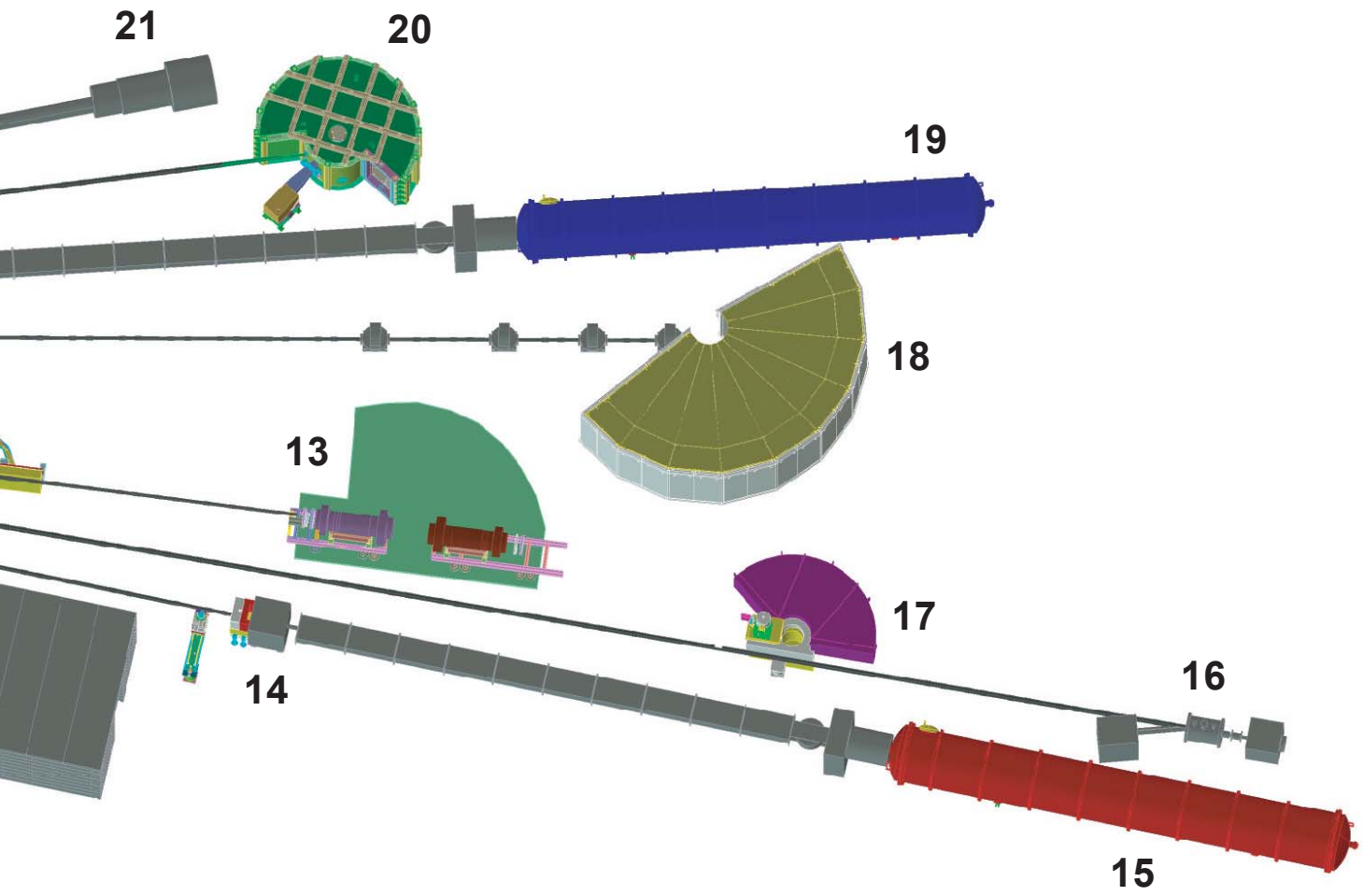

13 Spin Echo Spectrometer offering neV energy resolution, based upon Jülich design, sponsored by NIST, Jülich and ExxonMobil — part of CHRNS.

14 Prompt Gamma Activation Analysis cold neutron fluxes allow detection limit for H of 1 μg to 10 μg. Focused beams are available for profiling.

15 NG-7 30 m SANS for microstructure measurements sponsored by NIST, ExxonMobil, and the University of Minnesota.

16 Neutron Physics Station offering three cold neutron beams having wavelengths of 0.5 nm, 0.9 nm, and "white" that are available for fundamental neutron physics experiments.

17 Fermi Chopper hybrid time-of-flight (TOF) Spectrometer for inelastic scattering with incident wavelengths between 0.23 nm and 0.61 nm chosen by focusing pyrolytic graphite crystals. A simple Fermi chopper pulses the beam.

18 Disk Chopper TOF Spectrometer a versatile time-of-flight spectrometer, with beam pulsing and monochromatization effected by 7 disk choppers. Used for studies of dynamics in condensed matter, including macromolecular systems — part of CHRNS.

19 NG-3 30 m SANS for microstructure measurements sponsored by the National Science Foundation and NIST — part of CHRNS.

20 Backscattering Spectrometer high intensity inelastic scattering instrument with energy resolution < 1 μeV, for studies of motion in molecular and biological systems — part of CHRNS.

21 NG-1 8 m SANS for polymer characterization being modified to 10 m and to be made available for CHRNS use along with its current use by the NIST Polymers Division.

22 Vertical Sample Reflectometer instrument with polarization analysis capability for measuring reflectivities down to 10^{-8} to determine subsurface structure.

23 Cold Neutrons for Biology and Technology vertical sample reflectometer, to be built with polarization analysis capability for measuring reflectivities down to 10^{-8}. It will have a position-sensitive detector for measuring off-specular reflections.

Removal of Unit 1

Biological shielding is removed and guides are disassembled prior to removing the Unit 1 cold source.

The bear trap is placed on special stanchions (white) to avoid misaligning the neutron guide stanchions (blue).

The "bear trap" transport device is moved into place to remove Unit 1.

Installation of Unit 2

Unit 2, the new cold source assembly, is moved into place (above) and rides a track (right) into the cold source thimble.

Connections to hydrogen condenser are welded into place.

Cold Source Replacement

Enclosed Unit 1 is moved (left) to storage area and aligned (below) with "winter bear den" under the watchful eye of NCNR director Mike Rowe.

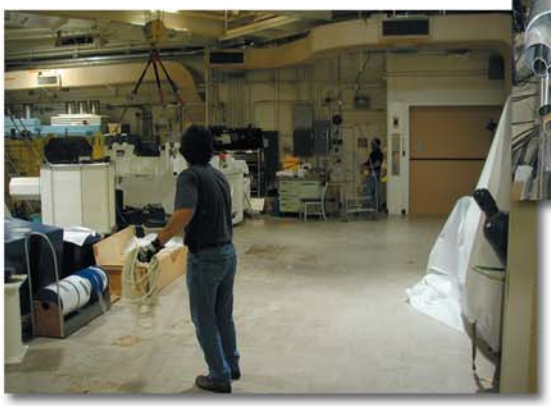

"Bear trap loaded with bear" (Unit 1) is guided toward exit for placement on a truck bed.

Unit 1 is sealed in storage.

Guide tube parts are aligned.

New guide tube assembly is prepared for placement.

The Advanced Liquid Hydrogen Cold Neutron Source

The 14 cold neutron instruments at the NCNR received a substantial increase in performance when the liquid hydrogen cold source, successfully operated since 1995 (hereafter called "Unit 1"), was replaced with an improved design (called "Unit 2") during last year's maintenance outage. The NCNR cold source is designed to maximize the useful intensity of neutrons in the wavelength band between 0.2 nm and 2.0 nm by providing a low temperature medium that further slows down the neutrons exiting the heavy water moderator/reflector of the NIST 20 MW reactor. The basic operating principles for the cold source are the same in both designs [1]. Using the large diameter cryogenic beam port at the NCNR reactor, a cryostat containing a thin, annular shell of liquid hydrogen is placed in a high intensity region of the reactor's reflector. Interaction with the slow moving hydrogen molecules modifies the neutron energy spectrum. A neutron guide tube system beginning close to the exit of the cryostat transports the intense cold neutron beams to the neutron scattering instruments. The radiation heat deposited in the moderator is removed by boiling of the liquid hydrogen. Stable operation of the cold source is maintained by a thermosiphon; cold liquid hydrogen flows by gravity into the cryostat from a helium cooled condenser and the hydrogen vapor from boiling returns to the condenser in a closed, convective circulation loop. The cryostat also includes a heavy water cooling jacket, insulating vacuum regions and helium containment vessel that surrounds all portions of the system containing hydrogen.

Following the commissioning of Unit 1, detailed simulations of the NCNR reactor and moderators became sufficiently accurate that it was possible to explore further optimization of the cold source geometry for improved performance using a sophisticated MCNP model of the NCNR source [2]. The Unit 2 design differs from Unit 1 in many key respects, as can be seen in Fig. 1. Most of the volume of the Unit 1 cryostat assembly was empty space, leaving a large void in the reactor reflector and lowering the neutron flux near the cryostat. The heavy water cooling jacket of Unit 2 was expanded to fill nearly half of the insulating vacuum void of Unit 1. This change reduced the void in the reflector and increased the neutron flux near the cryostat by about 40 % thus providing a cold neutron gain of the same magnitude. Because of these changes and to fully illuminate the rectangular aspect ratio of the NCNR guide system, the Unit 2 moderator chamber is smaller than the original and is an ellipsoidal annulus, rather than a spherical one. With a smaller vessel size, the thickness of the liquid hydrogen shell could be increased from 20 mm to between 25 mm and 30 mm without increasing the overall hydrogen inventory. Finally, the inner ellipsoid of the newer design is evacuated through a small vacuum port, removing most of the hydrogen vapor. In Unit 2, the cold neutron beam passes through only 20 mm of vapor, rather than through the 300 mm path

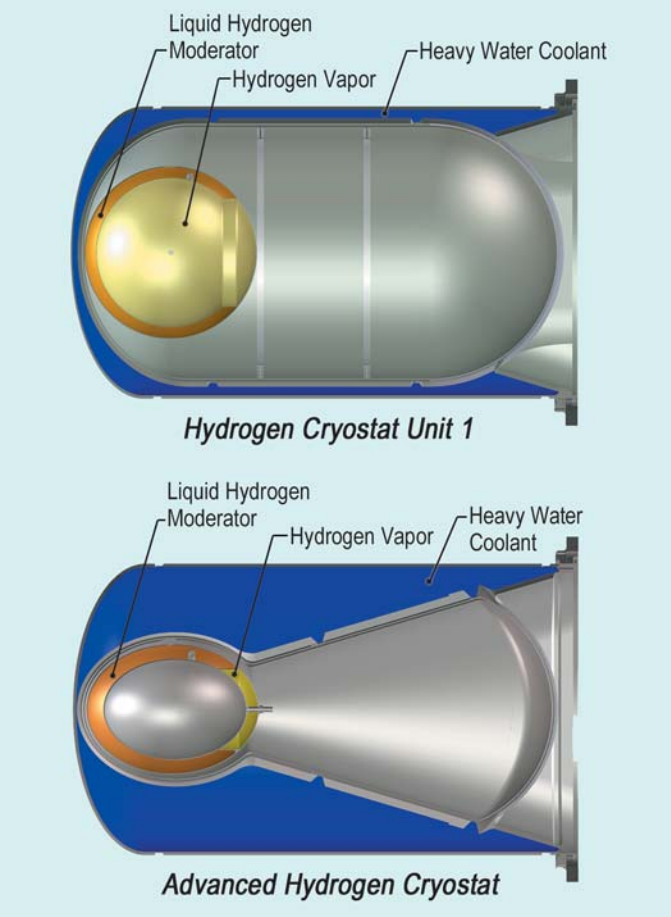

Fig. 1. Comparison between the original (top) and the advanced liquid hydrogen cold sources for the NIST research reactor. The heavy water volume is indicated in blue, liquid hydrogen in orange, and hydrogen vapor in yellow.

length in Unit 1. This results in less neutron adsorption by hydrogen. Collectively, these changes in the moderator chamber add another 15 % to 20 % to the predicted gain.

The complex geometry of Unit 2 posed many challenges for the design and fabrication of the cryostat. Complicated elliptical vessels were designed with the aid of finite element analysis to model their mechanical strength. Extensive pressure testing supported this detailed modeling. Because of the non-standard shapes, components were precisely cut from solid blocks of Aluminum-6061 using a high-speed mill at the NIST instrumentation shop. The geometry also placed high demands on the welding of the various components into a leak-tight cryostat satisfying stringent quality control tests. The entire cryostat system was completely fabricated, assembled, and tested at NIST. The replacement of Unit 1 with the new design was also a significant technical challenge. Detailed work planning was required to ensure that the highly radioactive Unit 1 could be safely removed with the least amount of disruption to the sensitive alignment of the neutron guide network. Radiation damaged neutron guides near the source were also systematically replaced during the installation. The installation was completed on schedule with a minimal dose exposure to the installation team.

When the reactor resumed normal operation on March 6, 2002, the thermal and neutronic performance of the new cold source was tested. Startup tests measured the helium refrigerator heat load as reactor power was increased. At 20 MW, the heat deposited in the source was measured at 1300 watts in excellent agreement with calculations. The cold neutron flux was monitored to ensure that the thermosiphon functioned smoothly and that the moderator volume remained full of liquid hydrogen as the evaporation rate increased to over 3 g/s at full power. Further tests established the normal operating parameters for the cryostat and verified the protection systems under various abnormal conditions.

The performance of the new source was benchmarked against Unit 1 by duplicating flux measurements of the intensity as a function of neutron wavelength at several Guide Hall instruments. Figure 2 is a plot of the cold source gain, defined as the ratio of intensities between Unit 2 and Unit 1, as a function of neutron wavelength. The figure includes both the gain factors measured at three spectrometers and as obtained from the MCNP Monte Carlo simulations [2]. While the agreement is excellent, the measured gains were actually somewhat greater than predicted, especially at long wavelengths. This additional gain is likely due to the new guide sections replaced during the cold source installation, an effect that is not included in the MCNP models. The new cryostat design also substantially reduces the number of fast neutrons from the cold source resulting in improved instrument signal-to-noise levels.

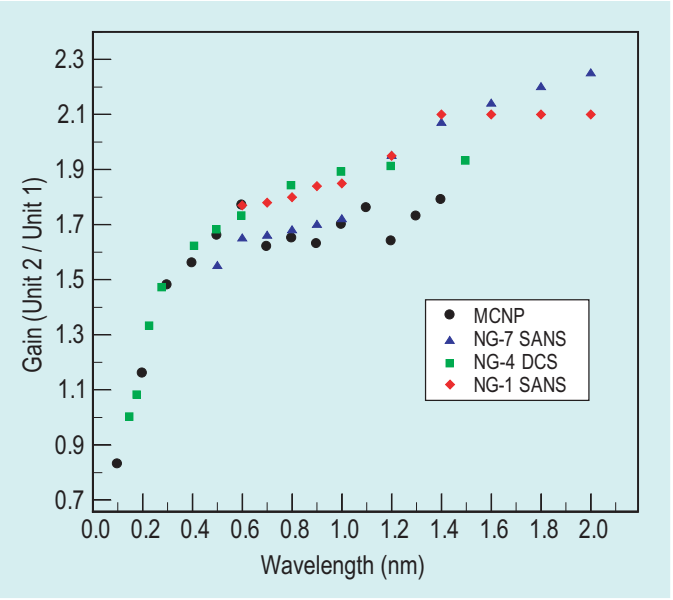

Fig. 2. Gains in cold neutron flux measured at the NG-7 and NG-1 small angle neutron scattering (SANS) instruments, and at the disk chopper spectrometer (DCS) on NG-4, compared to the predicted gains, based on Monte Carlo simulations using MCNP.

The advanced liquid hydrogen cold source has successfully met all of its design goals. Its success demonstrates how the effective use of detailed computer models to optimize a design can lead to substantial performance improvements. However, it also demonstrates that the complex geometry that results from such an optimization requires more complex stress modeling, new fabrication technologies and even more stringent quality assurance testing. Most importantly, the success of the Unit 2 cold source design significantly enhances the measurement capability of the cold neutron scattering instrumentation at NIST with intensity gains of nearly a factor of two in the important long wavelength region of the spectrum.

References

[1] R. E. Williams and J. M. Rowe, Physica B **311**, 117 (2002).

[2] J. F. Briesmeister (Ed.), MCNP – A General Monte Carlo N-Particle Transport Code, Version 4B, Los Alamos National Laboratory, LA-12625-M, Los Alamos, New Mexico (1997).

The Staff
NIST Center for Neutron Research
National Institute of Standards and Technology
Gaithersburg, MD 20899-8560

Neutron Spin Filters Based on Polarized ^{3}He

Spin-polarized neutrons are useful probes of magnetic matter since both the magnetic scattering of neutrons by unpaired electrons and the scattering of neutrons by nuclei of non-zero spin can be strong functions of the neutron spin state [1]. Unfortunately, the limitations of current polarizing and analyzing devices have substantially restricted the application of this powerful technique. ^{3}He spin-filters have the potential to yield broadband neutron polarizers and analyzers that can be used for cold, thermal, and epithermal neutrons. Such spin filters could make new classes of neutron scattering experiments possible.

For certain applications there are presently no suitable devices. For example, polarization analysis of scattered beams having wide angular divergence is impractical with reflection-based devices such as supermirrors because of their inadequate angular acceptance and small-angle scattering. At present, we are developing ^{3}He-based polarization analyzers for diffuse reflectometry and small-angle scattering (SANS) with neutrons, both of which require analysis of a large divergence beam. ^{3}He-based neutron spin filters would also be advantageous on crystal spectrometers since any monochromator or analyzer crystal can be used, rather than just Heusler alloy, greatly increasing the range and flexibility of the instrumentation. Furthermore, polarizing or analyzing thermal and hot neutrons at spallation sources, where the time-of-flight method is employed, often requires the broadband capability of ^{3}He spin filters. In addition to their utility for neutron scattering, polarized ^{3}He spin filters are also of interest for nuclear and particle physics studies with neutrons, such as determination of weak coupling constants and tests of the Standard Model via accurate measurements of decay correlation coefficients in polarized neutron beta-decay [2].

Neutron spin filters based on polarized ^{3}He rely on the strong spin-dependence of the neutron capture cross section for ^{3}He. For a sufficient thickness of 100 % polarized ^{3}He gas, essentially all of the neutrons with antiparallel spin would be absorbed, while nearly all of the neutrons with parallel spin would be transmitted, resulting in 100 % neutron polarization and 50 % transmission. In Fig. 1 we show calculated values of the neutron polarization P_n and neutron transmission T_n for ^{3}He polarization $P_{He} = 60$ %, an experimentally achievable value. Since there is a tradeoff between neutron polarization and transmission, we also show $P_n^2 T_n$, which is a useful figure-of-merit for many experiments. A transmission analyzer can be characterized either by the transmission asymmetry A or the flipping ratio F. For T_+ and T_- defined to be the transmissions for neutrons with polarization parallel and antiparallel to the ^{3}He polarization, respectively, the asymmetry is given by $A = (T_+ - T_-)/(T_+ + T_-)$ and the flipping ratio by $F = T_+/T_- = (1 + A)/(1 - A)$. The flipping ratio F is also shown in Fig. 1. The asymmetry for a spin filter used as an analyzer is the same as the neutron polarization produced when it is used as a polarizer. For the specific case of cold neutrons ($\lambda = 0.5$ nm), a spin filter used as a polarizer with $P_{He} = 60$ % and a pressure-length product of 7 kPa·m would yield $P_n = 90$ % and $T_n = 20$ %, or, when used as an analyzer, would give $A = 90$ % and $F = 19$.

We produce polarized ^{3}He gas by two optical pumping methods: spin-exchange, which is performed directly at high pressure (0.1 MPa to 0.3 MPa), and metastability-

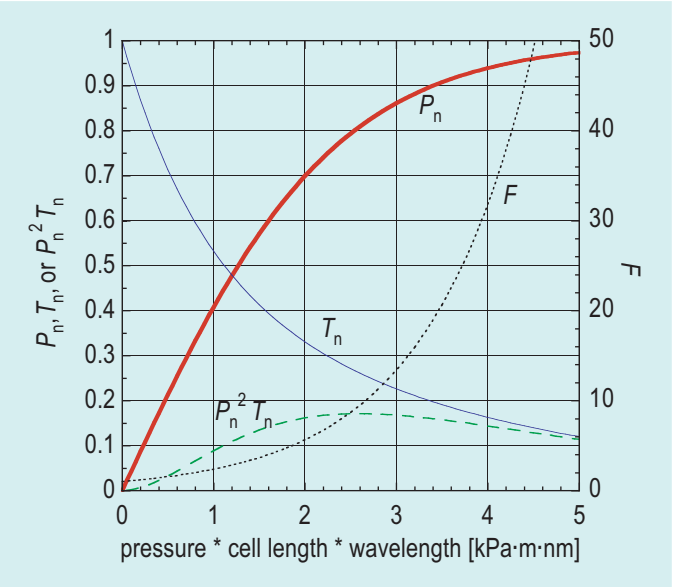

Fig. 1. Neutron polarization P_n (solid thick line), transmission T_n (solid thin line), a figure of merit given by $P_n^2 T_n$ (dashed line), and the flipping ratio F (dotted line) as a function of the product of ^{3}He pressure in Pa (assuming a room temperature cell), cell length in m and wavelength in nm. The calculations are shown for ^{3}He polarization P_{He}= 60 %. The scale on the right hand y-axis is used for the flipping ratio.

exchange, in which the gas is polarized at low pressure (≈ 100 Pa) and then compressed [3]. The spin-exchange method is convenient and well matched to continuous operation on a beamline, whereas the metastability-exchange method has a higher polarizing rate. At present, it has been more convenient (for either method) to polarize gas off-line and transport it to the beam line. Maintaining the polarization in the absence of optical pumping requires a homogeneous magnetic field and specially prepared glass cells with slow wall relaxation. We have produced cells with relaxation times as long as one month, dominated by the intrinsic dipole-dipole relaxation in the ^{3}He gas itself [4]. In the future, continuously operating spin filters can be installed directly on the neutron instrument.

Polarization analysis allows for separation of magnetic from nuclear scattering, and also separation of coherent from spin-incoherent scattering. In our first demonstration experiment for SANS, we used a ^{3}He spin filter to extract a small component of spin-incoherent scattering in the presence of strong coherent scattering [5]. We have continued with tests of separating magnetic from nuclear scattering.

Recently we carried out successful tests of a polarized ^{3}He spin filter on the NCNR NG-1 reflectometer. The first test experiment on a specular reflection was a careful comparison of results obtained with a ^{3}He analyzer to those obtained with the current technique that employs a supermirror analyzer. The test sample was an epitaxial $Mn_{0.52}Pd_{0.48}$/Fe (001) bilayer, for which chemical ordering and magnetic exchange-bias have recently been reported [6]. By varying the magnetic field on this sample, it was possible to test the ^{3}He analyzer under conditions of both significant and negligible spin-flip scattering. We employed a compact, magnetically shielded solenoid that was interchanged with the analyzing supermirror on the NG1 instrument. The solenoid adequately shielded the stray fields from the 0.6 T magnet and guide field magnets. The results obtained with the ^{3}He analyzer were identical to those obtained with the supermirror analyzer.

For efficient studies of diffuse scattering on a reflectometer, the ^{3}He analyzer will be combined with a position sensitive detector (PSD). Two issues not tested in the specular experiment are relevant in this case: (1) possible depolarization of neutrons that follow trajectories off the axis of the ^{3}He analyzer, and (2) possible background from the ^{3}He cell. We have established that most of the area of apertures in the magnetic shield is usable, with depolarization only occurring for a small range of extreme trajectories. We have also determined that small angle scattering from the cell is negligible and therefore should not pose an issue for the low neutron fluxes expected in diffuse scattering experiments. This series of tests established the suitability of polarized ^{3}He spin filters for diffuse reflectometry experiments, which we will pursue in the near future.

We are making continual improvements in the polarization and relaxation time of our ^{3}He cells. In the recent reflectometry experiments, the initial ^{3}He polarization was 57 %, resulting in a neutron flipping ratio of 31 and a transmission for the desired spin state of 24 %. The relaxation time of the polarized gas was 15 days on the beam line, which was somewhat reduced from the intrinsic value of 24 days for the cell due to a small fractional gradient of 3 x 10^{-4} cm^{-1} in the magnetic field of the shielded solenoid. Our aim is to increase the ^{3}He polarization to 70 % and obtain relaxation times at the dipole-dipole limit.

References

[1] R. M. Moon, T. Riste, and W. C. Koehler, Phys. Rev. A **181**, 920-931 (1969).

[2] *Fundamental Physics with Pulsed Neutron Beams, Research Triangle Park, North Carolina, June 1-3, 2000*, edited by C. R. Gould, G. L. Greene, F. Plasil, and W. M. Snow (World Scientific, Singapore, 2001).

[3] T. R. Gentile *et al*, J. Res. Natl. Inst. Stand. Technol. **106**, 709-729 (2001).

[4] D. R. Rich *et al*, Appl. Phys. Lett. 80, 2210 (2002).

[5] T. R. Gentile *et al*, J. Appl. Crystallog. **33**, 771-774 (2000).

[6] R. F. C. Farrow *et al*, Appl. Phys. Lett. **80**, 808 (2002).

T. R. Gentile and A. K. Thompson
National Institute of Standards and Technology
NIST Center for Neutron Research
100 Bureau Drive, MS 8461
Gaithersburg, MD 20899-8461

J. A. Borchers, J. W. Lynn, K. V. O'Donovan, and C. F. Majkrzak
National Institute of Standards and Technology
NIST Center for Neutron Research
100 Bureau Drive, MS 8562
Gaithersburg, MD 20899-8562

W. M. Snow and W. C. Chen
Indiana University
Department of Physics
Bloomington, IN 47405

G. L. Jones
Physics Department
Hamilton College
198 College Hill Road
Clinton, New York 13323

Development of an Ion-Implanted Phosphorus in Silicon SRM for the Semiconductor Industry

Silicon is the foundation material of the electronic age, lying at the base of the 200 billion dollar world-wide semiconductor industry. Silicon's properties are manipulated by precise implantation and distribution of other atoms (dopants), which makes the accurate measurement of impurity distributions imperative. SEMATECH (a consortium of semiconductor manufacturers) recently listed Standard Reference Material (SRM) implant of phosphorus in silicon as a high priority industrial need.

The U.S. semiconductor industry relies heavily on secondary ion mass spectrometry (SIMS) for characterization of the depth distribution of dopants in silicon. To achieve high accuracy in the concentration determination by SIMS, standards of known dopant concentration, conveniently provided by ion implants of certified dose, are required. Standard Reference Materials of boron and arsenic implants in silicon (SRMs 2137 and 2134 [1]) have already been developed by NIST as SIMS calibration standards.

The SIMS community in the United States undertook a round-robin study to calibrate the implanted dose of phosphorus in silicon by consensus. Dose determinations among laboratories varied by nearly a factor of 2, reflecting primarily the errors of the respective in-house standards (Fig. 1). These results demonstrate the need for a common phosphorus reference material to improve inter-laboratory reproducibility.

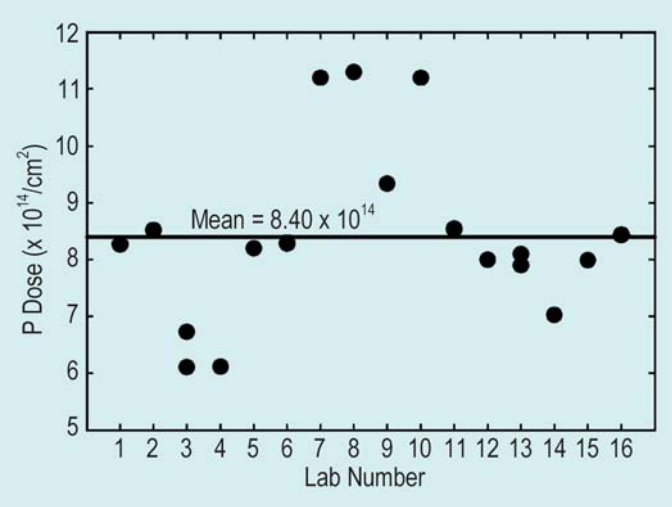

Fig. 1. Round-robin measurements of phosphorus in silicon by secondary ion mass spectrometry in 16 U.S. industrial laboratories, demonstrating the need for a common phosphorus reference material to improve inter-laboratory reproducibility.

In pursuit of a phosphorus in silicon SRM, a radiochemical neutron activation analysis (RNAA) procedure has been developed, critically evaluated, and shown to have the necessary sensitivity, chemical specificity, matrix independence, and precision to certify phosphorus at ion implantation levels in silicon [2, 3]. During sample irradiation, ^{31}P undergoes neutron capture to form ^{32}P, which is then separated from the matrix and measured by beta counting. The procedure is used here to assign a value to the quantity of phosphorus in SRM 2133 (phosphorus implanted silicon).

SRM 2133 was prepared by phosphorus implantation of a 200 cm diameter silicon wafer. The wafer was cut into 1 cm^2 pieces by means of a wafer saw, and twelve pieces were chosen for analysis. The area of each piece was determined by measuring its dimensions using a digital micrometer. During irradiation, ^{32}P may be produced via neutron capture by the implanted phosphorus, by bulk phosphorus impurity in the wafer, and by silicon. The latter two sources lead to measurement error, which must be corrected. These corrections were made by measuring silicon blanks, which were prepared by cutting a non-implanted silicon wafer into ~ 1 cm^2 pieces. Standards were prepared by deposition of standardized solutions of phosphorus on aluminum foils.

Samples, standards, and blanks were irradiated for 3 hours in irradiation tube RT1 of the NIST neutron source at a neutron fluence rate of 1.05×10^{14} $cm^{-2} \cdot s^{-1}$. Targets were then processed using the method developed previously [2, 3]. Silicon samples and blanks were mixed with a few milligrams of non-radioactive phosphorus (carrier) and dissolved in a mixture of nitric and hydrofluoric acids. Phosphorus was separated from the matrix first by precipitation as ammonium phosphomolybdate, then as magnesium ammonium phosphate. The latter was collected by filtration, washed with dilute ammonium hydroxide and ethanol, air dried, weighed, and packaged for beta-ray counting. The yield, (fraction of recovered phosphorus carrier), was determined gravimetrically, assuming a composition of $MgNH_4PO_4 \cdot 6H_2O$. Standards were processed using a similar procedure.

Counting of ^{32}P ($t_{1/2}$ = 14.28 d) was performed using a beta proportional counter. Purity of the ^{32}P from other radionuclides was ascertained by gamma-ray spectroscopy, and by monitoring beta count rates over a period of four half lives. No discernible contamination from other radionuclides was noted. ^{32}P count rates were adjusted for decay time, blank correction, and for differences in beta self-absorption.

NIST currently certifies elemental concentrations in SRMs using one of three modes: (1) a primary method at NIST with confirmation by other method(s); (2) two independent critically evaluated methods at NIST, and (3) one method at NIST and different methods by outside collaborating laboratories. Certification using a primary method is only possible when all potentially significant sources of uncertainty have been evaluated explicitly for the application of the method and the matrix under investigation. Therefore, in order to certify the phosphorus concentration in SRM 2133 using RNAA as a primary method it was necessary to evaluate all significant sources of uncertainty explicitly. For this set of measurements, we considered sources of relative uncertainty greater than 0.01 % to be significant. The results of a complete evaluation of all sources of uncertainty are listed in Table 1. This evaluation yielded an expanded relative uncertainty of 1.27 % (as defined by ISO and NIST), and gives an approximate level of confidence of 95 %. The measured phosphorus concentration is $(9.55 \pm 0.12) \times 10^{14}$ atoms·cm^{-2}.

In conclusion, we have successfully applied RNAA as a primary method for the certification of this new SRM. The observed relative expanded uncertainty of 1.27 % is smaller than the 3 % value needed by the semiconductor industry. This new SRM should greatly enhance the U.S. semiconductor industry's ability to achieve accurate and reproducible analytical results for this key dopant in silicon.

Table 1. Individual Uncertainty Components for Determination of Phosphorus in SRM 2133.

Source of Uncertainty	Uncertainty (1σ) %
Measurement Replication ($\sigma / \sqrt{n}$)	0.31
Measurement Replication (Standards) ($\sigma / \sqrt{n}$)	0.47
Measurement of Sample Area	0.012
Blank Correction	0.022
Blank Correction (Standards)	0.019
Volumetric Calibrations (Standards)	0.12
Concentration of Standard Solution	0.15
Mass Standard Solution on Foil	0.037
Radiochemical Impurity	0.13
Beta Self-Absorption	0.07
Beta Self-Absorption (Standards)	0.08
Carrier Yield Determination	0.10
Self-Shielding	0.024
Irradiation Geometry	0.09
Combined Uncertainty	0.63
Coverage Factor	2.0
Expanded Uncertainty	1.27

References

[1] R. R. Greenberg, R. M. Lindstrom, and D. S. Simons, J. Radioanal. Nucl. Chem, **245,** 57 (2000).

[2] R. L. Paul and D. S. Simons, *Characterization and Metrology for ULSI Technology*, ed. D. G. Seiler, A. C. Diebold, T. J. Shaffner, R. McDonald, W. M. Bullis, P. J. Smith, and E. M. Secula, American Institute of Physics, AIP Conference Proceedings 550, Melville, NY, 2001, pp. 677-681.

[3] R. L. Paul and D. S. Simons, *Silicon Front-End Junction Formation Technologies*, MRS Symposium Proceedings 717, ed. D. F. Downey, M. E. Law, A. Claverie, M. J. Rendon, Materials Research Society, Warrendale, PA, 2002, pp. 291-296.

R. L. Paul and D. S. Simons
Chemical Science and Technology Laboratory
National Institute of Standards and Technology
Gaithersburg, MD 20899-8395

New Thermal Neutron Prompt Gamma-Ray Activation Analysis Facility

Scientists from the Analytical Chemistry Division and the US Food and Drug Administration have maintained a thermal neutron prompt gamma-ray activation analysis (PGAA) facility at the NCNR for the past 25 years. The facility is used routinely for analysis of major and minor element compositions of a variety of biological, environmental and industrial materials. Recent applications include determination of: several elements in Standard Reference Material (SRM) 1575a Pine Needles; cadmium in SRM 2702 Inorganic Sediment; nitrogen and phosphorus in cattail samples in collaboration with Florida A&M University; boron in sapphire in collaboration with Southern University; and nitrogen, sodium, phosphorus, sulfur, chlorine, potassium, calcium, and cadmium in food, dietary supplements, and other food-related matrices.

A new thermal neutron PGAA instrument became operational in 2001, replacing the original thermal neutron PGAA instrument that was built in the late 1970s. The new instrument was designed and built to improve analytical sensitivities and limits of detection, and decrease the levels of radiation associated with use of the instrument. This was achieved by filtering the neutron beam to decrease the fast neutron and low energy gamma-ray components of the beam, designing the new facility components and support structure to minimize neutron capture gamma-rays, and installing an improved detection system. The new thermal neutron PGAA facility is shown in Fig. 1.

Fig. 1. New thermal neutron PGAA facility at VT-5.

A cylindrical sapphire beam filter 5.3 cm long and 4.3 cm in diameter was incorporated into the shutter assembly. This modification reduced the number of fast neutrons by a factor of 5, decreased the thermal neutron flux by approximately 12 %, and greatly reduced low-energy gamma-ray background. With the reduction in fast neutrons, the amount of hydrogenous shielding required to slow and capture the fast neutrons was reduced as compared with that needed in the old facility. As a result, the background count-rate for the 2223.3 keV capture gamma-ray of hydrogen has been reduced from about 1 count per second (cps) or the equivalent of about 0.5 mg, of hydrogen, to 0.05 cps or the equivalent of 25 µg of hydrogen.

A summary of the design changes for each component of the facility and their effects is shown in Table 1. The original beam tube and sample chamber were fabricated from concentric Plexiglas tubes, filled with a mixture of paraffin and boron carbide. The new sample chamber and beam tube were fabricated from aluminum and lined with a 2 mm thick flexible lithiated polymer (lithoflex). The beam tube is kept under vacuum to reduce background gamma-rays arising from neutrons scattered by air and captured in the surrounding materials. The new sample chamber can be evacuated to further reduce background associated with neutron scatter and capture in air. As a result of these design changes, the background count-rates from hydrogen, nitrogen, and boron have been reduced by a factor of 10 or more and carbon has been eliminated from the background. The count rate for aluminum is about the same in the new system, despite the large amounts of aluminum in the beam tube, beam stop, sample chamber and support structure.

The beam stop of the old facility was a separate unit. It consisted of a steel box containing a lithiated polycarbonate cube (30 cm on a side) surrounded by lead bricks. This unit was lifted into place on top of the beam tube each time the system was assembled. The new beam stop consists of an aluminum box welded onto the aluminum support structure, and is filled with a cube of borated polyethylene (20 cm on a side) surrounded by lead. The elimination of steel from the beam stop has greatly reduced the background count-rate from iron.

A new germanium detector with improved resolution and peak-to-Compton ratio was installed. This detector has a relative efficiency of 40 % (relative to a 7.6 cm cube of sodium iodide) and 2.0 keV (peak full-width-half-maximum) resolution for the 1332.5 keV gamma-ray line

Table 1. Comparison of original and new thermal neutron PGAA systems

Facility Component	Old PGAA System	New System	Effect
Beam Stop	Steel cube (61 cm on a side) Li_2CO_3 plug, cube of Li_2CO_3 in resin surrounded by lead bricks	Aluminum cube (43 cm on a side) ^6LiF polymer plug, borated polyethylene surrounded by lead bricks	Eliminate Fe background γ-rays from beam stop
Beam tube	Plexiglas concentric tubes with a mixture of boron carbide in paraffin, and Li_2CO_3 in paraffin between them; Teflon film end windows; air filled beam tube	Al tubing lined with ^6LiF polymer capped at each end with Al and center windows of a Mg alloy. Upper and lower sections evacuated, lithiated polyethylene shielding on outer two sides	Reduce H and eliminate N background γ-rays
Sample Chamber	Walls fabricated from B_4C in resin with Teflon windows covered with fused enriched Li_2CO_3 plugs in front of and across from the detector window	Welded Al plate covered with ^6LiF polymer shielding; Mg alloy thin windows in front of and across from the detector covered with the same Li_2CO_3 plugs; chamber may be evacuated	Reduce B and eliminate N background γ-rays
Detection system	Ge detector (27 % relative efficiency) in a NaI Compton suppressor	Ge detector (40 % relative efficiency) in a BGO Compton suppressor	Eliminate Na background γ-rays
Support Structure	Al tripod frame with a cage to hold the beam stop	Al tripod frame. The beam tube and beam stop are attached to the frame and the detection system placed on rails	Improve structure stability
Component Set-Up	Four separate pieces (beam tube, Al tripod, beam stop, detection system) that are assembled individually	Assembled as one unit with a removable Ge detector	Improve safety and ease of system set-up

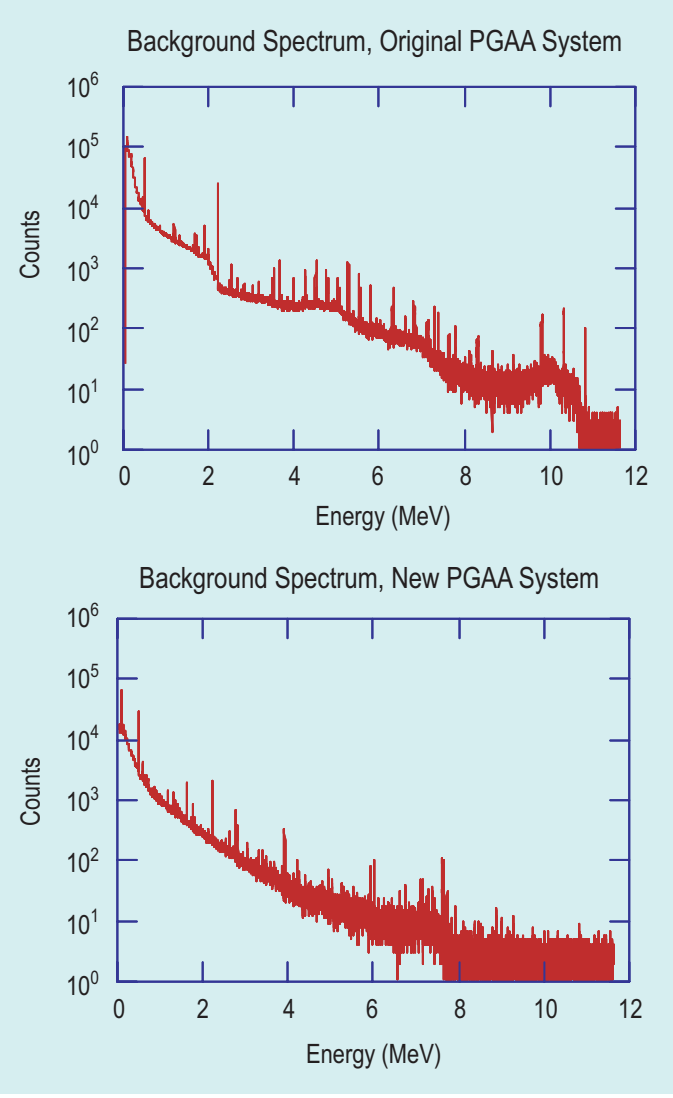

Fig. 2. Comparison of the background spectra collected with the old PGAA system (top) and the new system (bottom).

from ^{60}Co. The original sodium iodide Compton suppression system was replaced with a bismuth germanate suppressor. This modification eliminated sodium gamma-ray background.

The goal of reducing background radiation and improving analytical sensitivity and detection limits has been achieved. A comparison of spectra from background counts from the old and the new PGAA systems is shown in Fig. 2. The reduction in the background count-rates in the low energy region is evident. This reduction will greatly improve the detection limits for elements with neutron capture gamma-rays in the low energy region. With the sample chamber evacuated, nitrogen capture gamma-rays have been eliminated from the background. Elimination of the sodium background has improved the detection limit for this element. Improvements in shielding have resulted in a decrease in the background count-rates of hydrogen, boron, carbon, iron, and germanium, improving detection limits for those elements as well.

E. A. Mackey and R. M. Lindstrom
Analytical Chemistry Division
National Institute of Standards and Technology
Gaithersburg MD, 20899-8395

D. L. Anderson
Elemental Research Branch
Food and Drug Administration
College Park, MD 20740-3835

P. J. Liposky
NIST Center for Neutron Research
National Institute of Standards and Technology
Gaithersburg MD, 20899-8561

Performance Enhancements of the CHRNS 30-m SANS Instrument

Two changes made to the optics of the CHRNS 30-m SANS instrument during the installation of the NCNR's new cold source have increased the flux at the sample *and* the low-Q resolution of the instrument.

The increase in flux, over and above that provided by the new cold source, comes from replacing the instrument's cooled bismuth-beryllium filter with an "optical filter" of the type shown schematically in Fig. 1. The optical filter replaces 10 m of straight neutron guide and its 40 cm long Bi-Be filter with an inclined guide section with a high critical angle supermirror reflective coating. The optical filter channels cold neutrons, with wavelengths as short as 3 Å, out of the line-of-sight of fast neutrons and gamma rays from the source. The cold neutrons delivered to the SANS instrument undergo an even number of reflections in the optical filter to emerge in the horizontal direction, but displaced 14 cm vertically. To accommodate the beam displacement, the entire SANS instrument had to be raised; a non-trivial task that required detailed engineering analysis, careful planning and skilled execution.

The design of the optical filter was refined with the aid of detailed Monte Carlo calculations of the angular and spectral distribution of neutrons transmitted by the optical filter. Figure 2 shows the calculated and measured gain in flux at the sample, due to the optical filter alone, for the supermirror reflectivity model shown in the inset. These results demonstrate that the optical filter transmission is about the same as the previous crystal filter for wavelengths around 5 Å, but becomes substantially better at longer wavelengths where absorption in the crystal filter becomes significant.

The optics for the CHRNS SANS instrument were further improved by installing a system of refracting lenses and prisms near the sample position to focus 17 Å neutrons onto the detector at its maximum distance, 13 m, from the sample. A similar lens system, consisting of 28 biconcave single crystals of MgF_2 for focusing 8 Å neutrons, has been in use on the NCNR's other 30-m SANS instrument on guide NG-7 for nearly two years [1]. The refracting power of the lenses increases with the wavelength squared, but so does the distance the neutron falls between the sample and detector due to gravity. The vertical spreading of the focus for a beam with a wave-

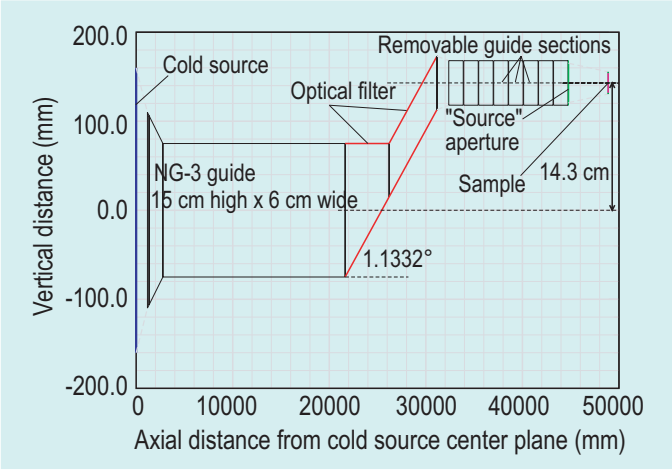

Fig. 1. Schematic elevation of the NG-3 optical filter (note vertical scale is exaggerated for clarity). The inclined section shown in red is coated with supermirror with critical angle approximately 3.2 times that of natural nickel. The removable guide sections are in the pre-sample flight path of the NG-3 SANS instrument.

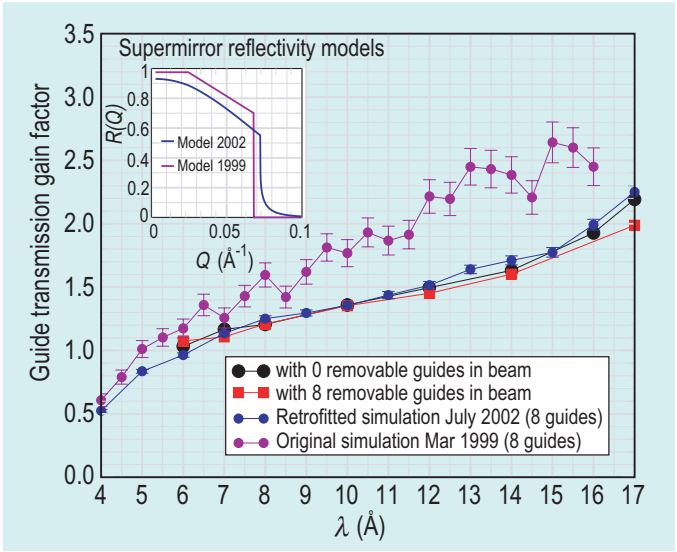

Fig. 2. Transmission gains of the NG-3 optical filter. The black circles are measured with no removable guides in the beam. The red squares are measured with 8 removable guides in the beam. The violet circles are the original Monte Carlo simulated gain predictions (March 1999) using the supermirror reflectivity model shown in the inset. The blue circles are simulated gains (July 2002) using the refined reflectivity model shown in the inset. These "hindsight" simulations predict the measured gains well for $M = 3.2$ supermirror with $R(Q = 0) = 0.930$ and RMS surface roughness equal to 10 Å with $R(Q = 0.069\ Å^{-1}) = 0.55$.

length spread typical of a SANS instrument, about 10 % to 15 % FWHM, restricts the utility of the lenses alone to wavelengths less than 10 Å. The new development implemented on the CHRNS SANS instrument is to follow the lenses with prisms that refract in the vertical direction to counteract the effect of gravity.

Figure 3 depicts the arrangement of lenses and prisms now installed on the CHRNS SANS instrument. Seven MgF_2 biconcave lenses focus 17 Å neutrons at the detector, 13 m from the sample. For this distance a single prism with an apex angle of 161° would cancel the beam spreading due to gravity for all wavelengths [2]. Such a prism, however, would have to be 250 mm long at its base to intercept the full beam height transmitted by the lenses (≈ 2 cm). A more practical scheme, as shown in Fig. 3, is to stack two sets of prisms, with each prism 30 mm long and 5 mm high with an apex angle of 143°, to give the same anti-gravity effect. In this scheme, the bottoms of each prism are coated with Gd_2O_3 to eliminate surface reflections.

The effectiveness of the lens/prism combination can be seen in Fig. 4 that compares circularly averaged SANS data from voids in an irradiated crystal of aluminum obtained with pinhole collimation and with the focusing optics. The data for the lens/prism system extend to a minimum scattering vector Q = 0.00045 Å^{-1}, nearly a factor of two lower than the pinhole collimation. Furthermore, the scattered intensity is 3 times higher with the lens/prism system because a larger area of the sample can be illuminated without degrading the Q-resolution. With pinhole collimation, intensity at the detector is roughly

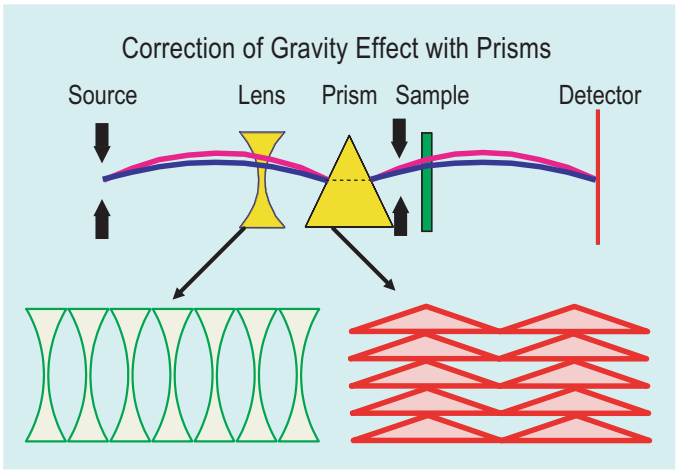

Fig. 3. Schematic diagram of the configuration of lenses and prisms used on the 30-m CHRNS SANS instrument. The seven biconcave lenses focus 17 Å neutrons at the detector, 13 m from the sample, and the double stack of prisms refracts the beam vertically to cancel the effect of gravity.

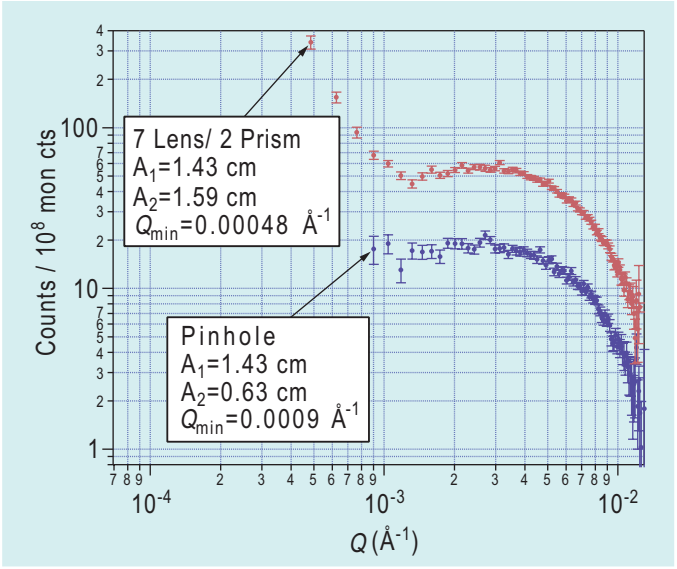

Fig. 4. SANS from voids in an aluminum crystal measured with and without the new focusing and gravity cancellation optics installed on the CHRNS SANS instrument. The optics halve the minimum accessible *Q*-value while increasing the scattered intensity roughly threefold.

proportional to Q^4_{min}, hence the lens/prism system represents an overall intensity gain of 48 compared with simply reducing pinhole aperture size to achieve the same minimum Q.

The new cold source and improvements in optics are enabling microstructural studies that link nanoscale with microscale features in, for example, polymer-clay nanocomposites, gels, and fluxoid lattices in superconductors.

References

[1] S.-M. Choi, J. G. Barker, C. J. Glinka, Y. T. Cheng, P. L. Gammel, J. Appl. Cryst. **33**, 793 (2000).

[2] E. M. Forgan, R. Cubitt, Neutron News **9(4)**, 25 (1998).

J. Cook, I. G. Schröder, S. R. Kline, B. Hammouda, and C. J. Glinka
NIST Center for Neutron Research
National Institute of Standards and Technology
Gaithersburg, MD 20899-8562

S.-M. Choi
NIST Center for Neutron Research
Present affiliation:
Korea Advanced Institute of Science and Technology
373-1, Guseong-dong, Yuseong-gu, Daejon,
Republic of Korea 305-701

Probing Nanoscale Disorder with Neutron Tunneling Spectroscopy

The presence of structural disorder can have a dramatic effect on macroscopic materials properties. At the atomic scale, structural disorder is typically described in terms of distributions of geometrical quantities such as bond lengths and bond angles that are determined from diffraction measurements. Alternatively, disorder can be quantified by determining the distribution of potential energies experienced by the atomic scale constituents of the system. The distribution is sharp for a highly ordered (crystalline) system, while it is broad for a disordered system. Rotational tunneling spectroscopy is a useful tool for characterizing the local molecular environment due to its exquisite sensitivity to the local potential [1]. This approach has been used to determine the distribution of rotational potentials felt by methyl iodide molecules adsorbed in a series of mesoporous silica glasses. The degree of confinement-induced disorder in the methyl iodide can then be directly related to the pore sizes in the glass.

The rotational potential felt by the methyl (CH_3) groups in methyl iodide (CH_3I) arises solely from interactions with the local environment including the neighboring molecules. The energies of the transitions between rotational states can be found by solving the Schrödinger equation for the model potential by $V_3(1-\cos(3\theta))/2$ in the angular coordinate about the C-I axis, θ. In the limit of an infinitely high barrier, V_3, the motion of the CH_3 group is that of a torsional oscillator. However, if the barrier is not too large, the wavefunctions will have significant overlap and quantum mechanical tunneling between the potential minima can occur. This results in a splitting of the rotational ground state. The energy of this splitting, which can be directly measured using cold neutron spectroscopy, has a nearly exponential dependence upon the barrier height. This strong dependence on V_3 is the reason why tunneling spectroscopy is so sensitive to the local molecular environment and, in particular, the quenched disorder of adsorbed molecular solids.

The porous hosts used in this investigation have a range of pore size distributions with differing nominal pore diameters and widths. Nominal pore diameters, <d>, determined via nitrogen adsorption/desorption isotherms range from 2.5 nm to 14.4 nm. In all cases but one (xerogel with <d> = 10.0 nm) the porous glasses are disks. The xerogel is a fine powder with a nominal particle size of 11 μm. Liquid methyl iodide (CH_3I) was condensed into the porous hosts until 95 % of the open pore volume was filled and then cooled to 5 K. Spectra were collected using the NIST High-Flux Backscattering Spectrometer with an energy resolution of 0.79 μeV.

The neutron scattering spectra display broad asymmetric lines indicative of a distribution of potential barrier heights. These distributions can be extracted from the neutron scattering data using a simple model in which a sum of Gaussian distributions of potential barriers (which yield an asymmetric tunneling line-shape) is used to fit the spectra [2]. A sum of two potential distributions is found to be sufficient to describe the data. One of these distributions is quite broad, indicating substantial disorder of the methyl iodide solid, while the other is much narrower suggesting a relatively high degree of order.

The relative weights of the two components show a pronounced dependence on <d>. Figure 1 shows that the fraction of the total integrated intensity that appears in the highly disordered component of the tunneling spectrum decreases monotonically as <d> increases. This behavior can be described with a simple model in which the relatively well-ordered component of the scattering is attributed to CH_3I molecules near the center of the pore while

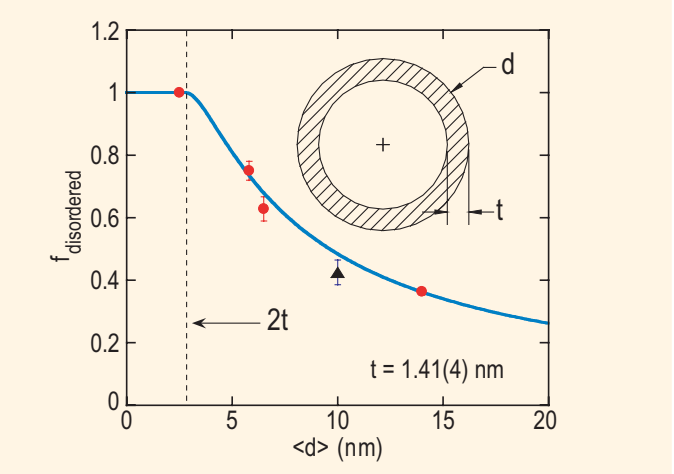

Fig. 1. Fraction of the total integrated intensity that appears in the disordered component of the tunneling spectrum as a function of the mean pore diameter. The solid line is a fit to the model discussed in the text. The dashed line is drawn at twice the disordered layer thickness. Inset shows the geometrical picture used in the model.

the highly disordered component is associated with a ring of thickness t of disordered molecules near the pore walls. Treating the pores as circular cylinders, the fraction of disordered molecules is just the ratio of the ring to circular areas: $f_{disordered} = 4t(<d> - t)/<d>^2$.

The solid line in Fig. 1 compares this model to the data for t = 1.41(4) nm, which corresponds to about three molecular layers. It is clear that this model provides an excellent fit to the data.

While the relative weights of the two components depend on the pore size, the mean values, $<V_3>$, and widths, σ_{V3}, of the two distributions of barrier heights are found to be roughly the same for each of the hosts. This indicates that the structure of the confined methyl iodide both near the surface and in the center of the pores does not depend strongly on either <d> or the width of the pore size distribution.

CH_3I molecules possess a relatively large electric dipole moment. This results in the molecules being anti-aligned in the bulk crystal structure [3]. Silica surfaces often have hydroxyl (OH) groups which would be expected to interact rather strongly with the dipole moment of the molecules and lead to a substantial surface-molecular interaction. The surface-molecule and molecule-molecule interactions can be of similar strength leading to structural frustration in the confined solid. Thus, one would expect that the disordered fraction and even the structure of the two components to be strongly influenced by changing the relative strengths of these interactions. In order to test this hypothesis, the surface of one set of porous disks (<d> = 5.8 nm) was chemically treated such that hydrophobic OCH_3 groups replaced the OH groups. This change significantly reduces the surface-guest interaction, and should therefore lead to a reduction of the disorder in the confined solid. The measured tunneling spectra for methyl iodide adsorbed in both the treated and untreated hosts (<d> = 5.8 nm) are shown in Fig. 2. As seen by the prominence of the narrower peaks, the more ordered component of the tunneling spectrum increases substantially for the methyl iodide confined in the glass with the hydrophobic surface as compared to the host with the hydrophilic OH groups. In fact, the disordered fraction decreases by about 25 %, which indicates that the thickness of the highly disordered layer is roughly two-thirds that of the untreated glass. Moreover the width of the tunneling line in the highly disordered component has also decreased substantially indicating that the structure of the methyl iodide near the hydrophobic surface is more bulk-like than it is near the hydrophilic surface.

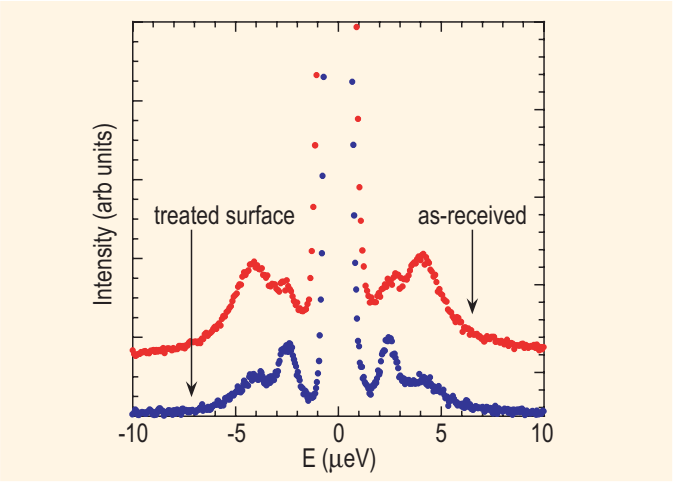

Fig. 2. Tunneling spectrum of confined CH_3I in 5.8 nm pores with and without surface treatment to make the surface hydrophobic. The hydrophobic surface results in a diminished disordered component.

In summary, the sensitivity of tunneling spectroscopy to small changes in the rotational potential has allowed us to probe the importance of surface-guest interactions in determining the disorder imposed by the confinement of methyl iodide within mesoporous glasses. It has been shown that the adsorbed species in the hydrophilic pores form a highly disordered layer with a thickness of approximately three molecular layers and that a more ordered region exists in the pore center. Interestingly, the molecular structures of these two regions do not depend strongly on either the average pore size or on details of the pore size distribution. When the surface chemistry is altered so as to reduce the importance of surface-guest interactions, both the thickness and molecular scale disorder of the region near the wall is greatly reduced.

References

[1] W. Press, in *Single-Particle Rotations in Molecular Crystals*, (Springer-Verlag, Berlin, 1981).

[2] R. M. Dimeo and D. A. Neumann, Phys. Rev. B **63**, 014301 (2001). R. M. Dimeo and D. A. Neumann, App. Phys. A **75** (in press). R. M. Dimeo, D. A. Neumann, Y. Glanville, and D. B. Minor, Phys. Rev. B **66**, 104201 (2002).

[3] M. Prager, J. Stanislawski, and W. Hausler, J. Chem. Phys. **86**, 2563 (1987).

R. M. Dimeo and D. A. Neumann
NIST Center for Neutron Research
National Institute of Standards and Technology, Gaithersburg, MD 20899-8562

Y. Glanville
The Pennsylvania State University
University Park, PA 16802-6300

D. B. Minor
Ceramics Division
National Institute of Standards and Technology
Gaithersburg, MD 20899-8520

The "Bucket Brigade" Mechanism of Proton Diffusion in Superprotonic Conductors

Proton diffusion plays a central role in many processes ranging from the regulation of biological functions to the production of electricity in fuel cells. The renewed emphasis on developing the next generation of portable sources of power requires the development of lightweight protonic conducting materials for use as electrolytic membranes [1]. Furthermore, understanding the atomic-scale mechanism of protonic diffusion in candidate materials is necessary to optimize their performance. Since neutrons are particularly sensitive to hydrogen, neutron scattering is an extremely valuable probe of proton dynamics (including diffusion). Moreover, because the wavelength of neutrons is comparable to interatomic distances, neutron scattering is capable of revealing the atomic-scale geometry of protonic motions in a way that is unmatched by other spectroscopic probes. Computational techniques also provide detailed atomistic information about proton incorporation and dynamics. Because of the simplicity of the scattering mechanism, computational results can be directly compared to neutron scattering data. Thus neutron scattering and computational methods are a powerful combination for understanding the performance of protonic conducting materials [2]. Here we briefly describe neutron vibrational spectroscopy (NVS) and quasielastic neutron scattering (QNS) measurements on superprotonic conductors of the general formula $MHXO_4$ (M = Rb, Cs, X = S, Se, etc.) that reveal detailed information on the proton-conduction mechanism.

The crystal structure of alkali-metal hydrogen sulfates and selenates consists of chains of XO_4 tetrahedra (Fig. 1), which are linked by hydrogen bonds, O-H··O. Due to the proximity of the proton site to the midpoint of the O-O separation, it is believed that the proton is dynamically disordered, yielding symmetric hydrogen bonds. However, at a sufficiently low temperature, one expects that the protons may order, giving rise to observable changes in the vibrational spectrum. Above room temperature, there is an orientational order-disorder transition to a phase in which the tetrahedra are dynamically disordered and which displays a very large protonic conductivity that should be observable by QNS.

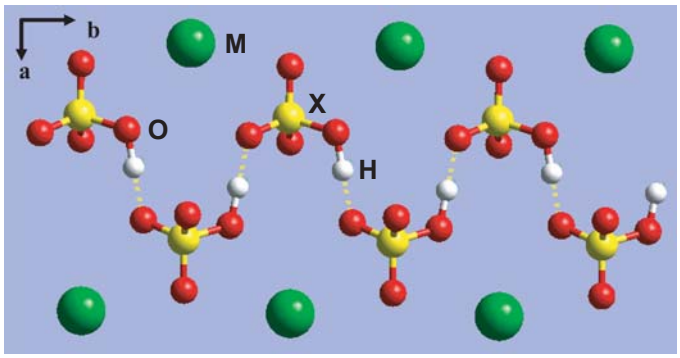

Fig. 1. Projection of the $MHXO_4$ structure, showing the zigzag pattern of the hydrogen bonds between XO_4 tetrahedra. Yellow dashed lines indicate the hydrogen bonds.

Figure 2 summarizes NVS results on $RbHSO_4$ measured using the Filter Analyzer Neutron Spectrometer. At low temperatures, the NVS spectrum shows sharp peaks at 83.3 meV and 99.7 meV. The temperature dependence of these peaks is quite unusual. The intensities decrease very rapidly with increasing temperature and almost disappear at temperatures as low as 200 K. In addition, while the high-energy mode softens, as expected, the low-energy mode hardens by about 2 meV as the temperature is increased. Near 200 K, these two modes collapse to form a broad feature around 95 meV. This suggests that there is significant proton motion even at this low temperature. We believe that this unusual behavior is related to dynamically disordered hydrogen bonds arising from breaking and reforming O-H bonds. Careful neutron diffraction studies in deuterated materials are underway to

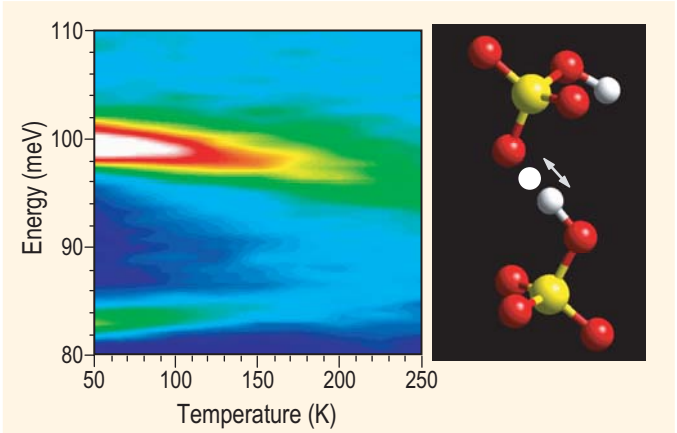

Fig. 2. Temperature-dependent NVS measurements of $RbHSO_4$. As discussed above, these results suggest very large amplitude proton motions are present at temperatures as low as ≈ 100 K. The right panel illustrates the dynamically disordered hydrogen bonding, which is most likely responsible for this unusual temperature dependence.

look for significant changes in the apparent locations or thermal factors of the protons at these temperatures. It should be noted that since this type of dynamical disorder is localized to two neighboring oxygen ions, it cannot be responsible for long-range protonic conduction.

To probe protonic diffusion directly, the temperature dependence of the QNS was measured for $CsH(SO_4)_{1-x}(SeO_4)_x$ ($x \approx 0.24$) above room temperature using the Fermi-Chopper time-of-flight Spectrometer. The data were fit as a function of the scattering vector Q (assuming both elastic and quasielastic components) in order to extract the Elastic Incoherent Structure Factor (EISF), which is defined as the fraction of the total scattering that is elastic. Figure 3 shows the EISF as a function of Q for several different temperatures. The fact that a non-zero EISF is observed even at 475 K indicates that, within the time window of the measurement (< 20 ps), the hydrogen motion is localized rather than diffusive. Moreover, the fact that the EISF changes with temperature indicates the existence of non-energetically equivalent proton-sites. The best fit to the EISF (shown by the solid lines in Fig. 3) was obtained assuming two types of hopping motions for the protons between pairs of inequivalent sites. The agreement between the data and the model is excellent. The two jump distances, 1.4 Å and 4.5 Å, are essentially independent of temperature (see Fig. 4). Looking at the structure, these can easily be identified as the reorientation of the SO_4-H group around the quasi-threefold (1.4 Å) and the quasi-twofold (4.5 Å) axes (Fig. 4). The ratio of the times that the proton spends in each of the two sites depends exponentially on temperature as expected (solid lines in the upper left panel of Fig. 4). For the short-distance reorientation, the time ratio goes rapidly to unity around 405 K, just before the super-protonic phase transition, indicating that the two sites are equally populated. For the long-distance reorientation, the ratio approaches 0.2 at the highest temperature.

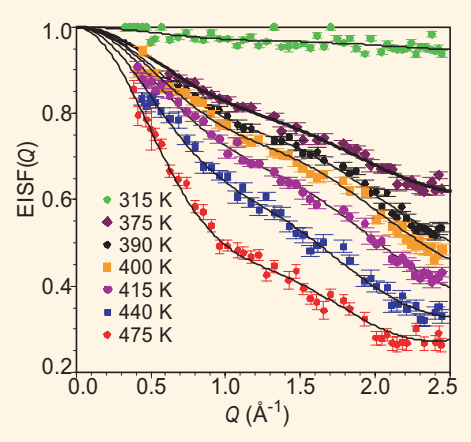

Fig. 3. EISF (dots) and fits (solid lines) at different temperatures for $CsH(SO_4)_{1-x}(SeO_4)_x$ ($x \approx 0.24$).

These findings are consistent with a previous neutron-powder-diffraction study on the high-temperature phase of $CsHSO_4$, which revealed four different orientations of each tetrahedron [3]. Most probably the four orientations mimic the dynamical orientational disorder of the tetrahedra that we observe by QNS. We also note that the two types of dynamic orientational disorder shown in Fig. 4 do not result in long-range protonic conduction since the motions are localized on a single tetrahedron. However, when one combines these two motions with the dynamically disordered hydrogen bond implied by NVS, the mechanism of protonic conduction can be understood. Namely, the protons move between two neighboring tetrahedra via dynamically disordered hydrogen bonds. The tetrahedra then reorient, allowing the protons to move to a third tetrahedron, again via the dynamically disordered hydrogen bonds. Thus the tetrahedra play the role of a "bucket brigade" by accepting a proton from an adjacent tetrahedron then turning and handing it the tetrahedron on the other side. On the atomic scale, superprotonic conductivity occurs in the $MHXO_4$ family of compounds due to this efficient mechanism of transporting protons through the lattice.

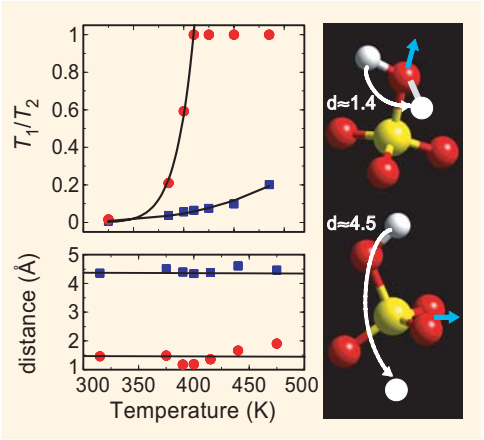

Fig. 4. Top: Temperature dependence of the ratios of the residence times T_1 to T_2 for the pair of two-site hopping motions identified by QNS. Bottom: The two jump distances obtained from QNS as a function of temperature. These distances correspond to the two reorientational motions shown on the right. The red circles correspond to the motion depicted on top while the blue squares correspond to the motion shown on the bottom.

References

[1] *National Hydrogen Energy Roadmap*, DOE, Germantown, MD, 2002.

[2] T. Yildirim, B. Reisner, T. J. Udovic, and D. A. Neumann, Sol. State Ionics **145**, 429 (2001).

[3] A. V. Belushkin, C. J. Carlile, W. I. F. David, I. R. Ibberson, L. A. Shuvalov, W. Zajac, Physica **B174**, 268 (1991).

T. Yildirim, D. A. Neumann, and T. J. Udovic
NIST Center for Neutron Research
National Institute of Standards and Technology
Gaithersburg, MD 20899-8562

Motion in Intermediates Along the Protein-Folding Pathway: *cytochrome c*

Proteins are long macromolecular chains consisting of amino acid repeat units that, in the native state, adopt a well defined and intricately folded three-dimensional conformation. The ability to predict *a priori* the native three-dimensional structure of a given amino acid sequence, the so called "protein folding problem," is essential for the full promise of genetic therapies to come to fruition [1]. In fact, many apparently unrelated diseases (*e.g.*, Alzheimer's, Mad Cow, cystic fibrosis, and even many cancers) result from protein folding gone wrong.

In order to obtain detailed knowledge of the protein folding mechanism, extensive characterization of the relevant interactions, structure and dynamics is required at each step of the protein-folding pathway. To this end, researchers have been investigating the properties of proteins in the native, partially unfolded and the completely unfolded states to obtain "snapshots" of the relevant behavior of intermediates along the folding pathway, yielding information intended to facilitate rationalization of folding mechanisms.

To deepen our understanding of the molecular motions involved in protein folding and, hence, the role of dynamic behavior on the overall folding mechanism, we employed quasielastic neutron scattering (QENS) as a dynamical probe of several folded states of the electron transfer protein *cytochrome c* (see Fig. 1). QENS provides

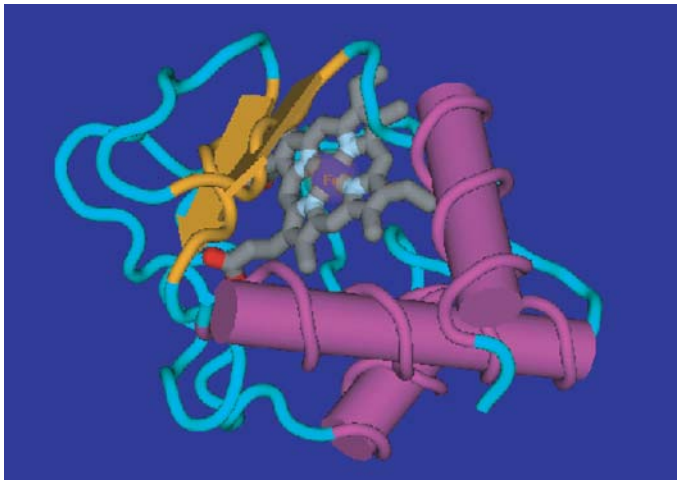

Fig. 1. The native state of *cytochrome c*.

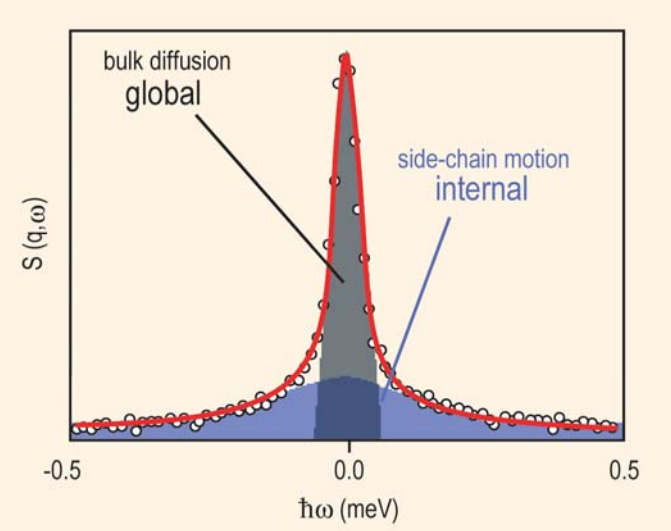

Fig. 2. Illustration of the general quasielastic neutron scattering profile of a protein in solution indicating the narrow scattering from the global diffusion and the broad scattering due to the internal side chains of the amino acid residues.

a method for directly probing the internal dynamics of biomolecules on the picosecond time scale and Angstrom length scale. In this technique neutrons exchange energy and momentum with the nuclei of the sample, allowing the forms, geometry, amplitudes and time-dependence of the motions involved to be determined. By making use of the large incoherent cross section of hydrogen nuclei and the capabilities of the Disk-Chopper Spectrometer at ≈ 32 μeV resolution it was possible to collect data on five different *cytochrome c* folded states (in order of increasing unfolding): native (N), salt induced molten globule (MG), alkaline denatured (D_{alk}), acid denatured (D_{acid}) and guanidine hydrochloride unfolded (U).

In a typical QENS experiment of this sort, a monochromatic beam of neutrons is scattered by a buffered solution containing the protein, the contribution of the scattering from the buffer is removed, and the resulting profile is considered to be that resulting from just the protein [2, 3]. Figure 2 depicts the general neutron scattering profile from a protein in solution, illustrating the distinct scattering from global (bulk translational and rotational diffusion) and internal (protein side-chain) dynamics. A profile of this sort is analyzed with a two Lorentzian fit model — a narrow Lorentzian to fit the global motion and a broad Lorentzian to fit the internal

motions. The two Lorentzian fit model permits the average ensemble time scale of global and internal side-chain motions to be ascertained separately.

The half width at half maximum of both Lorentzian fit functions, corresponding to the global and internal motions as a function of scattering vector squared (q^2) are given in Fig. 3. An effective diffusion coefficient (D_{eff}) is determined from the slope of Γ_{global} as a function of q^2. As evident from the tabulated results, D_{eff} generally decreases as the protein unfolds reflecting the correspondingly higher specific molecular volume of non-native folding states. The exception lies with the acid denatured state that, due to the strong electrostatic interactions present in the system, shows a near native D_{eff}.

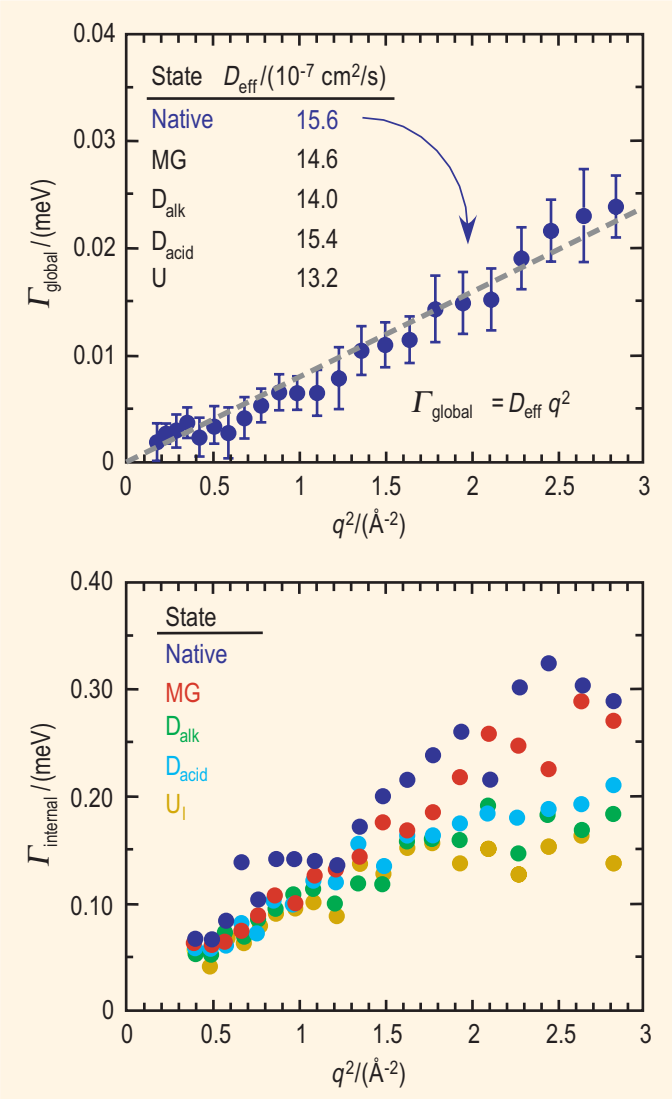

Fig. 3. Plot of the half width at half maximum of the global (top, native only) and internal (bottom) Lorentzian as a function of scattering vector squared. The tabulated effective diffusion coefficients are given for each folded state of *cyt c*.

A decrease in the relative time scale of the internal motions is observed as a function of protein unfolding. It is believed that the rather close-packed native structure provides more sharply defined, short-range interactions between the proximate side chains of the amino acid residues. Upon unfolding of the protein, these interactions are diminished by the increased separation between side chains and small, weakly interacting buffer molecules between them.

The results of this study demonstrate the type of dynamic information that can be determined from QENS experiments performed on a protein in several different structural states. As the nature of the unfolding medium displays a critical role in the internal dynamics of the unfolded states of *cytochrome c*, any attempts to correlate features between different folding states should take this into account. In combination with other characterization techniques, information of this sort will prove beneficial to the understanding and development of accurate protein folding mechanisms.

References

[1] A. R. Dinner, M. Karplus, Angew. Chem. Int. Ed. **40**, 4615 (2001).

[2] Z. Bu, D. A. Neumann, S-H. Lee, C. M. Brown, D. M. Engelman, C. C. Han, J. Mol. Biol. **301**, 525 (2000).

[3] J. Perez, J.-M. Zanotti, D. Durand, Biophys. J. **77**, 454 (1999).

A. Pivovar and D. A. Neumann
NIST Center for Neutron Research
National Institute of Standards and Technology
Gaithersburg, MD 29899-8562

Neutron Reflectivity from Biomimetic Membranes: Improving Reliability through Wavelet Analysis

Understanding such key biological processes as molecular recognition, protein insertion, and molecular self-assembly in *living* biological membranes remains a challenge. Membrane materials mimicking biological ones (biomimetic membranes) provide model systems to address this issue, and, because of its special sensitivity to hydrogen, neutron reflectivity (NR) offers a unique way to reveal thin film structures in biomimetic membranes.

The feasibility of using phase-inversion techniques in NR to reveal such structural details has been demonstrated [1]. It is possible to directly measure the real part, $r_I(Q)$, of the complex reflection coefficient $r(Q)$ as a function of wavevector Q and to mathematically invert it to obtain the scattering length density (SLD) depth profile $\rho(x)$ of the film. There remains much to do, however, in defining the reliability of the results, especially in accessing the unavoidable reduction of spatial resolution induced by data truncated at a maximum wavevector, Q_{max}. Wavelet analysis provides a systematic and useful approach to the problem [2].

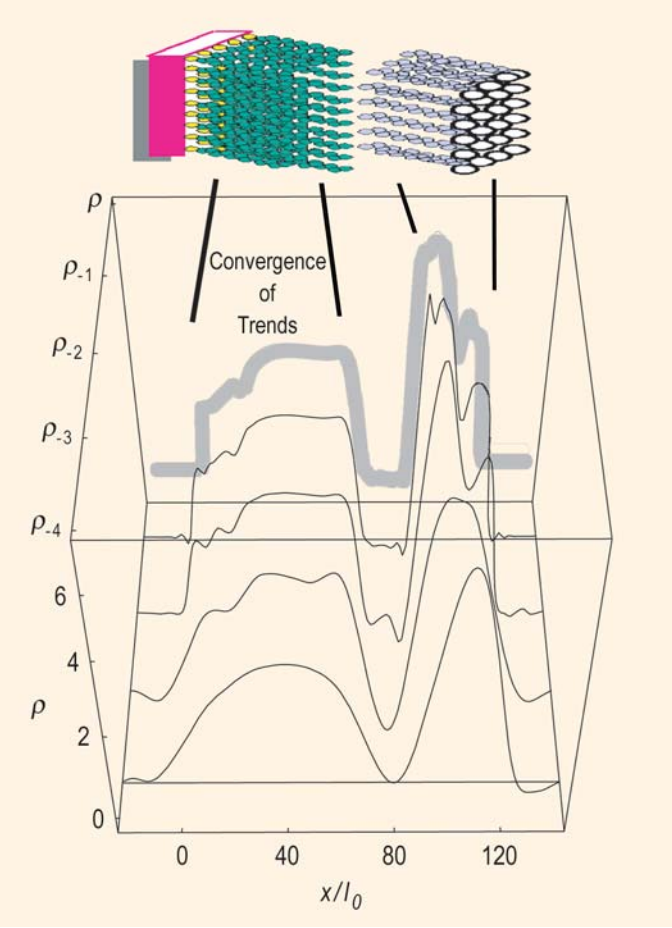

Fig. 1. Diagram of model (top) for which the computed scattering length density $\rho(x)$ is the thick grey curve. Trends converge: $\rho_{-4}(x)$, $\rho_{-3}(x)$, . . .,→$\rho(x)$.

In using Wavelet MultiResolution Analysis (WMRA), SLD profiles are characterized by a finest length scale $R_0 \approx 1$Å and coarser scales, $R_j = 2^{-j}R_0$, with j negative. $\rho(x)$ is viewed as a coarse "trend" $\rho_J(x)$ at resolution level J, with added "detail" $\Delta_J\rho(x)$ giving the trend at the next finer scale, $\rho_{J+1}(x) = \rho_J(x)+\Delta_J\rho(x)$. Relative to a base scale of resolution R_J, the SLD profile thus can be represented by the trend plus all remaining detail, $\rho(x) = \rho_J(x)+\sum_{J\le j}\Delta_j\rho(x)$. The experimental $\rho(x)$, associated with a given $Q_{\max}$ determined by the instrument, is a blurred representation of the veridical SLD. It can be thought of as a coarse image bracketed by neighboring trends for this $Q_{\max}$.

WMRA provides spatially localized orthonormal bases for this description. A family of wavelets called Daubechies-8 seems well suited to NR analysis. For illustration, we use a realistic SLD profile obtained by molecular modeling to represent a hybrid lipid membrane on a thin gold film (diagram on top of Fig. 1), a biomimetic system typical of those being studied in many laboratories. The model $\rho(x)$, seen in the back panes of Figs. 1 and 2, consists of the gold layer, a hydrogenated alkanethiol layer, and a deuterated lipid monolayer.

Figures 1 and 2 depict the convergence of the WMRA descriptions of $\rho(x)$ as trend and detail. The "overall" shape of $\rho(x)$ effectively is determined by the trend $\rho_{-4}(x)$ and detail $\Delta_{-4}\rho(x)$, *i.e.*, by trend $\rho_{-3}(x)$. However, emergence of the prominent double peaked structure of the lipid head group near x/l_0 needs detail $\Delta_{-3}\rho(x)$. Subsequent detail mainly acts to sharpen the edges between the film's components.

Figure 3 shows the effective contributions of the trend and the successive spatial detail to the reflection coefficient $r(Q)$, each calculated exactly. The edge-sharpening detail seen in Fig. 3 is not revealed in the reflection spectrum below $QR_0 \approx 0.6$. Figure 4 shows the "smeared" $\rho(x)$ obtained by direct inversion of the reflec-

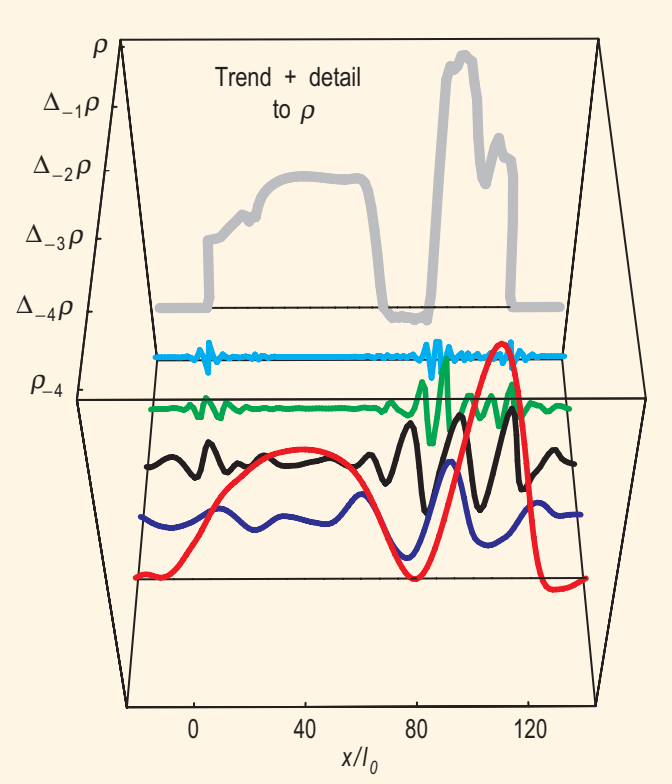

Fig. 2. Trend plus detail converges: $\rho_{-4}(x)+\Delta_{-4}\rho(x)+\Delta_{-3}\rho(x), \ldots, \rightarrow \rho(x)$.

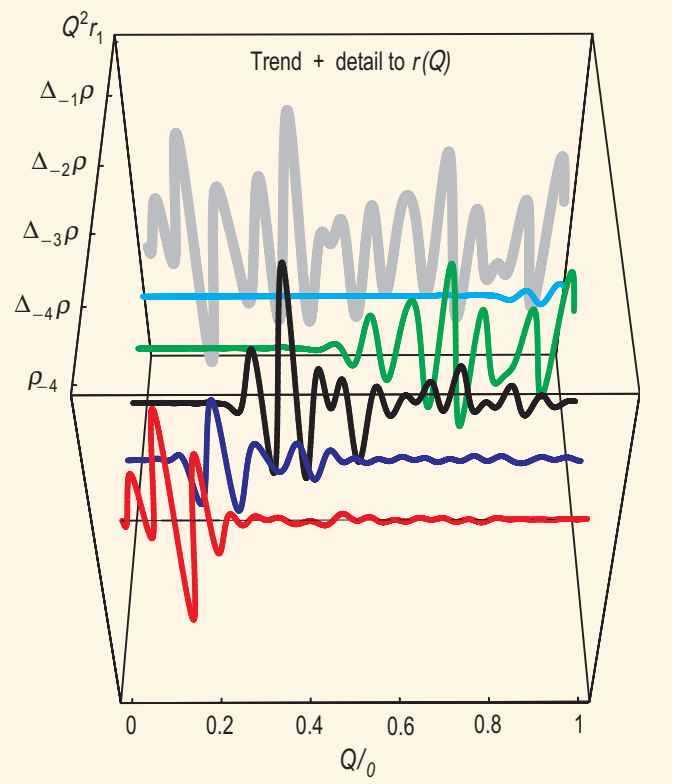

Fig. 3. Effective contributions to $Q^2r_1(Q)$ generated by the trend $\rho_{-4}(x)$ (in red) and the details $\Delta_j\rho\ (x)$ for j = -4, -3, -2, -1 shown in Fig. 2. The $Q^2r_1(Q)$ contributions are labeled by the SLD's that produced them.

tion from $\rho(x)$ using data truncated at $Q_{max} \approx 0.2$ Å^{-1}. This is seen to fall "between" the trends $\rho_{-4}(x)$ and $\rho_{-3}(x)$, stemming from low-pass filters with roll-offs at $Q \approx 0.2$ Å^{-1} and $Q \approx 0.4$ Å^{-1}, respectively. This is expected from the fact that the Fourier transforms of trends and detail overlap to a degree. Thus, a "pure" trend cannot be observed in the truncated data.

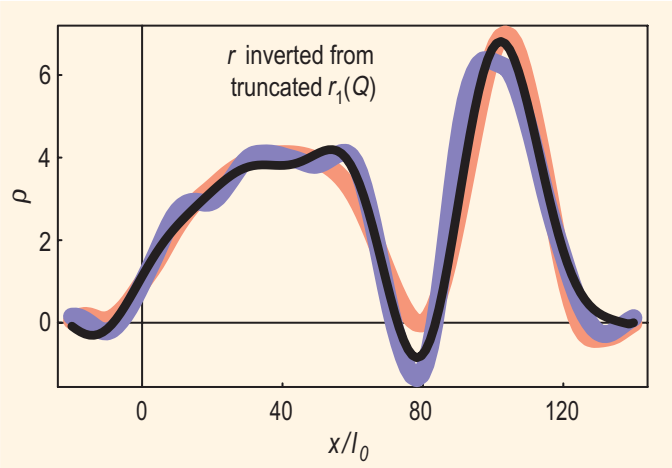

Fig. 4. Inverted $r_1(Q)$ (black) using only data truncated at $Ql_0 = 0.2$. Trends $\rho_{-4}(x)$ (red) and $\rho_{-3}(x)$ (blue) of the actual $\rho(x)$.

Wavelet analysis thus provides a systematic method for assessing the correctness of density profiles measured by NR. It promises to add reliability in unraveling structures of importance in biomimetic membranes.

References:

[1] C. F. Majkrzak, N. F. Berk, S. Krueger, J. Dura, M. Tarek, D. Tobias, V. Silin, C. W. Meuse, J. Woodward, and A. L. Plant, Biophysical J., **79,** 3330 (2000).

[2] Wavelets were first applied to x-ray reflectivity with different focus and using different techniques by I. R. Prudnikov, R. D. Deslattes, and R. D. Matyi, J. Appl. Phys., **90**, 3338 (2001).

N. F. Berk and C. F. Majkrzak
NIST Center for Neutron Research
National Institute of Standards and Technology
Gaithersburg, MD 20899-8562

Protein Adsorption to Metal-Chelating Lipid Monolayers

The adsorption of proteins to surfaces, especially lipid layers, plays a critical role in biochemical processes within living systems. These include membrane signaling and recognition, toxin detection, and mitigating the effects of toxin/biowarfare agents. Specific issues to be addressed are: protein orientation and surface density, monolayer versus multilayer adsorption, specific versus non-specific interactions, and lateral order and conformational changes upon adsorption including denaturization of protein [1].

In this work neutron reflection is combined with grazing incidence x-ray diffraction (GIXD) to study the interactions of the protein myoglobin with Langmuir monolayers of synthetic lipids. Neutron reflection is used to determine the adsorbed amount and to obtain information regarding the orientation and conformation of the adsorbed myoglobin [2]. GIXD is used to study the response of the lipid layer that occurs upon protein binding.

For lipid layers we have used the synthetic lipid distearyl imino-diacetate (DSIDA) that contains receptors for the metal ion Cu^{2+}. The use of metal ion coordination to target the adsorption of proteins to lipid membranes has been studied extensively. This method uses specific coordination interactions between Cu^{2+} and naturally occurring histidine units in myoglobin.

A Langmuir monolayer of 100 % DSIDA was spread onto the surface of buffered D_2O or H_2O (Fig. 1) and then compressed to a surface pressure of ≈ 40 mN/m where it forms a solid condensed phase layer (see GIXD data below). A dilute solution of $CuCl_2$ was injected under the condensed DSIDA monolayer. The Cu^{2+} ions chelate at the imino-diacetate site as indicated in Fig. 1.

Neutron reflectivity data for the condensed lipid layer with added Cu^{2+} ions are shown in Fig. 2 for both the H_2O and D_2O buffered subphases. Myoglobin was then injected into the subphase and neutron reflectivity data were taken repeatedly to monitor the time dependence of protein adsorption. The adsorbed protein layers reached quasi-equilibrium at ≈ 14 h after adding myoglobin into the solution. Only final sets of reflectivity data with adsorbed protein (for both H_2O and D_2O subphases) are shown in Fig. 2. The very large change in the reflectivity after

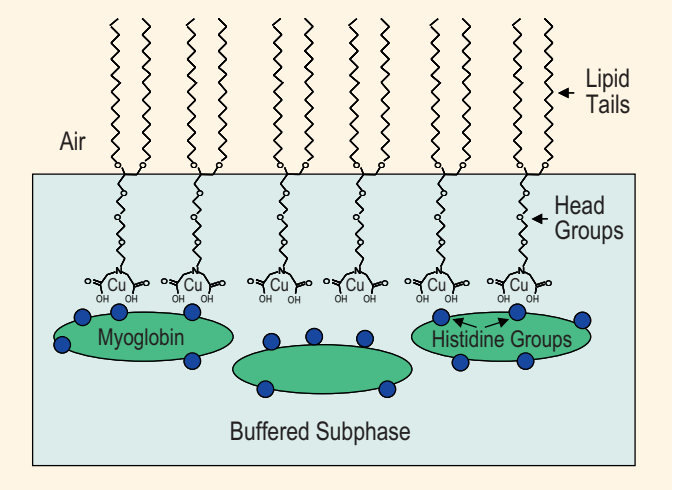

Fig. 1. Schematic of histidine groups on myoglobin adsorbing to distearyl imino-diacetate (DSIDA) molecules at chelated Cu^{2+} ion sites.

protein injection indicates a significant adsorption of protein under the lipid layer.

Solid lines in Fig. 2 are fits to the reflectivity data from which the segment concentration profile of protein can be obtained. Simultaneous fits to both sets of data show that the dimension of the quasi-equilibrium adsorbed myoglobin layer is 36 Å +/- 2 Å, and that the segment volume fraction of protein is ≈ 50 %. Unit cell dimensions of myoglobin from its crystal structure are (a, b, c) =

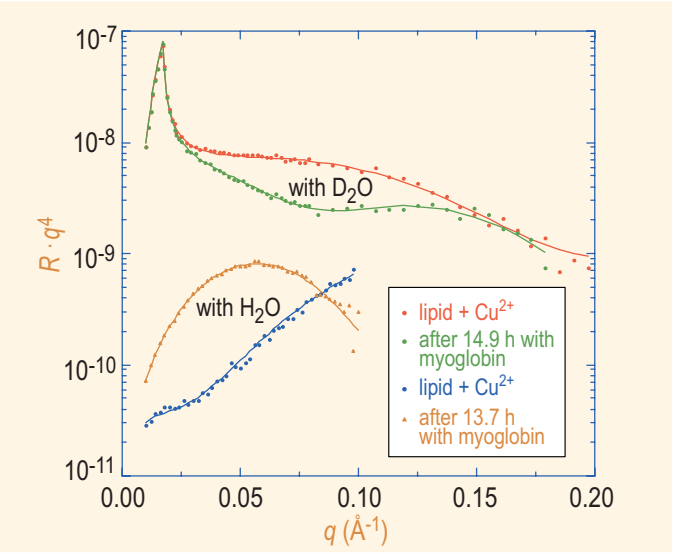

Fig. 2. Neutron reflectivity for 100 % DSIDA on buffered D_2O and H_2O subphases with and without myoglobin in the subphase. Solid lines are fits to the data as described in the text.

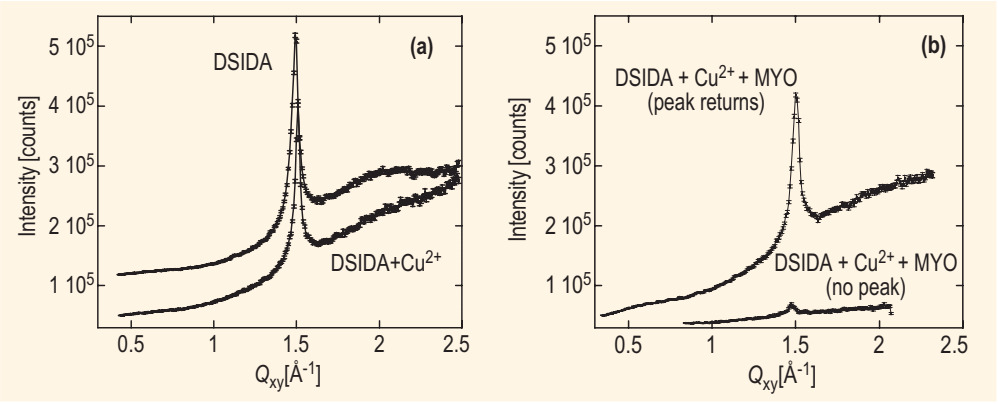

Fig. 3. Surface diffraction peak at a constant surface pressure of 40 mN/m: (a) 100 % DSIDA and also with Cu^{2+}, (b) 1.9 h (no peak) and 4.4 h (peak returns) after myoglobin injection.

(64.84, 30.98, 34.92) Å. Thus, the protein in all likelihood is bound to the lipid layer in its native state, *i.e.*, not denatured.

If no $CuCl_2$ is added to the subphase, then no change in the neutron reflectivity signal is observed upon injection of myoglobin. Alternatively, if we inject a strong Cu scavenging agent (EDTA) in the subphase after the protein adsorption, the reflectivity reverts back to that of the pure condensed lipid layer. This clearly shows that we are observing very specific binding of the protein to the chelated Cu^{2+} sites on DSIDA.

Important insight has been revealed in complementary GIXD data from the DSIDA system. Figure 3a shows the surface diffraction peak from the tails of a condensed DSIDA monolayer at an in-plane wavevector Q_{xy}= 1.50 Å^{-1}. This corresponds to a hexagonal packed lipid layer with a nearest neighbor spacing of 4.21 Å. Insertion of Cu^{2+} ions into the layer does not seem to affect the 2-D crystalline order of the lipid layer except for a slight change in lattice spacing.

When myoglobin is added to the subphase at a constant surface pressure of 40 mN/m, the diffraction peak arising from the hexagonal packing of the DSIDA tails (at Q_{xy}= 1.50 Å^{-1}) is drastically reduced at short times (Fig. 3b). This indicates a large perturbation in the 2-D crystallinity of the lipid layer upon insertion of protein. The surface diffraction peak, however, reappears after a few hours (Fig. 3b). The peak is slightly shifted to a higher value of Q_{xy}, and the distribution of intensity normal to the surface (not shown) indicates a substantially increased tilt of the lipid tails. By contrast, no change in the diffraction peak is observed after addition of myoglobin when the surface layer is maintained at a constant area (after initial compression to 40 mN/m).

We hypothesize that the protein is able to insert into the lipid monolayer when it is maintained at a constant pressure of 40 mN/m, but does not insert when at constant area (surface pressure in this case rises from 40 mN/m to 43 mN/m). Thus far, all the neutron reflection data have been obtained at constant surface area. In future work we will examine adsorption to lipid monolayers composed of 100 % DSIDA at constant surface pressure. We expect to see very different arrangement of the protein adsorbed layers for conditions at which the protein inserts into the lipid monolayer versus when it does not.

In summary, a combination of neutron reflectivity and GIXD has proven to be a very powerful way to study both the protein adsorption to lipid monolayers as well as structural changes that the lipid layer itself undergoes as the protein is adsorbed. Because of different contrast conditions for neutrons and x-rays, neutron reflectivity profiles are very sensitive to the adsorption of the protein, while GIXD is ideally suited for examining in detail any changes in the 2-D ordered structure of the lipid layer itself.

This successful study opens up a rather large field to examine other important lipid-protein interactions such as insertion of biological toxins into a lipid layer. Preliminary studies of neutron reflectivity and GIXD to examine the adsorption of cholera toxin to monolayers of glycolipids (a class of lipids containing sugar molecules which are found on cell surfaces) show extraordinary promise in this regard.

References:

[1] K. M. Maloney, D. R. Shnek, D. Y. Sasaki, and F. H. Arnold, Chemistry & Biology, **3**, 185, (1996).

[2] M. S. Kent, H. Yim, D. Y. Sasaki, J. Majewski, G. S. Smith, K. Shin, S. K. Satija, and B. M. Ocko, Langmuir **18**, 3754,(2002).

M. Kent and H. Yim
Sandia National Laboratory
Albuquerque, NM 87185

S. K. Satija
NIST Center for Neutron Research
National Institute of Standards and Technology
Gaithersburg, MD 20899-8562

J. Majewski
Los Alamos National Laboratory
Los Alamos, NM 87545

Hydration State of Single *cytochrome c* Monolayers on Soft Interfaces via Neutron Reflectivity

Water is critical, not only for the correct folding of proteins but also for the maintenance of this folded structure. The internal molecular motions in proteins, which are necessary for biological activity, are very dependent on the degree of flexibility which is determined by the level of hydration. The number of water molecules hydrating a functioning protein is thus an issue of great interest. Given an appropriate model system, neutron scattering, particularly sensitive to hydrogen, provides a way to measure this water content.

Previous optical spectroscopy studies have shown that yeast *cytochrome c* (YCC) covalently bound to a soft interface (Fig. 1.) and partially hydrated by a moist helium atmosphere can be fully functional with respect to the oxidation-reduction chemistry of its iron porphyrin prosthetic group [1, 2, 5, 6]. This system thus provides an opportunity to examine the water distribution required to maintain the structure and function of the protein YCC.

Unlike x-rays, neutrons scatter very differently from hydrogen and deuterium. This fact allows the water distribution in the monolayer profile structure of YCC to be obtained by comparison. The neutron scattering length density profile derived from neutron reflectivity for a YCC monolayer hydrated by D_2O is compared to the profile for identical hydration with H_2O.

The silicon surface layer of an iron-silicon (Fe/Si) or iron-gold-silicon (Fe/Au/Si) multilayer solid substrate can bind a self-assembled monolayer (SAM) to form the soft surface used to tether the YCC monolayer. (See diagrams at the top of Fig. 3.) Such a multilayer substrate has two key advantages in a neutron (or x-ray) reflectivity experiment: a multilayer substrate dramatically enhances this scattering for momentum transfer normal to the substrate surface, and a multilayer substrate also provides an important reference profile structure for the unique interferometric phasing of the reflectivity data.

Neutron reflectivities (Fig. 2) were collected on the NG-1 reflectometer for both H_2O and D_2O hydration cases for two such SAM/YCC samples. One SAM formed a nonpolar surface (-CH_3/-SH = 6:1 mixed endgroups), and

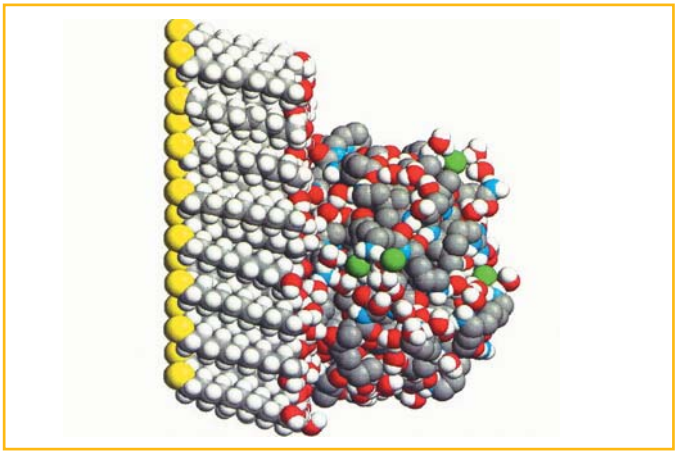

Fig. 1. Molecular dynamics "snapshot" of YCC tethered to the soft surface of an uncharged-polar self-assembled monolayer (SAM).

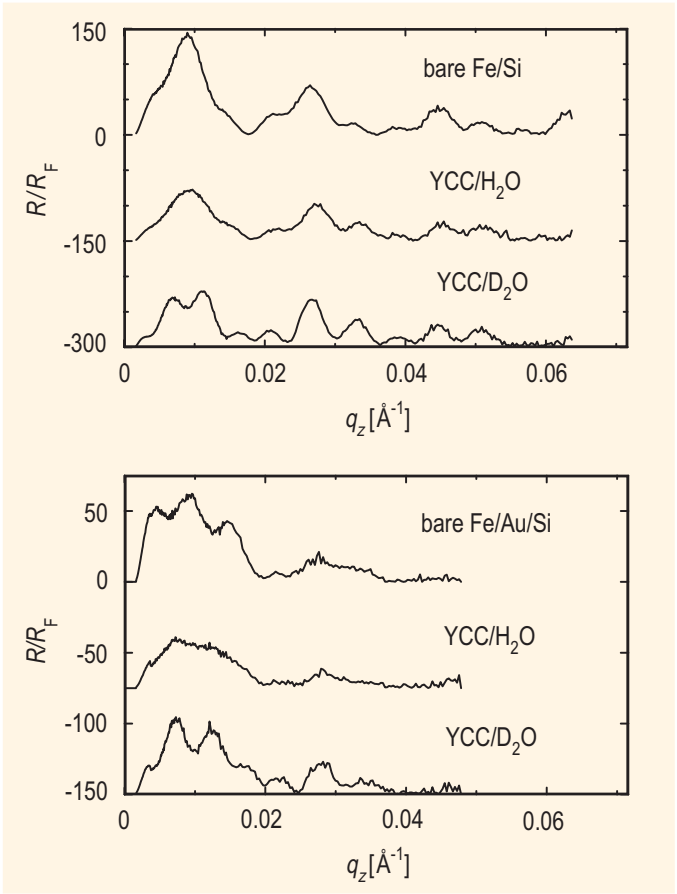

Fig. 2. Top: normalized reflectivity data with incident neutron spins parallel to the iron magnetization for the bare multilayer substrate, substrate plus nonpolar SAM plus YCC/D_2O, and substrate plus nonpolar SAM plus YCC/H_2O. Bottom: data for similar arrangements with the uncharged polar SAM on a Fe/Au/Si substrate. In the top plot the H_2O data are offset by 150 units and the D_2O data by 300 units on the ordinate, and in the bottom plot the H_2O data are offset by 75 units and the D_2O data by 150 units on the ordinate. (Note: $q_z = 2\sin\theta/\lambda$.)

the other SAM formed an uncharged polar surface (-OH/-SH = 6:1 mixed endgroups). These data were analyzed using a new interferometric phasing method that makes use of two features: the neutron scattering contrast between the Si and Fe layers in a single reference multilayer structure, and a constrained refinement approach using the finite extent of the gradient of the profile structures for the systems [3]. The water distribution profiles for the two SAM/YCC monolayers provided by this analysis are shown in Figs. 3a and 3b.

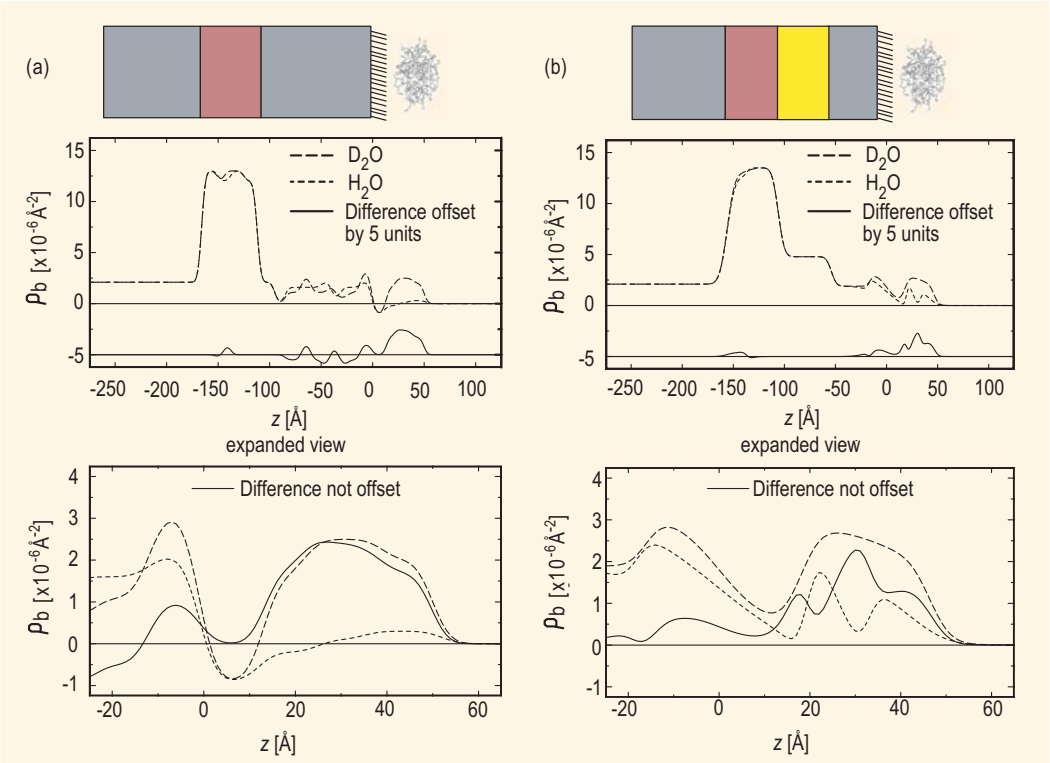

Fig. 3. The absolute neutron scattering length density profiles for partial hydration with D_2O and H_2O and their difference profile for both the nonpolar SAM (a) and the uncharged polar SAM (b) cases. The boundaries for the *cytochrome c* protein region of the profiles used for calculation of the amount of water hydrating the protein are *z* = 10 Å and *z* = 60 Å. Schematics of the composite structures are shown above their respective scattering length density profiles approximately to scale.

For hydration with D_2O, these profiles show that the protein monolayer is 3 Å to 4 Å closer to the substrate surface for the uncharged-polar SAM compared to the nonpolar SAM. This finding is in excellent agreement with simulations of these systems [3, 4], and arises because residues on the protein's surface interact strongly with the polar SAM's hydroxyl endgroups via hydrogen-bonding, thus drawing the YCC closer to the SAM surface.

Given these water distribution profiles, the number of water molecules hydrating the YCC monolayer at each SAM can be calculated. Allowing for proton exchange in the *cytochrome c* molecule itself (≈ 17 polypeptide backbone hydrogens and ≈ 104 side chain hydrogens), we obtained values of ≈ 167 water molecules/YCC at the uncharged polar SAM (exposed to He at 81 % relative humidity) and ≈ 297 water molecules/YCC at the nonpolar SAM (exposed to He at 88 % relative humidity) with relative errors of order 20 % to 25 %. These findings allow quantitative comparison to molecular models, opening an important window to understanding the role of water in protein functioning.

References:

[1] J. A. Chupa, J. P. McAuley, R. M. Strongin, A. B. Smith, J. K. Blasie, L. J. Peticolas, and J. C. Bean, Biophys. J. **67**, 336 (1994).

[2] A. M. Edwards, J. K. Blasie, and J. C. Bean, Biophys. J. **67**,1346 (1998).

[3] L. R. Kneller, A. M. Edwards, C. E. Nordgren, J. K. Blasie, N. F. Berk, S. Krueger, and C. F. Majkrzak. Biophys. J. **80,** 2248 (2001).

[4] C. E. Nordgren, D. J. Tobias, M. L. Klein, and J. K. Blasie. Biophys. J., in press.

[5] J. M. Pachence, S. M. Amador, G. Maniara, J. Vanderkooi, P. L. Dutton, and J.K. Blasie. Biophys. J. **58**, 379 (1990).

[6] J. M. Pachence, and J. K. Blasie. Biophys. J. **59**, 894 (1991).

L. R. Kneller, N. F. Berk, S. Krueger, and C. F. Majkrzak
NIST Center for Neutron Research
National Institute of Standards and Technology
Gaithersburg, MD 20899-8562

J. K. Blasie, A. M. Edwards, and C. E. Nordgren
Department of Chemistry
University of Pennsylvania
Philadelphia, PA 19104

Direct Measurement of the Reaction Front in Chemically Amplified Photoresists

The semiconductor industry is rapidly approaching the need to fabricate sub-100 nm structures to continue performance increases in integrated circuits. Photolithography remains the enabling technology for the fabrication of integrated circuit patterns. Although industry is able to commercially produce 130 nm features, lithographic materials and processes are not fully available for the production of sub-100 nm structures. New materials must be able to produce structures with dimensional tolerances of 2 nm to 5 nm, dimensions near the size of the polymer chain molecules in the imaging layer.

Current imaging layers, chemically amplified photoresists, are multi-component materials consisting of a polymer resin initially insoluble in an aqueous base developer solution, a photoacid generator (PAG), and other additives. A schematic diagram of the fabrication process and an example structure are shown in Figs. 1 and 2. The patterns are generated in the resist by exposure to UV radiation through a mask. In the exposed areas, the PAG decomposes, forming an acid species. Upon baking, the acid diffuses and catalyzes a deprotection reaction rendering the insoluble resist soluble in a developer. The soluble regions are then removed with the aqueous base developer. Control over this process is dominated by the events in the transitional region between exposed and unexposed areas of the photoresist.

The initial development of chemically amplified photoresists was a key technological breakthrough furthering the continued use of optical photolithography for the fabrication of sub micrometer features. The importance of chemically amplified photoresist concepts is illustrated by the industry-wide use of these materials in the fabrication of state-of-the-art devices today and into the foreseeable future. With the imminent need for sub-100 nm feature

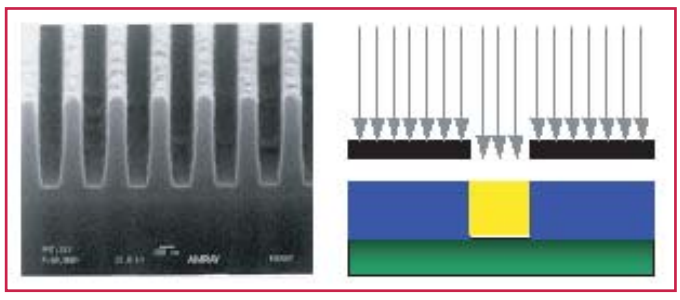

Fig. 1. At left, SEM image of a lithographically fabricated structure with a nominal critical dimension of 150 nm and 300 nm pitch. At right, schematic illustration of patterning through a mask to create the structure.

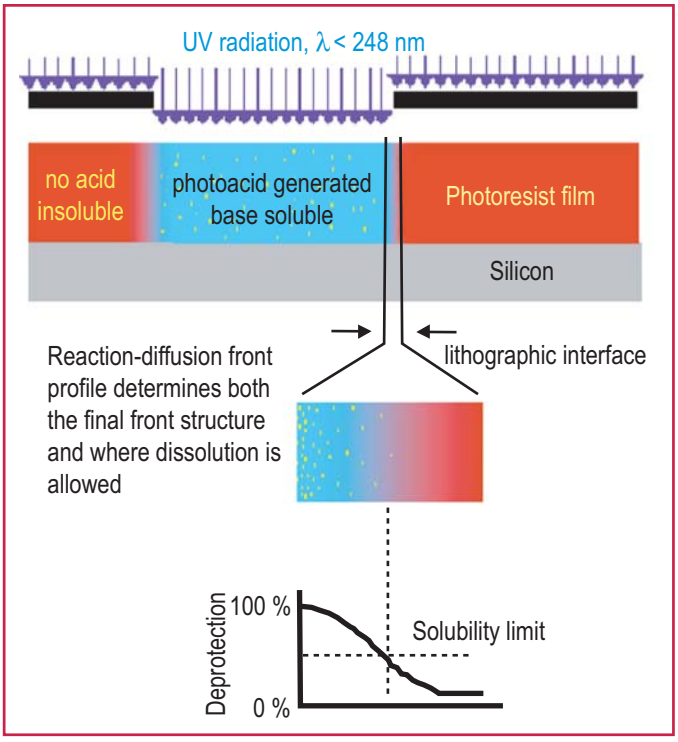

Fig. 2. Schematic diagram of the reaction-diffusion process in chemically amplified photoresists. The transitional region between exposed and unexposed regions is particularly important for critical dimension and roughness control.

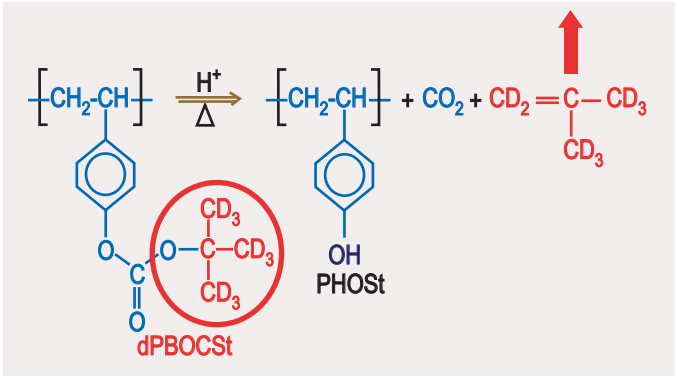

Fig. 3. General deprotection reaction in a chemically amplified photoresist. Deuterated molecular parts with strong contrast to neutrons are shown in red.

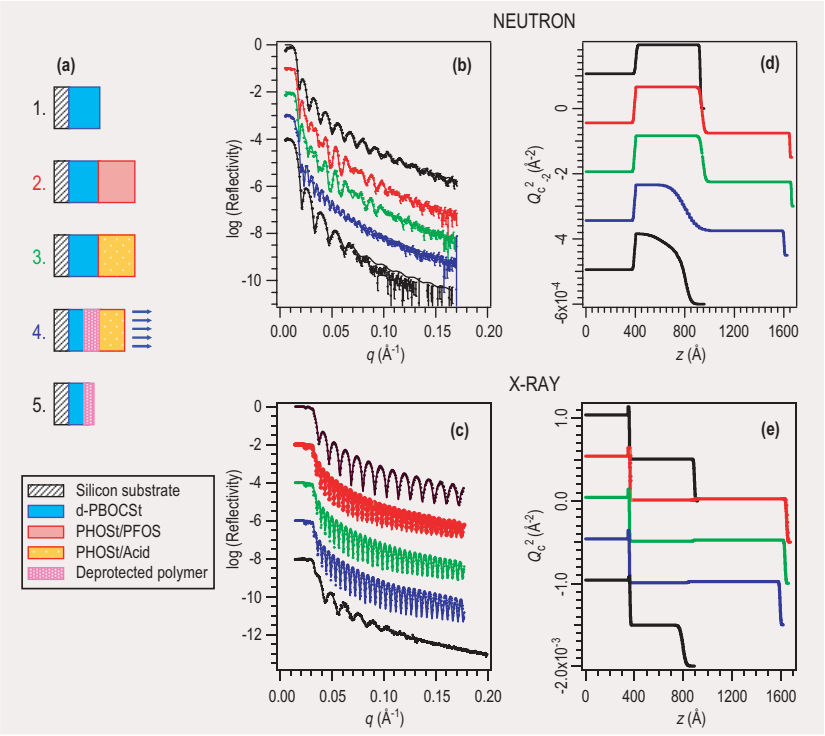

Fig. 4. (a) schematic diagram of the processing steps including the application of each film layer, exposure to UV radiation, a post-exposure bake (PEB) and development. (b) and (d) show the NR data and compositional depth profile and (c) and (e) show the XR data and density depth profiles from each step.

sizes, nanometer level control over the spatial evolution of the deprotection reaction front and the subsequent development steps is needed. The current level of understanding of the acid-catalyzed reaction-diffusion process is not sufficiently detailed to achieve this goal.

To meet the need for spatially detailed data, we have developed, in collaboration with the IBM T. J. Watson Research Center and the University of Texas at Austin, an experimental methodology to directly measure the spatial evolution of the deprotection reaction front through each processing step. By using model photoresist polymers with a deuterated protection group, neutron and x-ray reflectivity (NR, XR) measurements are able to follow the compositional and density profiles of the reaction-diffusion process in an idealized transitional region in a bilayer film stack. Neutron contrast with the reaction is possible because the reaction products involving the deuterated protection group are volatile, as illustrated in Fig. 3.

The NR and XR results from a series of bilayer samples are shown in Fig. 4. NR and XR measurements were taken after each processing step from the spin-coating of each film layer through exposure and bake to the dissolution of the upper layer and any deprotected polymer. The data show that the deprotection reaction front broadens with time within the photoresist. The initial interfacial width was approximately 4 nm wide whereas the reaction front was nearly 20 nm wide. Upon development, the data show that the developed film remained sharply defined with a surface roughness of approximately 4 nm as well. Although the reaction front was much wider than the final interfacial width, the selectivity of the dissolution process allows for the fabrication of well-defined nanostructures with diffusive transport mechanisms.

The spatial detail afforded by the developed methodology can play an important role in not only the qualitative description of the reaction-diffusion process, but also with the quantitative determination of physical parameters and changes in any physical or chemical properties over the nanometer length scales required for control over the fabrication of sub-100 nm structures. In addition, the strategy developed here is general and can be adapted for the study of candidate photoresist materials being developed for future applications.

"[This work [1]] opens a window of opportunity to construct structure-property relationships between chemical transport mechanisms and ultimate resist resolution. It may also lead to insights into the ultimate, intrinsic resolution limits and critical dimension control of polymer-based imaging materials." [2]

References:

[1] E. K. Lin, C. L. Soles, D. L. Goldfarb, B. C. Trinque, S. D. Burns, R. L. Jones, J. L. Lenhart, M. Angelopoulos, C. G. Willson, S. K. Satija, and W. L. Wu, Science, **297**, 372 (2002).

[2] E. Reichmanis and O. Nalamasu, Science, **297**, 349 (2002).

E. K. Lin, C. L. Soles, R. L. Jones, J. L. Lenhart, and Wen-li Wu
Polymers Division
National Institute of Standards and Technology
Gaithersburg, MD 20899-8541

S. K. Satija
NIST Center for Neutron Research
National Institute of Standards and Technology
Gaithersburg, MD 20899-8562

D. L. Goldfarb and M. Angelopoulos
IBM
T.J. Watson Research Center
Yorktown Heights, NY 10598

B. C. Trinque, S. D. Burns, and C. Grant Willson
University of Texas at Austin
Austin, TX 78712

Scaling of Membrane Phase Dynamics

Membrane phases are one example of the variety of complex fluid structures formed by surfactant molecules in solution. They are most commonly encountered in biological systems, but are also used extensively in a variety of commercial applications from personal care products to foods to paints. The diagram in Fig. 1 shows the regularly stacked lamellae of the L_α phase and the convoluted meandering channels of the "sponge" or L_3 phase. The topological distinctions between these two phases result in very different macroscopic properties. The anisotropic lamellar phases are birefringent and viscous, with complicated flow responses, while the isotropic sponge phases are clear and generally flow freely with constant viscosity. However, these very distinct phases are adjacent in the phase diagrams of many systems, and very dilute sponge phases exhibit a transient birefringence when shaken, which suggests a shear-induced transition to a lamellar state. Due to the experimental challenges of studying both the structure and rheology of such dilute phases, the exact nature of the transient birefringence has remained somewhat controversial.

Both sponge and lamellar structures have scaling properties: their characteristic lengths (see Fig. 1), the channel width, ξ, and the smectic periodicity, d, scale with the ratio of the membrane thickness, δ, to the membrane volume fraction, ϕ. The dynamics of these phases are dominated by thermodynamic fluctuations of the membranes, which also scale with these parameters. Cates and Milner predict the scaling relationship and shear response to be expected for an isotropic diblock copolymer phase [1]. They note that this phase is topologically similar to sponge phases, and therefore expect the relationship to extend to such systems as well. Their analysis indicates that flow should dampen fluctuations normal to both the flow velocity ($\boldsymbol{V}$) and the velocity gradient ($\boldsymbol{\nabla V}$), eliminating channels in those directions. This would result in a quasi-first order phase transition to a lamellar state with its membranes parallel to the ($\boldsymbol{V,\nabla V}$) plane, *i.e.*, perpendicular to Z, (conventionally the "a" orientation) occurring at a critical shear rate: $\dot{\gamma}_c \sim k_B T/\eta_s \xi^3 \sim k_B T(\phi/\delta)^3/\eta_s$, where k_B is the Boltzmann constant, T is the temperature, and η_s is the solvent viscosity.

From the equation, it is clear that transient birefringence, occurring at low shear rates, requires very dilute samples, *i.e.*, having small ϕ. Furthermore, the ϕ^3/η_s dependence suggests that increasing solvent viscosity to slow membrane fluctuations would relax this requirement. Taking our lead from previous microemulsion work [2], we found that dextrose could be dissolved at volume fractions up to 40 % in the heavy brine solvent (0.2 mol of NaCl in D_2O to make a 1 L solution) of cetylpyridinium chloride/hexanol membrane systems without altering their phase diagrams. The maximum dextrose addition changes η_s from 1.1 mPa·s to 13.6 mPa·s. Then for a series of sponge samples having membrane volume fractions from

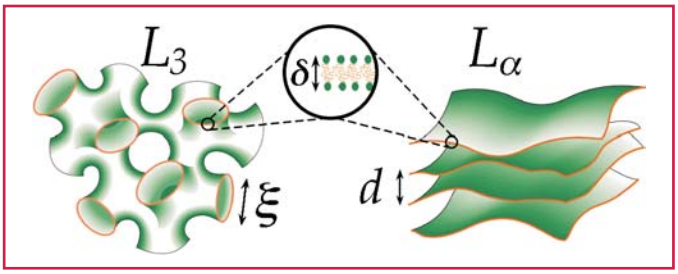

Fig. 1. Representations of two types of membrane morphologies: the sponge (L_3) and lamellar (L_α) phases with their corresponding characteristic lengths.

3 % to 10 %, the factor ϕ^3/η_s can be varied by more than two orders of magnitude. Plots of the reduced viscosity and shear stress (Fig. 2b) versus the rescaled shear rate parameter, $\dot{\gamma}\eta_s/\phi^3$, display master curve behavior, clearly showing that these macroscopic responses measuring the dynamics of this system scale as predicted. The corresponding scaled micro-structural response parameters, explored by Couette SANS (Fig. 2c, d) likewise exhibit excellent scaling behavior. Moreover, the strong correlation between these macroscopic and microscopic responses leads to a detailed picture of the mechanisms involved.

The response exhibits three distinct regions [3]. (See Figs. 2 and 3.) At low shear rates (Region I), the sponges show their familiar constant viscosity Newtonian behavior and isotropic scattering. No structural changes occur since the applied shear rate is much less than the dynamic response rate of the channels. In region II, when the shear rate approaches this rate, the density of connections in the gradient direction ($\boldsymbol{\nabla V}$) decreases, leading to a gradual

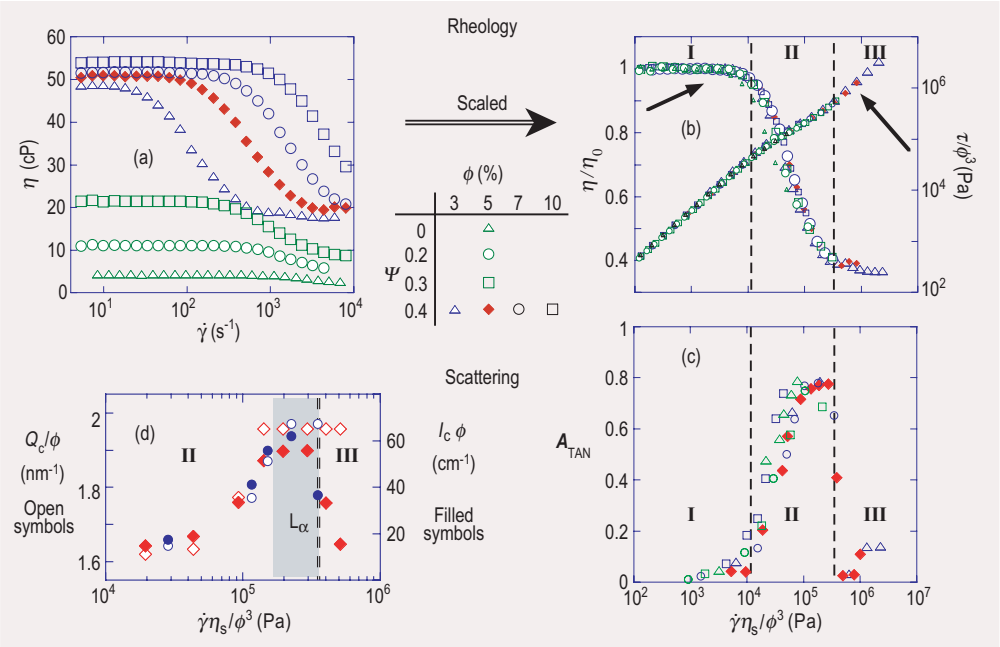

Fig. 2. (a) Rheological data for a range of membrane volume fractions (ϕ) and dextrose concentrations (ψ). (b) The same plotted to show master curve behavior, indicative of scaling. (c) The corresponding master curve variation of the scattering anisotropy, A_{TAN} / $(I_Z - I_{\nabla V})/(I_Z + I_{\nabla V})$, and (d) the rescaled correlation peak position and intensity. Regions I, II and III are discussed in the text.

over only a narrow range of shear rates in region II before collapsing at the onset of region III to a structure with correlations on length scales >> ξ, which is only observed for samples with sufficiently high solvent viscosities and low membrane concentrations. While more work remains to determine the nature of this final structure, we note that it has been predicted that suppression of fluctuations by shear should eventually destabilize a bulk lamellar system [4].

While the magnitude of the critical shear rates are consistent with theory and we have now confirmed the scaling behavior of the shear response, the nature of the transition and the orientation of the shear-induced smectic state are not as predicted. The theory does not, in fact, extend straightforwardly to the topologically similar sponge phases as expected, and a more sophisticated model is needed to fully explain the details of shear response in this class of systems.

development of smectic order in that direction, and thus causing the observed decrease in viscosity. At shear rates high enough to totally eliminate the channels along ∇V the intensity $I_{\nabla V}$ saturates, indicating the appearance of a lamellar phase with the membranes fully-aligned *parallel* to Z. In view of the theory, this is an unexpected result: the order develops in the so-called "c" orientation, indicating that it is fluctuations in the gradient direction (∇V) that are being suppressed rather than in the vorticity (Z) direction of the predicted "a" orientation. Also the complete lack of a rheological stress plateau (Fig. 2a) and the gradual change of the peak position (Fig. 2d) both preclude the possibility of the transition being first order. The aligned lamellar phase remains stable

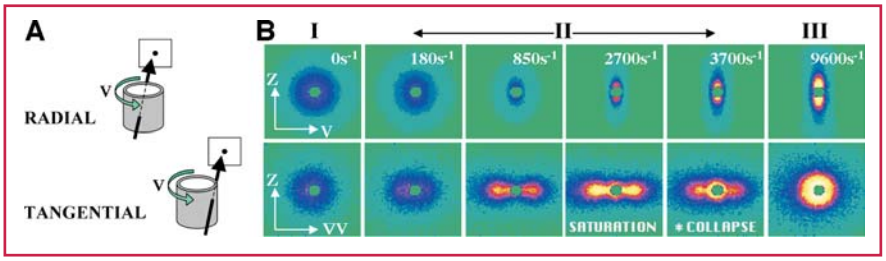

Fig. 3. (a) Schematic of the beam incidence on the Couette SANS cell in radial and tangential geometries. (b) Scattering patterns in radial and tangential geometries for a ϕ = 0.05, ψ = 0.4 sponge sample at a range of shear rates over the three rheological regions.

References:

[1] M. E. Cates and S. T. Milner, Phys. Rev. Lett. **62**, 1856 (1989).

[2] Chen V., PhD Thesis, University of Minnesota (1988).

[3] L. Porcar *et al.,* Phys. Rev. Lett., in press.

[4] S. Ramaswamy, Phys. Rev. Lett. **69**, 112 (1992), and R. Bruinsma and Y. Rabin, Phys. Rev. A **45**, 994 (1992).

L. Porcar
Oak Ridge National Laboratory
Oak Ridge, TN 37831-6393
Present address:
University of Maryland, College Park, MD 20742

W. A. Hamilton and P. D. Butler
Oak Ridge National Laboratory
Oak Ridge, TN 37831-6393

G. G. Warr
The University of Sydney
Sydney, NSW 2006, Australia

Observation of Liquid-Glass-Liquid and Glass-Glass Transitions in the L64/D_2O Copolymer Micellar System

The glassy state of matter is ubiquitous, ranging from ordinary window glass to polymers to proteins. Yet, the nature of the transition between liquid (L) and glassy (G) states remains one of the unsolved problems in the physics of condensed matter. Mode-coupling theory (MCT), originally developed for supercooled simple liquids, makes predictions of liquid-glass (L-G) and glass-glass (G-G) transitions in a colloidal suspension. Here we present small-angle neutron scattering (SANS) and photon correlation spectroscopy (PCS) measurements confirming these predictions.

In a recent series of papers [1, 2] MCT predicts that in colloidal systems with a sufficiently short-range effective inter-particle attractive interaction one can observe two types of kinetic glass transitions (KGT). The KGT can be the result of a "cage effect," originating from the excluded volume effect of the particles at high volume fractions and at high temperatures, or the result of a particle bonding to its nearest neighbors at low k_BT and at all volume fractions.

One particularly interesting feature in this novel state of matter is the occurrence of two distinct amorphous glassy states called respectively the "repulsive glass" (G_R) and the "attractive glass" (G_A), as the result of the two distinct mechanisms for the structural arrest mentioned earlier. With PCS and SANS measurements, we succeeded in detecting both these transitions in L64/D_2O micellar system at high volume fractions [3].

L64 is a symmetric tri-block copolymer of composition $(PEO)_{13}(PPO)_{30}(PEO)_{13}$. Above 20 °C, the copolymers self-assemble into spherical micelles each with PPO segments packed into a compact core and PEO segments forming a corona around it. The short-range attraction arises from the overlap of PEO chains in the corona regions when two micelles approach one another. The depth of the attractive well increases with temperature

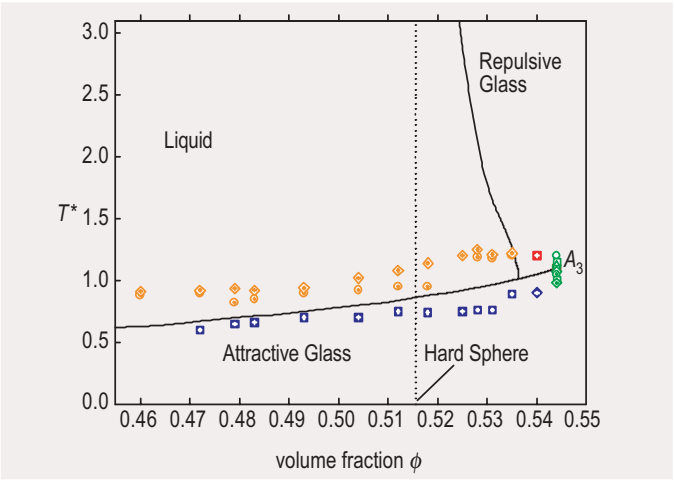

Fig. 1. The lines represent phase boundaries (in T^*- φ plane) determined by mode-coupling theory for a colloidal system with a short-range attraction ($\varepsilon = 0.03$). The phase points shown are for the L64/D_2O micellar solution. (Liquid state: orange, glassy states: blue, red, and green.) The results confirm the existence of the attractive branch in the predicted glass-transition boundary, and the G_A-G_R transition.

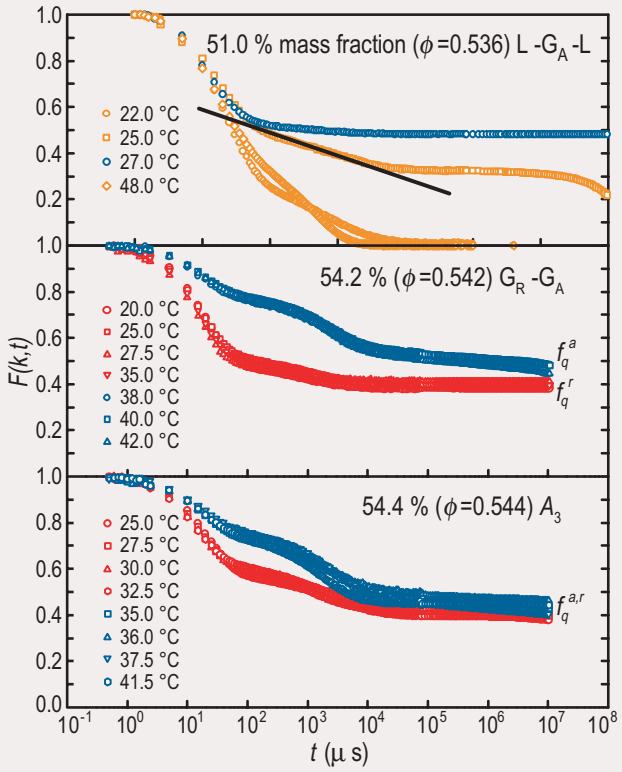

Fig. 2. The ISF as measured by photon correlation spectroscopy at three different volume fractions, φ, at different temperatures. (Data follow the same color scheme as in Fig. 1.) The top panel shows the re-entrant L-G_A-L transition. The line highlights a region of logarithmic time dependence preceding the plateau in the liquid state just before the transition [4]. Evidence of the G_A-G_R transition can be seen in the middle panel. By comparing the long-time limit of the ISF's with the predictions of mode-coupling theory (MCT), the two different types of the glasses can be identified by their respective Debye-Waller factors. The bottom panel is for a volume fraction of 0.544, which is the A_3 end point predicted by MCT. f_q^a and f_q^r become identical, confirming the prediction.

because water becomes an increasingly poor solvent as temperature rises.

If the interaction is modeled by a square-well potential, the crucial control parameters of the phase behavior are: the volume fraction, $\varphi = \pi\rho d^3/6$, the effective temperature, $T^* = k_B T/u$, and the fractional well-width parameter, $\varepsilon = \Delta/d$. ρ is the number density of the spheres, d its hard core diameter, Δ its attractive well-width, and $-u$ its well-depth.

The calculated glass-transition lines, for the case of $\varepsilon = 0.03$ [2], are shown in Fig.1 in the (T^*, φ) plane. On going from higher to lower T^*, at volume fractions less than 0.5365 L-G_A transitions occur, and at volume fractions greater than this value, one has a possibility of observing G_R-G_A transitions.

Figure 2 shows normalized photon correlation functions (coherent intermediate scattering functions, ISF) measured at $q \approx 0.001$ Å^{-1} and at three different volume fractions, as a function of temperature [3]. For the φ where the L-G_A transition is possible, one can see that in the L state, the long-time limit of the ISF, f_q, is zero, while in the G_A state, $f_q^a \approx 0.4$ to 0.5, which is the value of the Debye-Waller factor of the glassy state. The KGT is thus characterized by a discontinuous change of f_q. At $\varphi = 0.542$, we observe the G_R ($f_q^r \approx 0.4$) to G_A transition ($f_q^a \approx .7$). At $\varphi = 0.544$, which is called the A_3 singularity end point, our measured ISF's show identical values of $f_q^{r,a} \approx 0.4$ in the two glassy states, confirming the theory.

Figure 3 shows scaling plots of SANS intensity distributions at four volume fractions, and at different temperatures, spanning the regions of the phase diagram where the L, L-G-L, G-G, and two identical glasses (A_3 point) are located. The scale is set by a unique length parameter, the average inter-particle distance.

Verification of mode-coupling theory predictions through photon-correlation spectroscopy and small-angle neutron scattering measurements on a micellar system provides a basis for improved understanding of the glass transition in general.

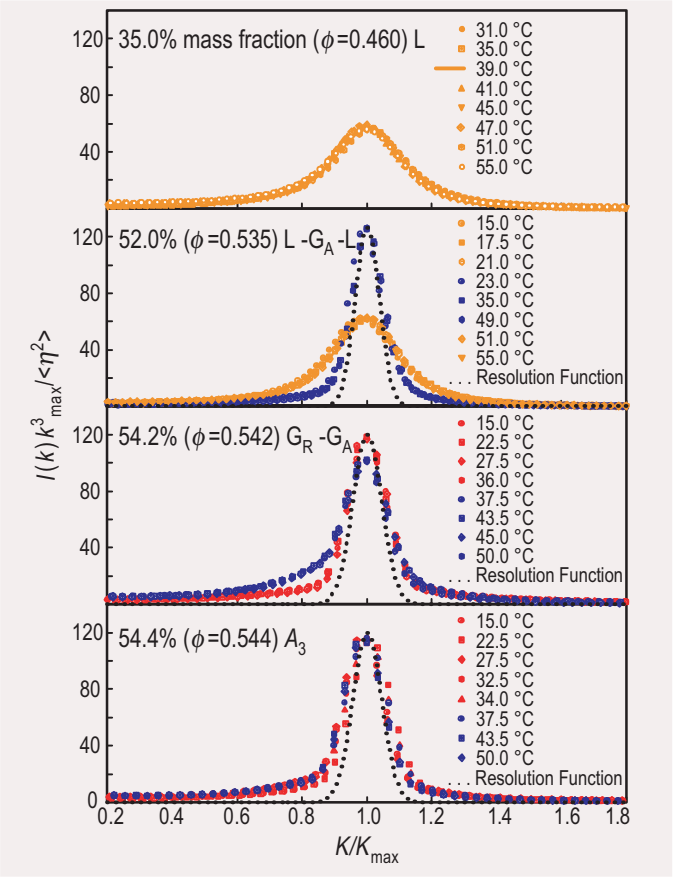

Fig. 3. SANS scaled intensity distributions vs. reduced scattering vector for the micellar solutions at four values of φ, at different temperatures. (Data follow the same color scheme as in Fig. 1.) The top panel is for $\varphi = 0.460$. All the scaled intensities are characterized by a unique length scale and collapse into a single master curve for all temperatures. The second panel is for $\varphi = 0.535$: the system is clearly characterized by two length scales. While the narrower peak is resolution limited, the broader peak is similar to the one observed in the first panel. If we identify the broader peak to represent the liquid state, then the narrower peak should represent the glassy state. The system thus shows a re-entrant L-G-L transition. The third panel is for $\varphi = 0.542$. Again, two length scales characterize the system. The narrower peak is resolution-limited and the slightly broader peak is also nearly so. The results can be interpreted as showing a transition between two amorphous solid states, i.e., a G-G transition. The last panel is for $\varphi = 0.544$, which is predicted as the A_3 point, at temperatures ranging from 15 °C to 50 °C. The two different types of glasses indeed become identical at this volume fraction.

References:

[1] L. Fabbian, W. Götze, F. Sciortino, P. Tartaglia, and F. Thiery, Phys. Rev. E **59**, R1347 (1999).

[2] K. Dawson, G. Foffi, M. Fuchs, W. Götze, F. Sciortino, M. Sperl, P. Tartaglia, Th. Voigtmann, and E. Zaccarelli, Phys. Rev. E **63**, 011401 (2001).

[3] W. R. Chen, S. H. Chen, and F. Mallamace, Phys. Rev. E **66**, 021403 (2002).

[4] F. Mallamace, P. Gambadauro, N. Micali, P. Tartaglia, C. Liao, and S. H. Chen, Phys. Rev. Lett. **84**, 5431 (2000).

S.-H. Chen and W.-R. Chen
Massachusetts of Institute of Technology
Cambridge, MA 02139

F. Mallamace
Massachusetts of Institute of Technology
Cambridge, MA 02139

and

University of Messina
Messina, Italy

Early-Stage Compositional Segregation in Polymer Blend Films

Wetting plays an important role in diverse applications ranging from insecticide sprays to detergency. This interest, in part, has motivated a great deal of fundamental research involving the spreading (wetting) of a liquid on a solid surface. Polymer blends are of great commercial importance and therefore their thermodynamic and phase separation behaviors have been widely studied.

The structure and properties of thin blend films are governed by the interplay between phase separation and surface segregation driven by polymer-surface interactions. The nature of the segregation depends on whether the mixture forms a stable one-phase fluid or phase-separates [1, 2]. In the former case, the surface-enrichment-layer (SEL) grows and stabilizes to an equilibrium value. In the latter case the initially formed SEL breaks into droplets for partial wetting and grows unsteadily for complete wetting [1]. The late stage evolution of the surface enrichment layers thus exhibits "non-universal" growth laws, depending on the phase stability, wetting characteristics of the blend, confinement, as well as on the details of the polymer-surface interaction potential [2]. The universality of surface segregation at the early-stage, however, has not been explored, partly because the compositional changes are normally rapid [3, 4]. We therefore designed a measurement that can access the short time and small length-scale surface-enrichment regime.

A critical blend film near the glass transition of the polymers is utilized so that the chain dynamics are greatly slowed down even under thermodynamically strong segregation conditions. The polymers are deuterated poly(methyl methacrylate) (dPMMA) and poly(styrene-*ran*-acrylonitrile) (SAN). This polymer blend has a lower critical solution temperature (LCST) below T_g as revealed by small-angle neutron scattering measurements. A 445 Å film of dPMMA/SAN (50/50 by mass) was obtained by spin-casting from a common solution. After drying at a temperature slightly below T_g, the films were annealed in a vacuum oven at (130 ± 0.1) ˚C for various times ranging from 1 min to 36 h. After drying and after each step of annealing, the film was measured using neutron reflectivity (NR). An atomic force microscopy study indicated that the film roughness was below 6 Å throughout the measurement.

Figure 1 shows NR spectra after several annealing intervals. The spectra were analyzed using a model-fitting scheme. The best fits are shown as the solid curves, and their corresponding compositional profiles are shown in Fig. 2. The inset of Fig. 2 shows the evolution of the dPMMA volume fraction in the depletion zone (ϕ_d) and at the surface (ϕ_s). The former decreases monotonically, suggesting that equilibrium has not been achieved, while the non-monotonic variation of the latter is due to the surface relaxation at the initial time.

The surface excess, $z^* = \int[\phi(x) - \phi_d]dx$, is shown in Fig. 3, and can be fit to a power law $t^{0.41\pm0.01}$ for early times (solid line), and a stretched exponential form for the entire time (dashed curve). The latter gives $z^*(\infty) = 72$ Å at the saturation. z^* starts to deviate from the power-law behavior at about 9 h (indicated by the arrow in Fig. 3) corresponding to $z^* = 40$ Å and $\xi_s = 57$ Å, where ξ_s is the surface correlation length characterizing the decay of the surface enrichment composition. These crossover scales in the kinetics are comparable to the bulk correlation length length $\xi_b \approx 60$ Å, suggesting a transient saturation. After that, the SEL will grow unsteadily, entering the later stage of the wetting layer growth [4].

The inset of Fig. 3 shows that ξ_s nearly follows a power law of $t^{0.25\pm0.01}$, except for initial times. Note that

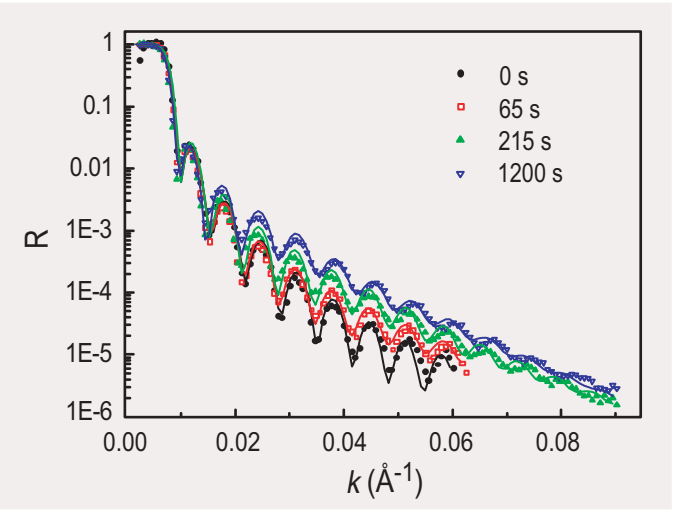

Fig. 1. Selected neutron reflectivity spectra after various times at 130 ˚C.

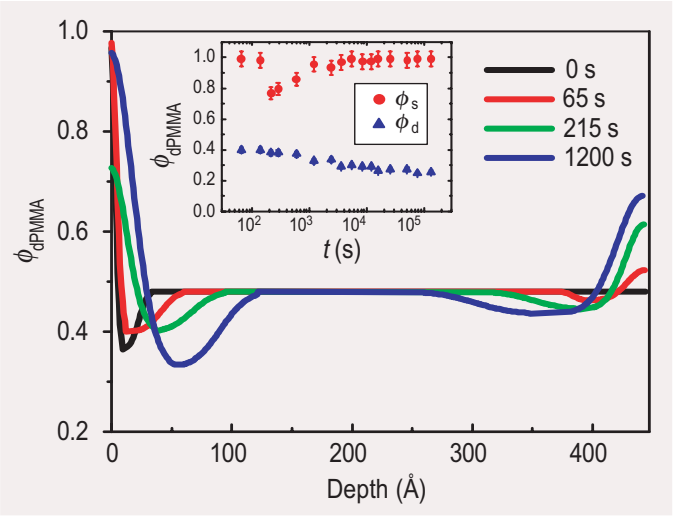

Fig. 2. ϕ_{dPMMA} profiles that give the best fit. The inset shows the evolution of surface composition, ϕ_s (circles) and depletion layer composition, ϕ_d (triangles).

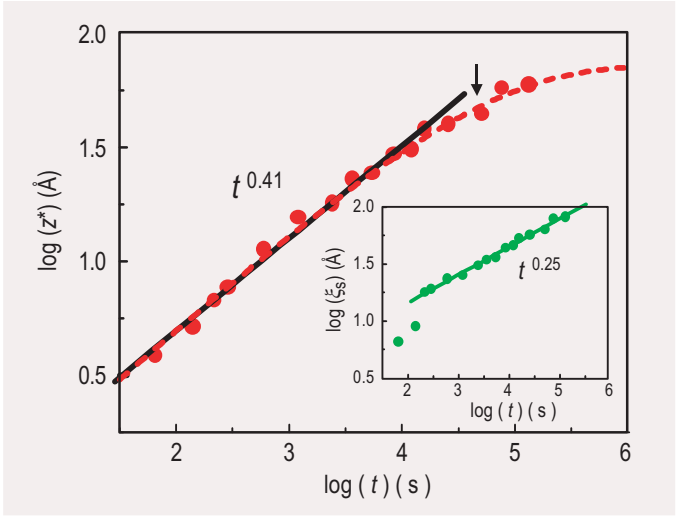

Fig. 3. z^* with a power-law fit (solid line), $t^{0.41}$, and a stretched exponential function (dashed curve). The arrow denotes a $z^* \approx 40$ Å and the transition to slower growth. The inset shows the surface correlation length.

right after drying, $z^*(0) = 4$ Å, indicating a segmental scale of saturation from processing the film (spin-casting and drying). Thus, the initial "anomaly" of ϕ_s and ξ_s may reflect the relaxation of the highly non-equilibrium compositional profiles. While most of the previous work focused on the kinetics after the formation of the initial layer on the order of the correlation length, the transient early-stage of the SEL has received little attention. The interpretation of the apparent power law growth will thus require further investigation.

In summary, during the early stage of surface segregation, enrichment at a monomer length-scale occurs first, followed by a segregation layer that grows to the order of the bulk correlation length, ξ_b, which coincides with the radius of gyration of polymers deep in the two-phase regime. Thus, the two observed distinct surface saturation states correspond to the characteristic scales of macromolecules. However, at near criticality, previous studies suggest a large discrepancy between ξ_s and ξ_b, pointing to the need to consider three length scales: that of the monomer, the molecular size, and the size of compositional fluctuations. The extent of universality in the early stage growth kinetics therefore needs further investigation. The present study is the first to quantitatively examine this important phenomenon.

References:

[1] S. Dietrich, in *Phase Transitions and Critical Phenomena*, ed. by C. Domb and J. L. Lebowitz, Academic Press, London (1988) Vol. 12.

[2] K. Binder, J. Non-Equilib. Thermodyn. **23**, 1 (1998), and references therein.

[3] S. Puri and K. Binder, J. Stat. Phys., **77**, 145 (1994); S. Puri and K. Binder, Phys. Rev. E, **49**, 5359 (1994).

[4] H. Wang, and R. J. Composto, Phys. Rev. E, **61**, 1659 (2000).

H. Wang, J. F. Douglas and C. C. Han
Polymers Division
National Institute of Standards and Technology
Gaithersburg, Maryland 20899-8542

S. K. Satija
NIST Center for Neutron Research
National Institute of Standards and Technology
Gaithersburg, Maryland 20899-8562

Magnetic Cluster Sizes in Magnetic Recording Disks

The equivalent of Moore's law for magnetic recording is that the areal density of magnetically written bits increases at 60 % to 100 % per year, and, of equal interest to the consumer, the cost per megabyte decreases at 40 % to 50 % per year. To achieve this, the noise in the magnetic media must be continuously reduced, which is accomplished by decreasing the size of the magnetic clusters — regions of the media that are magnetically coupled. The cluster size must decrease, since the media noise primarily results from the finite cluster size; the bit transitions are narrower when the clusters are smaller. Presently, cluster sizes are believed to be about 10 nm to 15 nm, but accurate knowledge of the size distribution and even the average size is lacking. A common assumption is that the cluster size is identical to the crystalline grain size of the media [1], but this has not been demonstrated.

We have conducted Small Angle Neutron Scattering (SANS) measurements of the magnetic cluster size in actual recording disks and quantified the size distribution. The measurements were performed at NG-7 30 m SANS instrument with unpolarized neutrons with wavelength of 7 Å and a relative wavelength spread of 11 %. Since SANS is caused by both physical and magnetic inhomogeneities, it is necessary to separate these contributions and to isolate the magnetic cluster SANS. This was done with two separate measurements. Data were first taken for disks in an initial, high noise state where there are a maximum number of interfaces between magnetic clusters. This is accomplished by first fully magnetizing the disks in a circumferential direction. Then, the disks were scanned with a recording head field in the opposite direction and with a strength approximately equal to the remnant coercivity of the media. This causes approximately half of the magnetic clusters to reverse direction, leaving a maximally noisy state. In this state, the SANS contains contributions from the physical film structure (grains) and the magnetic film structure (magnetic clusters). Data were then obtained with a magnetic field of 0.6 T applied parallel to the disk surface. This field orients the magnetic moments in the clusters predominantly along the field and, by examining the Q-dependence of the SANS, we can determine the SANS from the physical film structure. Subtracting the zero field and 0.6 T spectra leaves the desired magnetic SANS [2, 3].

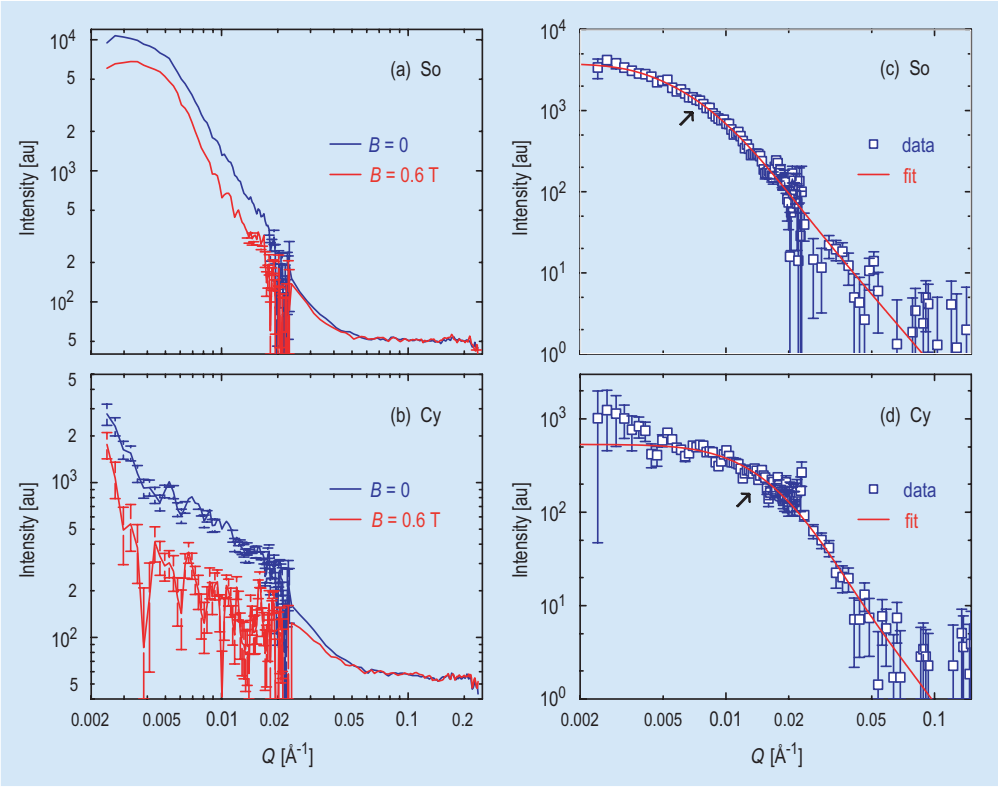

Fig. 1. SANS intensity for magnetic disks So and Cy, averaged around the incident beam direction which was perpendicular to surface of the disks. In (a) and (b) the blue lines show data for no applied field (high noise state), while red lines show data for a 0.6 T field. Two sample-to-detector distances were used, with Q ranges of 0.0025 Å^{-1} to 0.025 Å^{-1} and 0.025 Å^{-1} to 0.3 Å^{-1}. In (c) and (d) the blue squares are the magnetic SANS, the difference of the zero and 0.6 T scattering intensities in (a) and (b). The red line shows the best fit to a model described in the text. The arrows mark the approximate Q where the slope of the data changes.

The disks, denoted So, To and Cy, are those used in three product generations. The magnetic media in each two-sided disk was a Co-Pt-Cr alloy (25 nm to 40 nm thick) sandwiched between a carbon layer and one or more nonmagnetic underlayers. The disks were sliced into eight pieces and stacked to create 16 magnetic layers for the SANS measurements. The relative signal-to-noise ratio (S_0/N_m) varied from 0 db (So) to 3 db (To) to 6.5 db (Cy).

SANS data for both magnetic fields are shown in Fig. 1a and 1b. Subtracting these two spectra leaves the desired magnetic SANS, which are shown in Fig. 1c and 1d. It is apparent that for increasing S_0/N_m (So to Cy) there is an increase in the Q where the slope changes, which establishes that the disks with higher S_0/N_m have smaller average cluster size. In addition, there is a distribution of cluster sizes, since there are no oscillations in the data and the change in slope is gradual.

To determine the cluster size distribution, we have modeled the cluster shapes as cylinders, since TEM shows the physical grains adopt a columnar morphology. The magnetic SANS data are well fitted using a log-normal distribution of cluster sizes. These distributions are shown in Fig. 2, while the fits to the data are shown in Fig. 1. Such magnetic cluster size distributions have not been reported before for recording media, and allow us to draw several important conclusions.

First, these results show that the media S_0/N_m is inversely correlated with the magnetic cluster size. This is apparent from Fig. 2 when one recalls that S_0/N_m increases from So-To-Cy. This provides firm experimental verification of the models that have proposed smaller clusters give larger S_0/N_m [1]. A second conclusion follows from a comparison of the magnetic cluster size to the physical grain size, shown in the inset to Fig. 2. The average cluster size is slightly larger than the average grain size, and, for the most advanced media (Cy), this difference is < 10 %. This shows that the intergranular magnetic interactions are not very strong, especially for the advanced media; hence, the size of the media noise sources scales with crystalline grain size. This result validates previous (implicit or explicit) assumptions [1, 4].

The cluster size distribution is quite broad with a log-normal *r* of about 0.5. Recent models of the magnetic recording properties of media have begun to include microstructural disorder [1], and have shown that the magnetic cluster size distribution has significant effects on these properties. Thus, the exact cluster size distribution is important for these models. Our results provide empirical

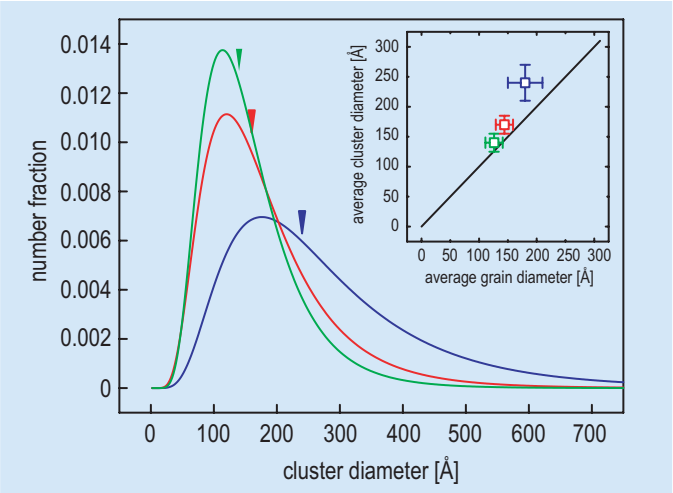

Fig. 2. Green, red and blue curves show the best-fit distributions for disks Cy, To and So, respectively. The triangles mark the average cluster size. The log-normal *r* are 0.56, 0.52 and 0.46 for Cy, To and So, respectively. The inset shows the average magnetic cluster diameter versus the average physical grain diameter, obtained from x-ray diffraction and TEM.

data on this distribution, which, when incorporated into the models, will improve their reliability.

Our results have implications for magnetic recording technologies. While the lack of coupling is desirable from an S_0/N_m perspective, the broad distribution is not, since large clusters will contribute to noise and the small clusters will be thermally unstable. Reducing this distribution will be a major challenge for media designers. Finally, the methodology we have developed will be applicable to future media where the average cluster sizes are < 10 nm.

References:

[1] Y. Zhang and H. N. Bertram, IEEE Trans. Magn. **35**, 4326 (1999).

[2] J. Suzuki, K. Takei, Y. Maeda, Y. Morii, J. Magn. Magn. Mater. **184**, 116, (1998).

[3] J. F. Löffler, H.-B. Braun, W. Wagner, Phys. Rev. Lett., 85, 1990 (2000).

[4] M. F. Doerner, K. Tang, T. Arnoldussen, H. Zeng, M. F. Toney, D. Weller, IEEE Trans. Magn. **36**, 43 (2000).

M. F. Toney and K. Rubin
IBM Almaden Research Center
San Jose, CA 95120

S.-M. Choi
NIST Center for Neutron Research
Present affiliation:
Korea Advanced Institute of Science and Technology
Yuseong-gu, Daejon,
Republic of Korea 305-701

C. J. Glinka
NIST Center for Neutron Research
National Institute of Standards and Technology
Gaithersburg, MD 20899-8562

Dynamical Effects of Polar Nanoregions in Relaxor Ferroelectrics

Relaxor ferroelectrics exhibit exceptional piezoelectric properties. Single crystals of some of these materials can achieve ultrahigh strains under applied electric fields that are fully one order of magnitude larger than those attainable in conventional lead-zirconate-titanate (PZT) ceramics, which are widely used in solid-state actuators that convert electrical energy into mechanical energy. The additional properties of large electromechanical coupling and low dielectric loss suggest that industrial use of relaxors may revolutionize the areas of medical imaging, naval sonar, and other acoustic applications. Relaxors are further characterized by a markedly frequency-dependent dielectric susceptibility that is very broad in temperature. The recent neutron scattering studies briefly described here provide new insight on the behavior of these systems.

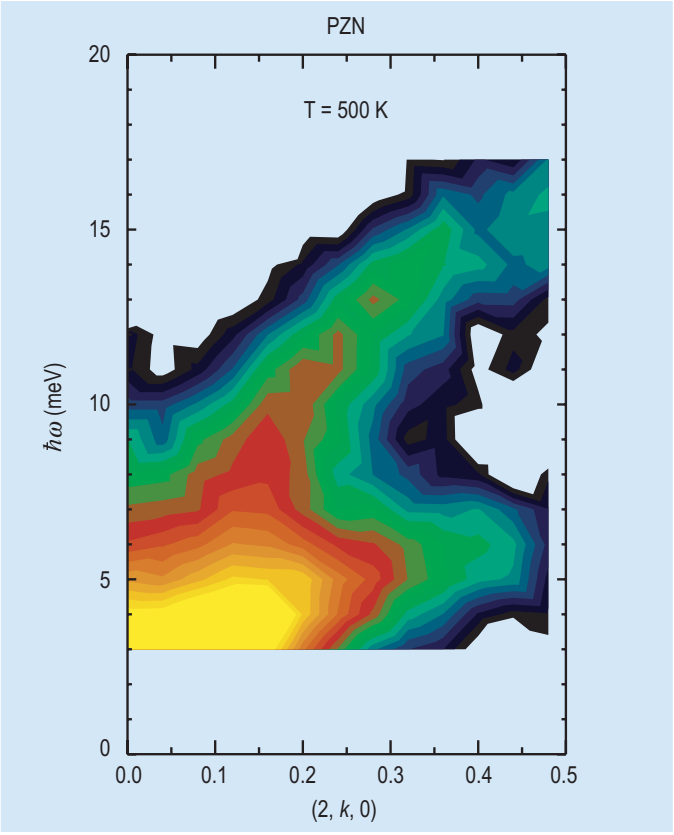

Fig. 1. Contour plot of the neutron inelastic scattering intensity measured in PZN in its cubic phase in the (200) Brillouin zone. The color scale varies logarithmically with intensity, and is limited in range to make the weaker features more visible.

A key feature that appears to be common to all of the relaxor compounds, and which is believed to play a fundamental role in producing the enhanced piezoelectricity, is the formation at high temperature of tiny regions of local and randomly-oriented electric polarization just several unit cells in size, also known as polar nanoregions (PNR). The existence of these PNR was inferred from the observation that the optical index of refraction in a variety of disordered ferroelectric systems deviates from a linear temperature dependence at a temperature T_d far above T_c [2].

$Pb(Zn_{1/3}Nb_{2/3})O_3$ (PZN) and $Pb(Mg_{1/3}Nb_{2/3})O_3$ (PMN) are two of the most studied compounds as their piezoelectric responses rank among the highest [1]. These compounds crystallize in the complex perovskite structure $Pb(B'B'')O_3$, where the B' and B'' atoms are generally heterovalent. Thus the relaxor compounds possess not only chemical disorder, but usually a mixed-valence character as well.

Our studies of PZN and PMN have focused on understanding the mechanism underlying the formation of the PNR, as well as their effect on the lattice dynamics. The latter are clearly manifest in neutron scattering measurements. The long-wavelength transverse optic (TO) phonons are heavily damped in energy below T_d in PZN, which gives rise to the anomalous "waterfall" feature shown in Fig. 1 [3]. This damping is strongly wavevector dependent, and becomes significant when the wavelength of the lattice vibration becomes comparable to the average size of the PNR, which is estimated to be of the order of 30 Å to 40 Å.

Subsequent experiments were performed above T_d = 620 K in PMN to look for a soft mode, given the obvious similarities to the classic soft-mode ferroelectric $PbTiO_3$. Surprisingly, the phonon damping persists well above T_d, as shown in Fig. 2 [4]. This implies that the PNR exist as dynamic entities above T_d, but are still effective at inhibiting the propagation of long wavelength phonon modes. Even more interesting is how the zone-center TO mode softens and broadens in energy as the temperature approaches T_d from above, and that only the zone-center TO mode becomes overdamped (no peak at non-zero energy) at T_d. Modes at higher wavevector q become overdamped too, but only below T_d. This behav-

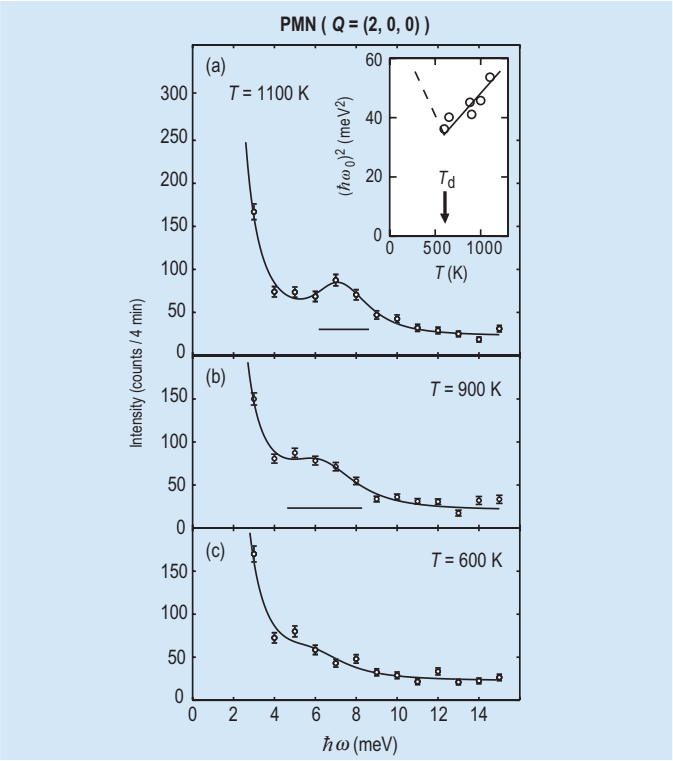

Fig. 2. Temperature dependence of the zone-center TO phonon in PMN measured at (200).

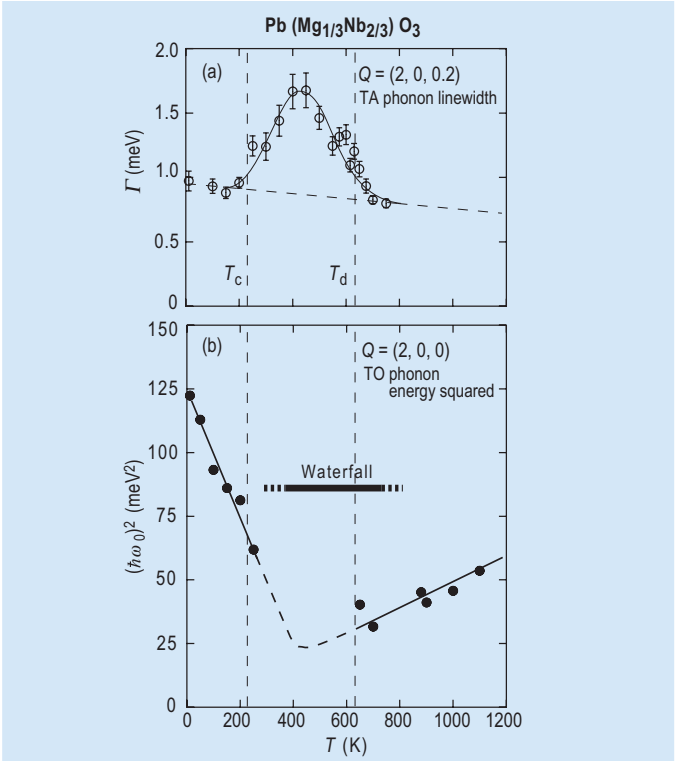

Fig. 3. Summary of the TA and soft mode dynamics in PMN between 10 K and 1100 K.

ior suggests that the zone-center TO mode condenses at T_d, thereby giving rise to the PNR. Consistent with this picture is the observation that the square of the zone-center TO mode energy varies linearly with temperature, as happens in normal soft-mode ferroelectrics. This is shown in Fig. 3, which summarizes the soft TO mode dynamics in PMN between 10 K and 1100 K [5].

An anomalous broadening of the acoustic modes, shown in the upper panel of Fig. 3, also occurs at T_d, as does the onset of diffuse scattering associated with the PNR. The diffuse scattering structure factors can be reconciled with those of the TO phonons in different Brillouin zones by postulating a uniform shift of the PNR along their polarization direction [6]. Furthermore, a model that couples the TA and TO modes is able to describe all of the observed phonon lineshapes extremely well [7]. This then suggests a novel idea in which PMN exhibits the condensation of a *coupled* soft TO mode at T_d. Such a coupled-mode would carry an acoustic component, and thus provide a natural explanation of the uniform shift of the PNR. If true, this would complete an elegant description for the dynamical formation of the PNR in PMN, and most likely other relaxors as well.

References:

[1] S.-E. Park and T. R. Shrout, J. Appl. Phys. **82**, 1804 (1997).

[2] G. Burns and F. H. Dacol, Solid State Comm. **48**, 853 (1983).

[3] P. M. Gehring, S.-E. Park, and G. Shirane, Phys. Rev. **B63**, 224109 (2000).

[4] P. M. Gehring, S. Wakimoto, Z.-G. Ye, and G. Shirane, Phys. Rev. Lett. **87**, 277601 (2001).

[5] S. Wakimoto, C. Stock, R. J. Birgeneau, Z.-G. Ye, W. Chen, W. J. L. Buyers, P. M. Gehring, and G. Shirane, Phys. Rev. **B65**, 172105 (2002).

[6] K. Hirota, Z.-G. Ye, S. Wakimoto, P. M. Gehring, and G. Shirane, Phys. Rev. **B65**, 104105 (2002).

[7] S. Wakimoto, C. Stock, Z.-G. Ye, W. Chen, P. M. Gehring, and G. Shirane, submitted to Phys. Rev. B.

P. M. Gehring
NIST Center for Neutron Research
National Institute of Standards and Technology
Gaithersburg, MD 20899-8562

S. Wakimoto and C. Stock
University of Toronto
Toronto, Ontario
Canada M5S 1A7

Z.-G. Ye and W. Chen
Simon Fraser University
Burnaby, British Columbia
Canada V5A 1S6

G. Shirane
Brookhaven National Laboratory
Upton, NY 11973

Emergent Excitations in a Geometrically Frustrated Magnet

A "Chinese" checkerboard having an equal number of black and white marbles cannot have every neighbor being the opposite kind, whereas a square checkerboard can. The triangular array on a Chinese checkerboard offers an example of "geometrical frustration". Frustration (*i.e.*, a condition in which some relation among the components cannot be satisfied simultaneously) is an important concept in understanding disordered states of matter. Systems in which a large diversity of states are involved are common in biology, chemistry and physics [1, 2]. Notable examples are glasses, liquids and proteins. Magnetic systems offer extreme examples of frustration in the form of spin lattices, where all interactions between spins cannot be simultaneously satisfied. Such geometrical frustration can lead to the emergence of qualitatively new states of matter, having "composite" degrees of freedom.

To explore this possibility, we examined magnetic fluctuations in $ZnCr_2O_4$ [3]. The B-site of this spinel lattice occupied by spin-3/2 Cr^{3+} leads to a magnet with dominant nearest neighbor interactions on the lattice of corner-sharing tetrahedra [4] shown in Fig. 1. Because the spin interaction energy is minimized when the four spins on each tetrahedron add to zero, interactions do not call for long-range order, but simply define a restricted phase space for fluctuations. Just as composite fermions can emerge from degenerate Landau levels in a two-dimensional electron gas, the near-degenerate manifold of states in a frustrated magnet is fertile ground for emergent behavior [5].

Neutron scattering provides the most effective tool to study possible composite spin degrees of freedom by directly probing the form factor of such entities. Fig. 2 (a,b) show the wave vector dependence of the low energy inelastic neutron scattering cross section in the spin-liquid phase of $ZnCr_2O_4$. The data exhibit broad maxima at the Brillouin zone boundaries, signaling the emergence of confined nano-scale spin clusters. Rather than Fourier-inverting the data, we consider potential spin clusters and test the corresponding prediction for the form factor against the data.

Individual tetrahedra would be prime candidates for such clusters, as they constitute the basic motif of the pyrochlore lattice. However, a tetrahedron is too small to account for the observed features. The next largest symmetric structural unit is the hexagonal loop formed by a cluster of six tetrahedra (Fig. 3). Two spins of each tetrahedron occupy the vertices of a hexagon while the other two spins belong to different hexagons. It is possible to assign all spins on the spinel lattice to hexagons simultaneously, thus producing N/6 weakly interacting degrees of freedom (Fig. 1). An outstanding fit is achieved for the antiferromagnetic hexagonal spin loops, as displayed in Fig. 2 (c, d). Thus, rather than scattering from individual spins, neutrons scatter from antiferromagnetic hexagonal spin clusters. In effect, $ZnCr_2O_4$ at low temperatures is not a system of strongly interacting spins, but a protectorate of weakly interacting spin-loop directors. Since the six hexagon spins are anti-parallel with each other, the staggered magnetization vector for a single hexagon, which shall be called the spin loop director, is decoupled from the 12 outer spins, and hence its reorientation embodies the

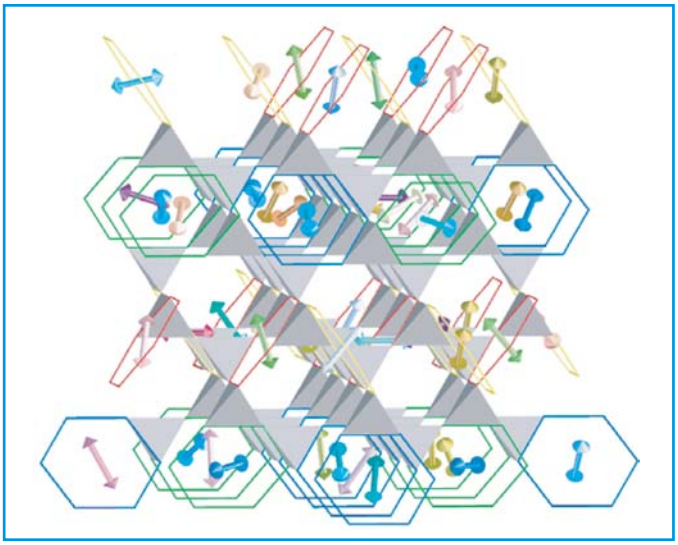

Fig. 1. The lattice of corner-sharing tetrahedra formed by the octahedrally coordinated B sites in a spinel structure with chemical formula AB_2O_4. A periodic assignment of all spins in the pyrochlore lattice is made to four different types of non-overlapping hexagons, represented by the colors blue, green, red, and gold. Every spin belongs to just one hexagon and each such hexagon carries a six-spin director. The resulting tetragonal structure of these hexagons has a unit cell of $2a \times 2a \times 3c$ and can be described by a stacking of two different types of three-layer slabs along the c-axis. The hexagon coverage on consecutive slabs is in fact uncorrelated, so that a macroscopic number of random slab-sequences can be generated.

long-sought local zero-energy mode for the pyrochlore lattice.

Composite degrees of freedom are common in strongly interacting many body systems. Quarks form hadrons; hadrons form nuclei; nuclei plus electrons form atoms; atoms form molecules that in turn are the basis for complex biological functionality. Planets, stars, galaxies and galactic clusters are examples of clustering on grander length scales. However, to our knowledge, the emergence of a confined spin cluster degree of freedom has not previously been documented in a uniform gapless magnet. The discovery is important because magnets offer an opportunity not afforded by the aforementioned systems, namely, to monitor emergent structure in complex interacting systems with microscopic probes such as neutron scattering and NMR. The collapse of a geometrically frustrated magnet into a director protectorate could for example be a useful template for exploring aspects of protein folding [2].

References:

[1] P. G. Debenedetti *et al*., Nature **410**, 259 (2001).

[2] P. G. Wolynes and W. A. Eaton, Physics World **12**, 39 (1999).

[3] S.-H. Lee, C. Broholm, W. Ratcliff, G. Gasparovic, Q. Huang, T. H. Kim, and S.-W. Cheong, Nature, in press (2002).

[4] S.-H. Lee *et al*., Phys. Rev. Lett. **84**, 3718 (2000).

[5] R. B. Laughlin and D. Pines, Proc. Natl. Acad. Sci. U.S.A. **97**, 28 (2000).

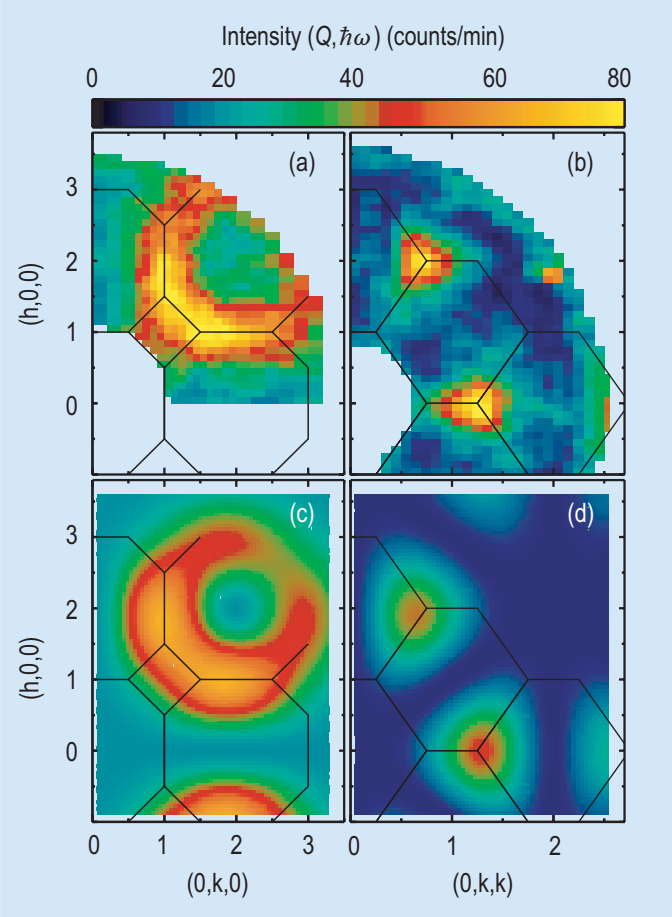

Fig. 2. (a), (b): Color images of inelastic neutron scattering intensities from single crystals of $ZnCr_2O_4$ in the (hk0) and (hkk) symmetry planes obtained at T = 15 K for $\hbar\omega$ = 1 meV. The data are a measure of the dynamic form factor for self-organized nano-scale spin clusters in the material. (c), (d): Color images of the square of the form factor calculated for antiferromagnetic hexagon spin loops averaged over the four hexagon orientations in the spinel lattice. The excellent agreement between model and data identifies the spin clusters as hexagonal spin loops.

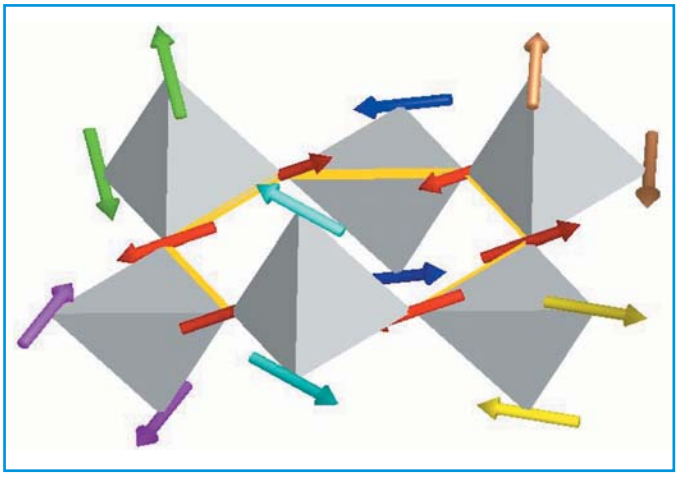

Fig. 3. Spin cluster surrounding a hexagon (shown in gold) in the pyrochlore lattice of Fig. 1.

S.-H. Lee, Q. Huang
NIST Center for Neutron Research
National Institute of Standards and Technology
Gaithersburg, MD 20899-8562

C. Broholm, G. Gasparovic
Department of Physics and Astronomy
The Johns Hopkins University
Baltimore, MD 21218

W. Ratcliff, S.-W. Cheong
Department of Physics and Astronomy
Rutgers University
Piscataway, NJ 08854

T. H. Kim
Francis Bitter Magnet Laboratory
Massachusetts Institute of Technology
Cambridge, MA 02139

Polaron Dynamics and the Glass Transition in Colossal Magnetoresistance Materials

The recent discovery of colossal magnetoresistance (CMR) effects in the manganese oxide class of materials (such as $La_{1-x}A_xMnO_3$ (A = Sr, Ca, Ba)) has rekindled intense interest in these systems, both because of their fundamental properties as well as their technological potential for read/write heads in magnetic recording media, sensors, and spin-polarized electronics. The role of local charge correlations and their competition with magnetic and electronic ground states is one of the most striking new features of the transition metal oxides such as cuprate superconductors and nickelates, but is most elegantly highlighted for these CMR manganites. Our neutron scattering results near optimal doping show that the short-range polaron correlations are completely dynamic at high T, but then freeze upon cooling to a temperature T_g. This glass transition suggests that the paramagnetic/insulating state arises from an inherent orbital frustration that inhibits the formation of a long range orbital- and charge-ordered state. Upon further cooling into the ferromagnetic-metallic state, where the polarons melt, the diffuse scattering quickly develops into a propagating, transverse optic phonon.

In the ground state these CMR materials are ideal isotropic ferromagnets. As the system is warmed through the Curie temperature of this half-metallic system the disorder in the spins begins to inhibit the hopping of the (magnetic) conduction electrons, and this in turn provides enough time for the lattice to distort and form polarons that trap the electrons. The ferromagnetic-paramagnetic transition is thus accompanied by a metal-insulator transition; cooling into the ferromagnetic state, or alternatively inducing a magnetization by application of a field, converts the insulator back into a metal, producing the CMR effect.

To investigate the dynamics of these polarons, we have carried out inelastic neutron scattering measurements on a single crystal of optimally-doped $La_{0.7}Ca_{0.3}MnO_3$ (T_C = 252 K) [1]. Fig. 1 shows the energy dependence of the polaron scattering at the peak of the polaron correlations [2]. The data reveal that there is a purely elastic component, indicating that the system still possesses order, and since spatially this order is short range in nature we interpret this as a *polaron glass*.

The data in Fig. 1 also exhibit dynamics, in the form of quasielastic scattering (peaking at zero energy). Figure 2 shows the temperature evolution of both the dynamic and purely elastic components, obtained on the optimally-doped CMR bilayer manganite $La_{1.24}Sr_{1.76}Mn_2O_7$ [3]. On decreasing the temperature from 460 K we see that the quasielastic scattering narrows in energy, with a width that decreases approximately linearly until $T \approx T^* \approx 310$ K while the integrated intensity of the scattering is approximately temperature independent. Below ≈ 310 K the behavior of the quasielastic width and intensity abruptly changes, and a new, purely elastic component, develops in the spectrum. The elastic scattering develops rapidly below T_g, and appears to track the resistivity of the material. This increase in the elastic intensity is accompanied by a concomitant decrease of the quasielastic intensity, while the energy width exhibits a change in slope, becoming approximately constant for $T_C < T < T_g$.

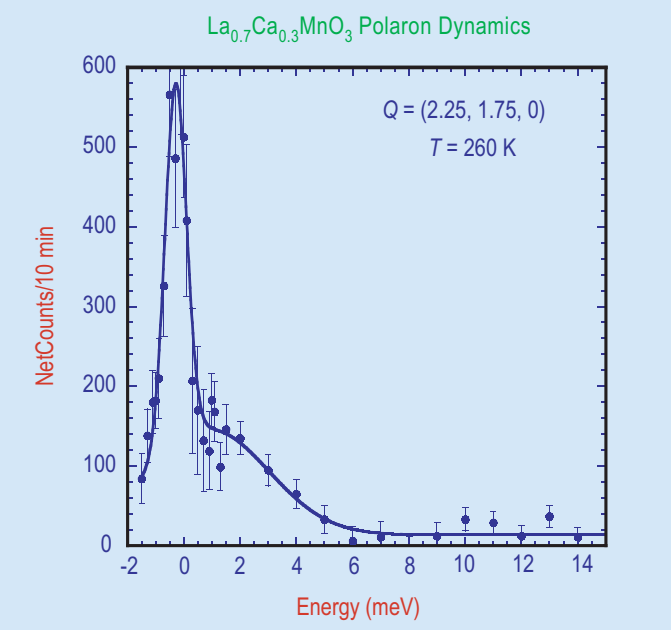

Fig. 1. Polaron dynamics at the peak in the correlation function at 260 K, just above T_C = 252 K, in $La_{0.7}Ca_{0.3}MnO_3$. The data reveal a pure elastic signal (indicating an ordered state) and dynamic quasielastic scattering.

To further probe the origin of this quasielastic scattering we compiled the map of the dynamical scattering above T^* shown in Fig. 3. The inelastic response shows that the dynamical scattering still has surprisingly

well-defined correlations at these elevated temperatures, demonstrating that the polarons are not isolated Jahn-Teller Mn^{3+} deformations, but are dynamically correlated. The dynamical correlation length obtained from these data is ≈ 12 Å, comparable in size to the static correlation length found at lower T. These dynamic correlations are still present up to 460 K, the highest T explored so far.

From our measurements we can identify three regimes. For $T > T^*$ the observed scattering is dominated by correlations that are completely dynamic. The quasielastic energy width from these correlations varies linearly with T, which is qualitatively what is expected for a continuous phase transition. The second regime occurs for $T_C < T < T^*$, and is dominated by frozen static polaronic correlations as revealed by the rapid development of the elastic component below T^*. The development of the elastic component is accompanied by a decrease of the quasielastic intensity, while the spatial correlations remain short range in nature. This behavior is clear evidence for a freezing transition, analogous to the freezing transition T_g found in structural glasses or geometrically frustrated spin-glasses. Our data strongly suggest that T^* represents a phase transition from a *polaronic liquid* to a *polaronic glass*. This polaron glass then melts at T_C as the ferromagnetic metallic state sets in.

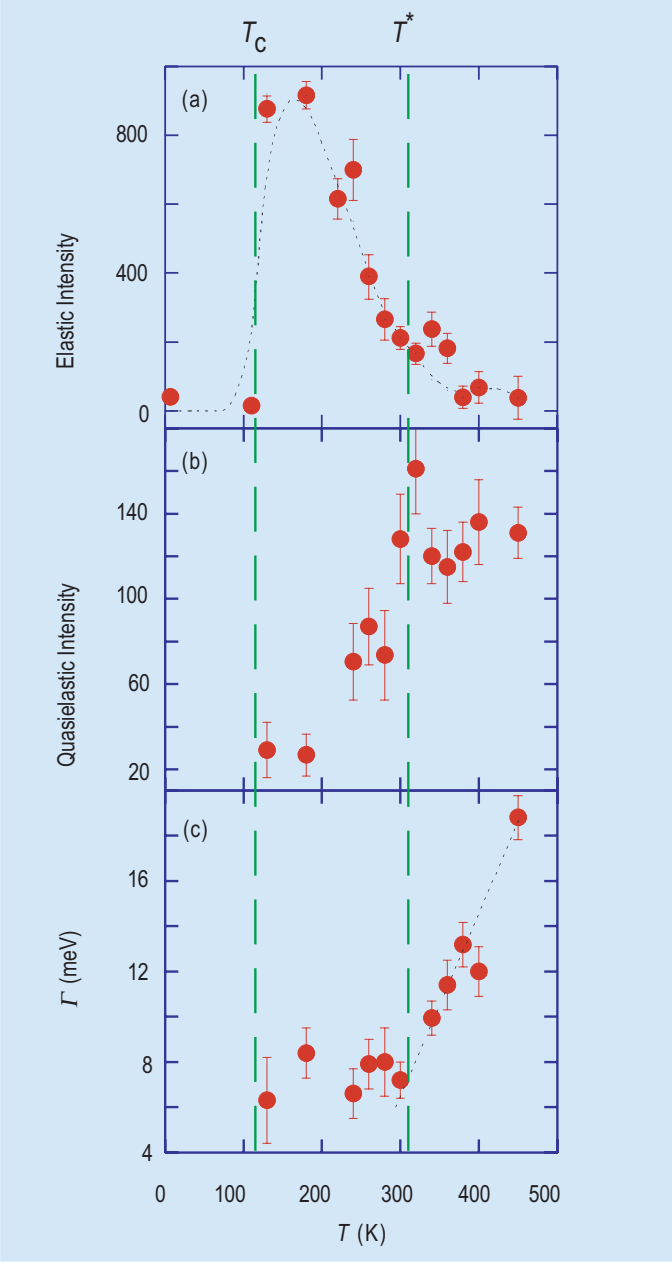

Fig. 2. Temperature dependence of the elastic (a) and quasielastic intensity (b) of the CMR bilayer manganite (T_C = 114 K). (c) Quasielastic width of the Lorentzian response. Dashed lines are guides to the eye. Error bars correspond to standard deviations obtained from the least squares analysis.

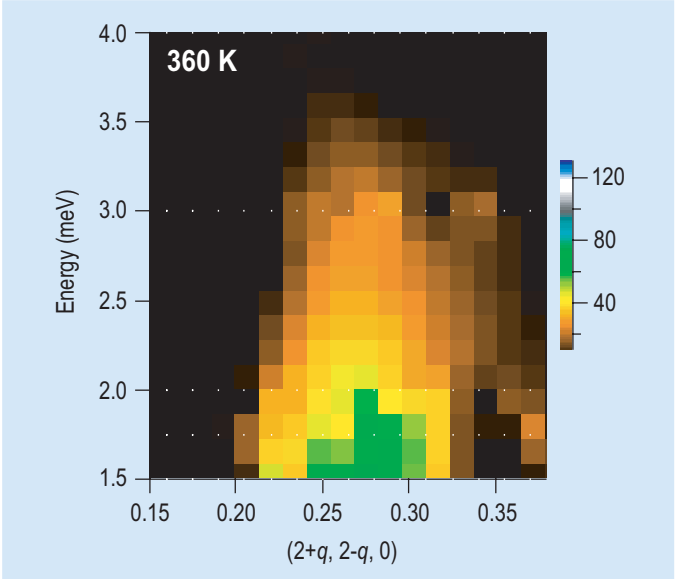

Fig. 3. Dynamic polaron correlations above the glass transition.

References:

[1] J. W. Lynn, F. M. Woodward, D. N. Argyriou, Y. Ren, Y. M. Mukovskii, A. A. Arsenov (preprint).

[2] C. P. Adams, J. W. Lynn, Y. M. Mukovskii, A. A. Arsenov, and D. A. Shulyatev, Phys. Rev. Lett. **85**, 3954 (2000); J. Appl. Phys. **89**, 6846 (2001).

[3] D. N. Argyriou, J. W. Lynn, R. Osborn, B. Campbell, J. F. Mitchell, U. Ruett, H. N. Bordallo, A. Wildes, and C. D. Ling, Phys. Rev. Lett. **89**, 036401 (2002).

J. W. Lynn and F. M. Woodward
NIST Center for Neutron Research
National Institute of Standards and Technology,
Gaithersburg, MD 20899

D. N. Argyriou, R. Osborn, and J. F. Mitchell
Argonne National Laboratory
Argonne, IL 60439

Quantum Impurities in the Two-Dimensional Spin One-Half Heisenberg Antiferromagnet

A phase transition is the transformation of a system from one state to another, *e.g.* from an ordered phase to a disordered phase. In magnetic iron for example, the ordered ferromagnetic phase gives way to the disordered paramagnetic phase when fluctuations overwhelm the forces tending to order the system. In thermal phase transitions the amplitudes of these fluctuations increase with temperature, and the transition occurs at a "critical" temperature T_C. By contrast, quantum phase transitions occur only at $T = 0$ K [1]. The relevant fluctuations are thus quantum mechanical in nature and can overwhelm the tendency to order when some other parameter of the system is varied. A conceptual example would be a ferromagnetic system at $T = 0$ that is continuously diluted with some non-magnetic material until it undergoes a transition to the paramagnetic state.

The hope for insight into the physics of high temperature superconductors has generated enormous interest in the case of the two-dimensional (2D) spin-½ square-lattice Heisenberg antiferromagnet ($S = ½$ SLHAF) because it models La_2CuO_4, the parent compound of the first high-temperature superconductor. It has been theorized that a quantum phase transition might occur in La_2CuO_4 by doping with static, non-magnetic, atoms [2]. We have investigated the properties of the 2D $S = ½$ SLHAF using complementary neutron scattering and numerical simulations. Our results demonstrate that the spin-diluted Heisenberg antiferromagnet $La_2Cu_{1-z}(Zn,Mg)_zO_4$ is a prototype system for square-lattice site percolation in the extreme quantum limit of $S = ½$ [3]. In the pure system ($z = 0$), magnetic Cu^{2+} ions form a 2D square lattice dominated by an antiferromagnetic nearest-neighbor exchange mediated by intervening oxygen ions, which leads to long-range antiferromagnetic order at low temperature. Replacement of the Cu spins with non-magnetic Zn^{2+} and Mg^{2+} ions randomly dilutes the antiferromagnetic sheets, weakening the antiferromagnetic order. With sufficient site dilution the system undergoes a geometric transition from having one infinite connected cluster of Cu spins below the percolation threshold to only finite disconnected clusters above the percolation threshold (around 41 %), as shown in Fig. 1. Our results demonstrate that random disorder and quantum fluctuations both play a strong role in determining the properties of this system near the percolation threshold.

Previous experiments [4] suggested that $La_2Cu_{1-z}(Zn,Mg)_zO_4$ might become disordered at zero temperature well below the classical percolation threshold because of quantum fluctuations. This question remained unresolved because of a lack of suitable samples, but high-quality single crystals of $La_2Cu_{1-z}(Zn,Mg)_zO_4$ grown at the T. H. Geballe Laboratory for Advanced Materials at Stanford University allowed us to solve this quantum percolation problem. Figure 2 shows the dilution dependence of the antiferromagnetic ordering (Néel) temperature T_N. Although a purely 2D system cannot have long-range order at nonzero temperature, small interlayer couplings allow long-range 3D order to occur when the 2D correlations become large enough. Monte Carlo calculations (also shown in Fig. 2) indicate that this occurs at correlation lengths of around 100 lattice constants for both the pure and diluted systems. Our results for $T_N(z)$ agree with previous measurements at lower concentrations [4], but we find that at higher concentrations T_N falls off more slowly and does not reach zero until the percolation threshold.

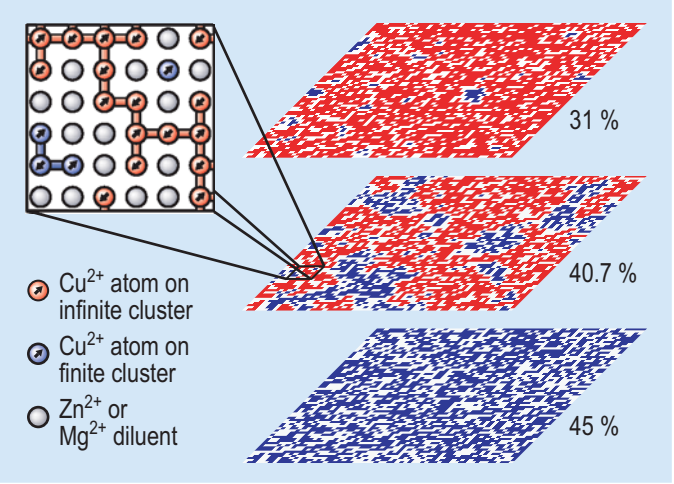

Fig. 1. A schematic of finite sections of the infinite lattice at dilution levels well below (31 %), just below (40.7 %), and above (45 %) the percolation threshold. Sites on the infinite cluster are shown in red, sites on finite disconnected clusters are blue, and diluents are in white. The inset is a close-up view for $z = 40.7$ %, showing the role that magnetic Cu and non-magnetic Zn/Mg ions play in the experimental system.

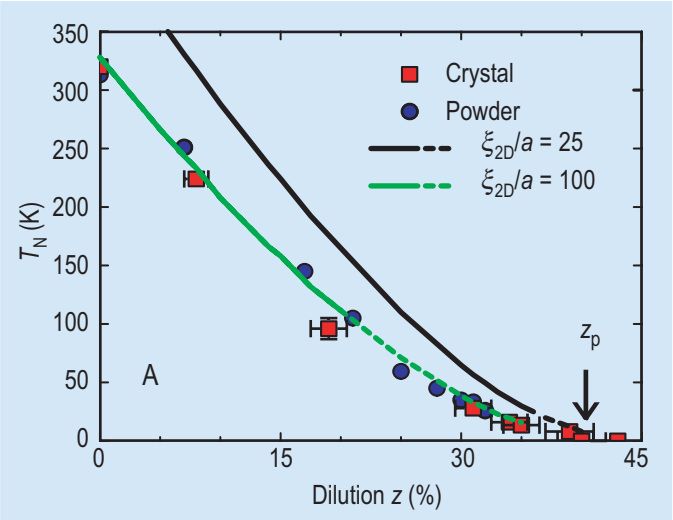

Fig. 2. Néel temperature phase diagram of $La_2Cu_{1-z}(Zn,Mg)_zO_4$. Single crystal results are from neutron diffraction, powder results are from SQUID Magnetometry. Lines are Monte Carlo results for the temperature at which spin-spin correlations reach the specified length.

To study the 2D static properties of $La_2Cu_{1-z}(Zn,Mg)_zO_4$, we measured the 2D instantaneous spin-spin correlation length ξ using a 2-axis energy-integrating technique in the paramagnetic phase above T_N. The results are shown in Fig. 3 (colored symbols) for a number of different concentrations and across a broad range of temperatures. Quantum Monte Carlo results for the nearest-neighbor Heisenberg model are shown as black symbols. There are no adjustable parameters in this comparison, and the experimental and Monte Carlo results match exceptionally well up to the percolation threshold. We can see that dilution not only weakens the correlations at a given temperature, but that it also slows down the rate at which they grow as the system is cooled. At low concentrations, ξ scales exponentially in inverse temperature. Near the percolation threshold, however, ξ exhibits power law behavior in inverse temperature, and above the percolation threshold it saturates at a finite length at low temperature.

We have shown that $La_2Cu_{1-z}(Zn,Mg)_zO_4$ is an excellent model system for studying percolation in a 2D $S = ½$ Heisenberg antiferromagnet. A long-range-ordered ground state persists up to the percolation threshold even though quantum fluctuations increase as dilution is increased. Further studies of the dynamics will provide more insight into the role of disorder in this quantum many-body system.

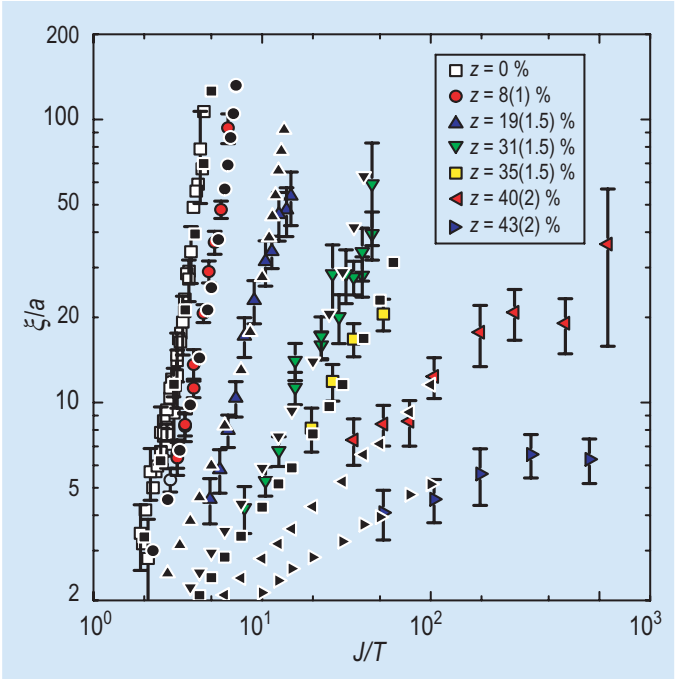

Fig. 3. Spin-spin correlation length (in units of the lattice constant) vs. inverse temperature (scaled by the nearest neighbor exchange energy J of the pure system) for different concentrations of non-magnetic ions. Colored symbols are experimental results, obtained from measurements of the static structure factor. Black filled symbols are quantum Monte Carlo results for z = (8, 20, 31, 35, 41, and 46) % dilution. Results for z = 0 % are from [5, 6]. No adjustable parameters are used in the comparison.

References:

[1] S. Sachdev, *Quantum Phase Transitions*, Cambridge University Press (Cambridge, 1999).

[2] Y.-C. Chen *et al.*, Phys. Rev. B **61**, R3772 (2000).

[3] O. P. Vajk *et al.*, Science **295**, 1691 (2002).

[4] M. Hücker *et al.*, Phys. Rev. B **59**, R725 (1999).

[5] R. J. Birgeneau *et al.*, Phys. Rev. B **59**, 13788 (1999).

[6] B. B. Beard *et al.*, Phys. Rev. Lett. **80**, 1742 (1998).

O. P. Vajk, P. K. Mang, and M. Greven
Stanford University
Stanford, CA 94305

P. M. Gehring and J. W. Lynn
NIST Center for Neutron Research
National Institute of Standards and Technology
Gaithersburg, MD 20899-8562

Automobile Sheet-Metal "Springback": Residual Stress Measurements and Modeling

A serious impediment to the use of lighter-weight, higher-strength materials in automobile manufacturing is the relative lack of understanding about how these materials respond to the complex forming operations that go into shaping a blank of metal into automobile body parts. One of the most vexing and costly problems is "springback" — the tendency of sheet metal to lose some of its shape when it is removed from the die. Springback is very pronounced with two of the likeliest candidates for weight reduction: high-strength steel and aluminum alloys, than it is with standard steel. Unless it is well managed and taken into account when the dies are designed, it leads to parts that are ill-fitting and deviate excessively from design intent.

American auto manufacturers, through the Springback Project of the USCAR consortium[1], are engaged in a major effort to predict springback by means of sophisticated finite element modeling ("FEM"). However, the accuracy of predictions of large strain plasticity under complex load histories, such as those applied during stamping processes, is uncertain because of incomplete validation of the FEM programs. Surprisingly, calculated residual stress, one of the key mechanical properties predicted by the state-of-the-art FEM codes, had not been compared with experimental measurements. The present work is the first comprehensive effort to determine the residual stresses of interest.

Diffraction provides a powerful means of very accurately measuring microstructure, strains (from which stresses are determined) and mechanical behavior in a way not possible with other techniques. More importantly, diffraction facilities available to the NCNR include neutron diffraction, laboratory x-ray diffraction and synchrotron x-ray diffraction (at Argonne's Advanced Photon Source). These constitute the full spectrum of diffraction probes of residual stress and microstructure for surface, sub-surface and bulk specimens. The test specimens employed for this study were two deep-drawn "Demeri" cups: one, thin-walled (≈ 1 mm) 6022-T4 aluminum; the second, thicker-walled (3.2 mm) steel. The latter is shown in Fig. 1.

Fig. 1. The deep-drawn steel cup. The aluminum cup was similar, except for wall thickness.

The objective of this project was to determine the residual stresses in the "simple" model specimens formed similarly to stamped auto parts. Modelers in the USCAR consortium would use FEM to predict the stress distributions to validate their codes. At this time, the modeling part of the project is still in progress.

Two distinct experimental studies were performed. The first utilized synchrotron x-rays to determine the stress distribution in a ring and pieces (Fig. 2) cut from the

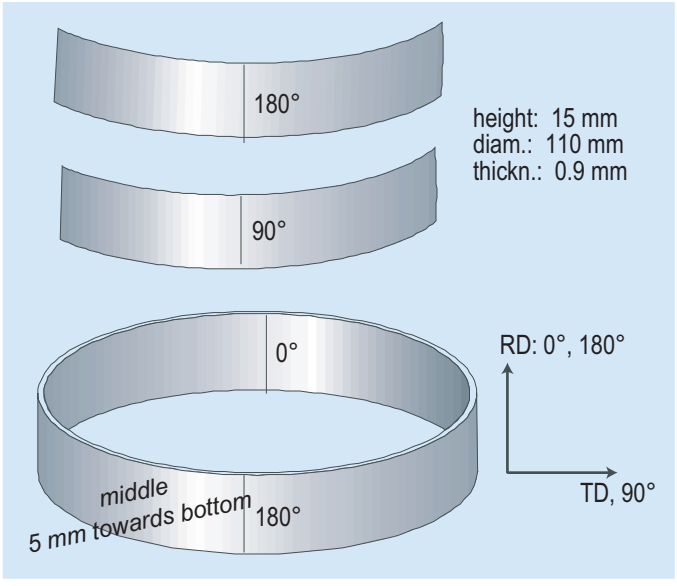

Fig. 2. Pieces cut from the aluminum cup and examined by synchrotron x-rays.

[1] USCAR is the umbrella organization of DaimlerChrysler, Ford and General Motors, which was formed in 1992 to further strengthen the technology base of the domestic auto industry through cooperative, pre-competitive research.

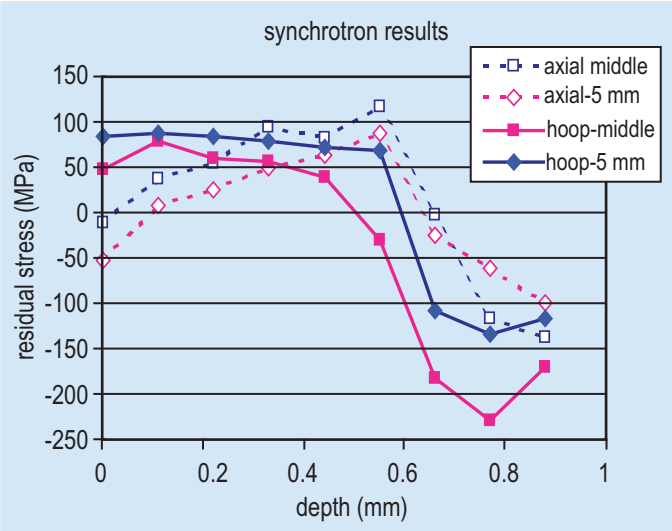

Fig. 3. Axial and hoop stresses for the 0.9 mm thick aluminum cup as determined by synchrotron x-rays.

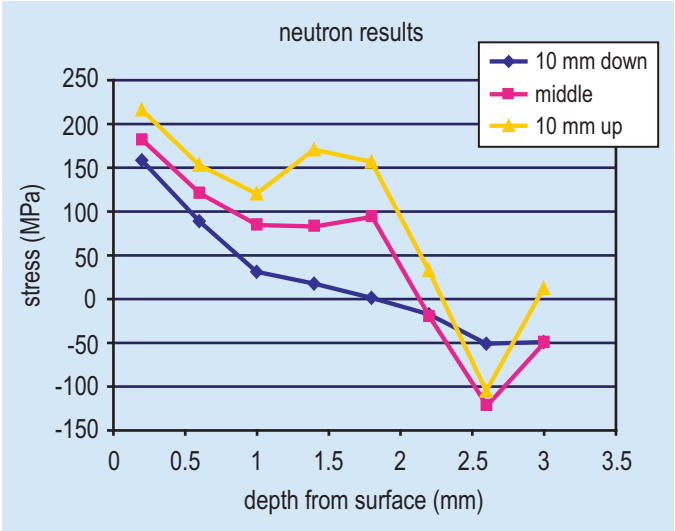

Fig. 4. Hoop stresses as a function of depth in the 3.2 mm thick steel cup, as determined by neutron diffraction.

aluminum cup (which except for wall thickness, was initially like the steel cup shown in Fig. 1). The critical point of this study is to determine the stress distribution in the ring and, ultimately, whether the FEM could predict it. Directly related to this was how the measured stress distribution compared with the simple linear depth dependence used in analytical calculations to predict the opening of the ring when cut.

The residual stresses determined from the x-ray diffraction measurements are shown in part in Fig. 3. Representative neutron diffraction results for the steel cup are shown in Fig. 4.

The more complete results shown for the aluminum ring, the first such measurements on deep-drawn cups, satisfy both symmetry and stress balance requirements. However, the stresses vary around the circumference and in the axial direction, and differ strongly from ideal bending stresses. So even for the "simple" model system, the plastic deformation process and the resultant stresses are very complex.

In summary, these results provide the first through-thickness stress distributions by which springback model predictions of residual stress can be tested. Furthermore, synchrotron radiation and neutrons are the only non-destructive methods that are able to provide the necessary accuracy and spatial resolution needed to obtain these results. Finally, successful modeling of springback requires successful prediction of these stress distributions.

References

T. Gnaeupel-Herold, H. J. Prask, R. J. Fields, T. J. Foecke, M. F. Shi, and U. Lienert, submitted to Mater. Sci. Eng. A

T. Gnäupel-Herold and H. Prask
NIST Center for Neutron Research
National Institute of Standards and Technology
Gaithersburg, MD 20899-8562

R. Fields
Metallurgy Division
National Institute of Standards and Technology
Gaithersburg, MD 20899-8553

D. Haeffner
Advanced Photon Source
Argonne National Laboratory
Argonne, IL 60439

E. Chu
Alcoa Technical Center
Alcoa Center, PA 15069-0001

Serving the Science and Technology Community

NCNR Partnership Celebration

This year marks the tenth anniversary of the start of user experiments in the NCNR guide hall. The NCNR has maintained working partnerships with a number of government agencies, industrial laboratories, and academic institutions since it was commissioned over 30 years ago. Several key partnerships are highlighted in this section. A special event celebrating NCNR partnerships and a decade of success was held on August 5, 2002, with a number of distinguished visitors in attendance. Addressing the audience were partnership representatives from both government and industry. The speakers noted the key role of partnerships in the growth and success of the NCNR and their impact on U.S. neutron science. Many of their comments referred to a recent report from the Office of Science and Technology Policy on the "Status and Needs of Major Neutron Scattering Facilities and Instruments in the United States." This report encourages the formation of partnerships such as those at the NCNR, especially between federal agencies, to promote effective stewardship of large federal research resources. The speeches and a guided tour of the facility for the visitors provided a satisfying perspective on the development of the NCNR into one of the world's leading and most productive neutron scattering facilities.

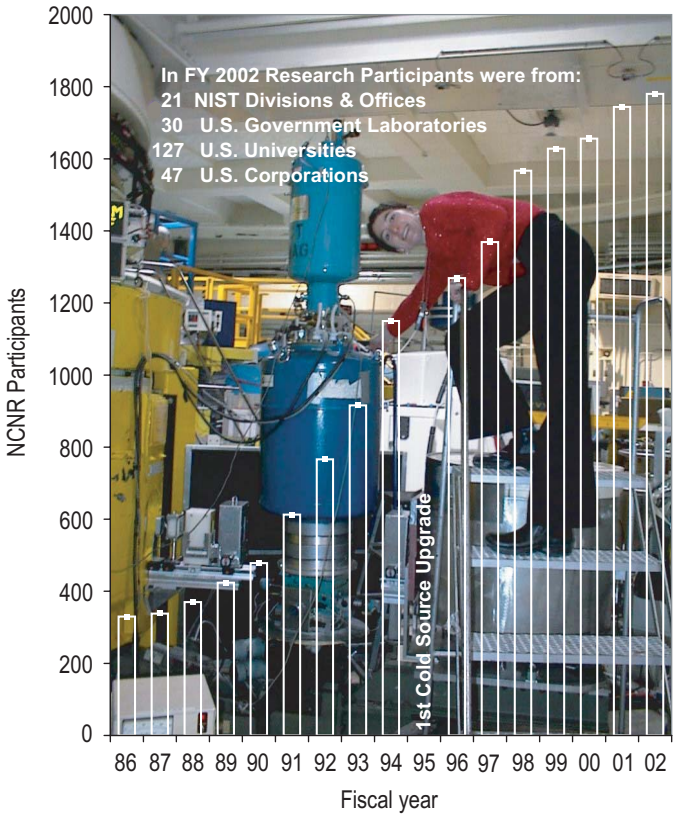

Fig. 1. Numbers of NCNR Research Participants over time.

The number of NCNR research participants has more than doubled over the last decade (Fig. 1) and has continued to increase, despite an extended shutdown for the installation of the advanced cold source and new cooling towers. As detailed in the recent OSTP report, the NCNR now accommodates more than half of all neutron users in the US.

The NCNR User Program

During the past year, we have made a significant shift toward entirely Internet-based proposal submission and review. Users have been sending proposals to us on our Web-page form for more than six years, but now it has become the exclusive method for standard submission of beam time proposals. Local beam time requests from NIST staff are managed through the same system. Peer reviews of proposals are also communicated to us electronically through a Web form, resulting in faster and more efficient decisions on instrument time, to the benefit of users and their research programs.

Two calls for proposals were made in the past year, and more than 390 proposals were received in response. The proposed experiments show increasing activity in research on soft condensed matter and bioscience, although more mature areas such as magnetism and polymer research have held their own. Proposals are now nearly equally divided between those for structural investigations, mainly SANS and reflectometry, and studies of dynamics, requesting one of the newer high-resolution spectrometers in the guide hall.

After a thorough review process by external referees and by the NCNR Program Advisory Committee (PAC), approved proposals were allocated beam time. The PAC is a panel of accomplished scientists with expertise across a broad range of neutron methods and scientific disciplines. It is the body primarily responsible for proposal review and

recommending user policies for the NCNR, working closely with the Center's Director and staff. Its current membership includes Sanat Kumar (Rensselaer Polytechnic Institute, chair), Robert M. Briber (University of Maryland), Michael K. Crawford (DuPont), Yumi Ijiri (Oberlin College), Dieter K. Schneider (Brookhaven National Laboratory), Kenneth Herwig (Oak Ridge National Laboratory), Michael Kent (Sandia National Laboratory), Robert Leheny (Johns Hopkins University), John Tranquada (Brookhaven National Laboratory), and Sossina Haile (California Institute of Technology).

The Center for High Resolution Neutron Scattering

One of the most important partnerships between the NCNR and another agency is with the National Science Foundation (NSF) through its support of the Center for High Resolution Neutron Scattering (CHRNS). Five instruments in the NCNR guide hall, and one in the thermal instrument area, are operated by CHRNS, comprising a crucial component of the user program. The instruments include a 30 m SANS instrument, the SPINS triple-axis spectrometer, the neutron spin-echo spectrometer, the high-flux backscattering spectrometer, the disk-chopper time-of-flight spectrometer, and the ultra-small angle scattering diffractometer. Most of the instrument time allocated by the PAC now goes to experiments carried out on CHRNS instruments. An additional SANS diffractometer on neutron guide NG-1, which up to now has been used primarily for NIST programmatic research, is being upgraded to a more powerful 10 m instrument with a new detector, and will be made available to CHRNS users. In aggregate, the CHRNS instruments provide structural information on a length scale from 1 nm to ≈ 10 μm, and dynamical information on energy scales from ≈ 30 neV to ≈ 100 meV. These are the widest ranges accessible at any neutron research center in North America.

Collaborations

Direct collaborations on specific experiments remain a common way for users to pursue their ideas using NCNR facilities, accounting for approximately half of the number of instrument-days. The thermal-neutron triple-axis spectrometers are mainly scheduled in this way. Most of the time reserved for NIST on these and all other NCNR instruments is devoted to experiments that are collaborations with non-NIST users. Collaborative research involving external users and NIST scientists often produces results that could be not obtained otherwise.

Fig. 2. Sanat Kumar, Dieter Schneider, and Rob Briber of the PAC consider proposals for beam time.

Another mode of access to the NCNR is through more formal research consortia. Groups of researchers from various institutions join forces to build and operate an instrument. Typically, a substantial fraction of the time on the instrument is then reserved for the consortium members, and the remaining time is allocated to general user proposals. For example, a group including ExxonMobil, the University of Minnesota, and NIST cooperates on the NG-7 30 m SANS instrument. Similar arrangements involving other consortia apply for the horizontal-sample reflectometer, the high-resolution powder diffractometer, the filter-analyzer spectrometer, and the neutron spin-echo spectrometer.

Cold Neutrons for Biology and Technology

An important new partnership with five universities, NIST and the National Institutes of Health is now proceeding with the design and construction of a new reflectometer dedicated to bioscience and biotechnology. The University of California at Irvine leads the consortium whose purpose is to provide a new national resource for investigations in structural biology. Research leaders from Penn State, Rice, Carnegie Mellon, Duke, and the Los Alamos National Laboratory are included in the consortium.

Independent Programs

There are a number of long standing programs located at the NCNR that involve other parts of NIST, universities, industrial laboratories, or other government agencies.

The **Nuclear Methods Group** (Analytical Chemistry Division, Chemical Science and Technology Laboratory) has as its principal goals the development and application of nuclear analytical techniques for the determination of elemental compositions with greater accuracy, higher sensitivity and better selectivity. A high level of competence has been developed in both instrumental and radiochemical neutron activation analysis (INAA and RNAA). In addition, the group has pioneered the use of cold neutron beams as analytical probes with both prompt gamma activation analysis (PGAA) and neutron depth profiling (NDP). PGAA measures the total amount of a particular analyte present throughout a sample by the analysis of the prompt gamma-rays emitted upon neutron capture. NDP, on the other hand, determines concentrations of several important elements (isotopes) as a function of depth within the first few micrometers of a surface by energy analysis of the prompt charged-particles emitted during neutron bombardment. These techniques (INAA, RNAA, PGAA, and NDP) provide a powerful combination of complementary tools to address a wide variety of analytical problems of great importance in science and technology, and are used to help certify a large number of NIST Standard Reference Materials.

A large part of the group's efforts is directed towards the exploitation of the analytical applications of the guided cold-neutron beams available at the NCNR. The Group's involvement has been to design and construct state-of-the-art cold neutron instruments for both PGAA and NDP and provide facilities and measurements for outside users, while retaining and utilizing our existing expertise in INAA and RNAA.

The Neutron Interactions and Dosimetry Group (Physics Laboratory) provides measurement services, standards, and fundamental research in support of NIST's mission as it relates to neutron technology and neutron physics. The national and industrial interests served include scientific instrument calibration, electric power production, radiation protection, defense nuclear energy systems, radiation therapy, neutron radiography, and magnetic resonance imaging.

The Group's research may be represented as three major activities. The first is Fundamental Neutron Physics including magnetic trapping of ultracold neutrons, operation of a neutron interferometry and optics facility, development of neutron spin filters based on laser polarization of ^{3}He, measurement of the beta decay lifetime of the neutron, and investigations of other coupling constants and symmetries of the weak interaction. This project involves a large number of collaborators from universities and national laboratories.

The second is Standard Neutron Fields and Applications utilizing both thermal and fast neutron fields for materials dosimetry in nuclear reactor applications and for personnel dosimetry in radiation protection. These neutron fields include thermal neutron beams, "white" and monochromatic cold neutron beams, a thermal-neutron-induced ^{235}U fission neutron field, and ^{252}Cf fission neutron fields, both moderated and unmoderated.

The third is Neutron Cross Section Standards including experimental advancement of the accuracy of neutron cross section standards, as well as evaluation, compilation and dissemination of these standards.

The **Polymers Division** of the Materials Science and Engineering Laboratory has several program elements at the NCNR covering the technological areas of electronics, multiphase polymeric, and biological materials. The purpose of the electronics materials program is to help the U.S. microelectronics industry address their most pressing materials measurement and standards issues. The structure of nanoporous thin films, used in integrated circuits as low-dielectric-constant insulators, is characterized through a combination of small angle neutron scattering (SANS), x-ray reflectivity, and ion scattering measurements. Advances such as vapor contrast matching techniques provide unique information about critical parameters such as the porosity, average pore size, and wall mass density. In addition, several instruments at NCNR provide unique high-resolution measurements that guide the development and fundamental understanding of next-generation polymeric photoresist materials for sub-100 nm lithography. Measurements include the segmental dynamics of the polymers that govern the mobility of an acid catalyst, direct measurement of the deprotection reaction that leads to patterned areas, and the structural characterization of lithographically prepared structures.

In the multiphase polymeric materials program, the objective is to understand underlying principles of phase behavior, local structure, and flow that control morphology and structure during processing of multiphase materials such as polymer blends and nanocomposites (polymers filled with clay platelets, carbon nanotubes, or triblock copolymer micelles). SANS and reflectivity measurements in equilibrium, in transient conditions, and under external

fields, provide essential information for general understanding as well as for specific application of polymer blend/alloy systems. For example, the structure induced by shear alignment of nanoparticle/polymer solutions has been elucidated with SANS, small angle light scattering, and rheological measurements. Customers include material producers and users, ranging from chemical, rubber, tire, and automotive companies, to small molding and compounding companies. The research focus on polymeric materials includes commodity, engineering and specialty plastic resins, elastomers, coatings, adhesives, films, foams, and fibers.

The biological materials initiative is committed to demonstrating the use of inelastic neutron scattering (INS) as a unique measurement tool for understanding the dynamics in several important biological systems. For example, INS has been used to elucidate changes in protein dynamics that occur in the final stages of protein folding. Likewise, INS and low frequency Raman scattering have been developed as measurement tools to identify the dynamical aspects of a good sugar or polyalcohol for protein stabilization and cryopreservation. Effective preservatives must suppress the high frequency motions that are precursors to protein unfolding and denaturation.

The **ExxonMobil Research and Engineering Company** is a member of the Participating Research Team (PRT) that operates, maintains, and conducts research at the NG-7 30 m SANS instrument and the NG-5 Neutron Spin Echo Spectrometer. Their mission is to use those instruments, as well as other neutron scattering techniques available to them at NCNR, in activities that complement research at ExxonMobil's main laboratories as well as at its affiliates' laboratories around the world. The aim of these activities is to deepen understanding of the nature of ExxonMobil's products and processes, so as to improve customer service and to improve the return on shareholders' investment. Accordingly, and taking full advantage of the unique properties of neutrons, most of the experiments use SANS or other neutron techniques to study the structure and dynamics of hydrocarbon materials, especially in the fields of polymers, complex fluids, and petroleum mixtures. ExxonMobil regards its participation in the NCNR and collaborations with NIST and other PRT members not only as an excellent investment for the company, but also as a good way to contribute to the scientific health of the nation.

The **U.S. Army Research Laboratory** is the current manager of a 30-year NCNR-Army partnership sponsoring a research team. This group performs materials research and engineering in support of Army needs and missions and works jointly with NIST/NCNR in developing and improving neutron methods and instrumentation. A key contribution of Army researchers at the NCNR is a highly successful neutron facility to map residual stress and texture within large components such as jet turbine blades and structural welds. This resource is critical to development and performance of industrial and transportation systems and military hardware.

The **Center for Food Safety and Applied Nutrition**, U.S. Food and Drug Administration (FDA), directs and maintains a neutron activation analysis (NAA) facility at the NCNR. This facility provides agency-wide analytical support for special investigations and applications research, complementing other analytical techniques used at FDA with instrumental, neutron-capture prompt-gamma, and radiochemical NAA procedures, radioisotope x-ray fluorescence spectrometry (RXRFS), and low-level gamma-ray detection. This combination of analytical techniques enables diverse multi-element and radiological information to be obtained for foods and related materials. The NAA facility supports agency quality assurance programs by developing in-house reference materials, by characterizing food-related reference materials with NIST and other agencies, and by verifying analyses for FDA's Total Diet Study Program. Other studies include the development of RXRFS methods for screening foodware for the presence of Pb, Cd and other potentially toxic elements, use of instrumental NAA to investigate bromate residues in bread products, and use of prompt-gamma NAA to investigate boron nutrition and its relation to bone strength.

The **Smithsonian Center for Materials Research and Education Nuclear Laboratory for Archeological Research** (SCMRE) has chemically analyzed over 24 000 artifacts by INAA at the NCNR over the last 25 years. SCMRE's research programs draw extensively upon the collections of the Smithsonian, as well as those of national and international institutions. The chemical analyses provide a means of linking these diverse collections together to study continuity and change involved in the production of ceramic objects. INAA data are used to determine if groups of ceramics have been made from the same or different raw materials. The ceramics then can be attributed to geographic regions, specific sources, workshops and even individual artists. The ability to combine chemical data for semi-complete or whole vessels with that derived from the analysis of materials recov-

ered from recent excavation programs provides many new opportunities for study. Museum vessels that are found to be similar and attributable to some geographic location provide a basis for exploring changing aspects of style, iconography, textual history and even ideology. In an integrative manner, the INAA program enhances the importance of collection materials for the study of the past.

A number of universities have also established long-term programs at the NCNR. The **University of Maryland** is heavily involved in the use of the NCNR, and maintains several researchers at the facility. **Johns Hopkins University** participates in research programs in magnetism, soft condensed-matter physics, bioscience, and in instrument development at the NCNR. The **University of Pennsylvania** is working to help develop biological applications of neutron scattering. It is also participating in the second stage construction of the filter analyzer neutron spectrometer, along with the **University of California at Santa Barbara, DuPont, Hughes, and Allied Signal**. **The University of Minnesota** participates in two PRTs, the NG-7 30 m SANS and the NG-7 reflectometer. The **University of Massachusetts** also participates in the latter PRT.

Eighth Annual Summer School

With support from the National Science Foundation, NCNR and CHRNS held their annual Summer School on Neutron Scattering from June 3-7, 2002. The subject matter of the school alternates in successive years between techniques designed to investigate structure, and those devoted to spectroscopy and dynamics. The course this year focused on structural studies with SANS and neutron reflectometry (NR). Forty graduate students and postdoctoral fellows from institutions across the US attended the Summer School this year. The format of the meeting in recent years has emphasized hands-on experience with CHRNS instruments. For much of the week, students in small subgroups circulated among various instruments set up to perform illustrative experiments, and analyzed data using NCNR-supplied resources. Among the experiments was a characterization by SANS of the structure of clay platelets dispersed in water. The neutron reflectometry experiments comprised measurements on thin films and multilayer materials. On the final day, the subgroups made presentations on the results of their studies. According to student evaluations, the school was highly effective in introducing them to the principles and practice of structural studies with neutron instruments.

Fig. 3. Eighth Annual Summer School on Neutron Scattering participants concentrate on neutron reflectometry results under the guiding hand of NCNR's Sushil Satija.

The NIST neutron source (NBSR) operated for 153 full power (20 MW) days or approximately 94 % of the scheduled time for this year. A typical operating year consists of seven cycles. A cycle has 38 days of continuous full power operation, followed by 11 days of shutdown maintenance, refueling, and startup preparations. This year, the NBSR was in a scheduled extended shutdown for maintenance and facility improvements until March 6, 2002. Those improvements included a new cold source, new transformers and switchgear for the building electrical system, a new plume-abatement cooling tower, and new shim arm seal assemblies. The new seal assemblies have characteristics superior to the old assemblies and provide greater assurance of dependable shim arm operation. The replacement of the electrical equipment and the cooling tower will increase the reliability of the NBSR over the next 25 years. In pursuit of that same goal, detailed inspections of vital systems and components were completed using ultrasonic probes, visual examinations, and remote examinations with miniature cameras and fiber-optic imaging equipment. The only major maintenance item scheduled for completion this shutdown was a determination of the status of the Thermal Column Tank Cooling System. After a thorough investigation, the capability of the Thermal Column was preserved by reconfiguring the cooling system and replacing original components within the biological shield. A new tank has been ordered and will be available if it becomes necessary to replace the tank in the future.

Seymour H. Weiss, Chief, Operations & Engineering

A number of important personnel issues were addressed in FY2002, including the effect of a surge of impending retirements on the NBSR. All licensed operators were requalified this year. Three new senior operators were licensed by the Nuclear Regulatory Commission, a new deputy chief for Operations was appointed, and significant progress was made on addressing recruitment and retention questions.

Thomas J. Myers, Deputy Chief, and Chief of Operations

Substantial changes to facility security were completed this year to fulfill the intent of the President's directives on homeland security. A vehicle exclusion area was established and surveillance equipment was improved. Other changes are on-going and Operations & Engineering is consulting with the U.S. Nuclear Regulatory Commission on security matters on a regular basis.

DAVE and Other Software Developments

Scientists at the NCNR, with support from the National Science Foundation via CHRNS, have developed a new software tool for the reduction, visualization, and analysis of neutron inelastic scattering data. DAVE, short for the Data Analysis and Visualization Environment, is an integrated suite of interactive software tools with a visual interface for treating and analyzing neutron inelastic scattering data sets. Using a powerful graphical interface, users can reduce their data from one of the inelastic spectrometers, make cuts through the scattering function, and fit them with the lineshape of their choice from a library of model functions.

The goal of the DAVE software package is to allow users, whose neutron scattering experience ranges from casual to expert, to reduce, visualize, and analyze their inelastic neutron scattering data sets with a minimum of effort by using a set of visually intuitive tools. The software has been in use on many of the inelastic neutron scattering instruments since January 2002 and was released to the user community in July. The source code is available from the NCNR website to run on PC, Linux, and Mac platforms. Project and download information are available at http://www.ncnr.nist.gov/dave.

New, easy to use software for reducing and fitting neutron reflectivity data is under active development at the NCNR. The new data reduction tools employ an intuitive graphical interface developed using open source software to read and process a variety of raw data files, including specular scans, background measurements, rocking curves, polarized beam, and slit scans. Using these new tools, the user can perform a variety of data correction and manipulation tasks to produce reduced data sets of the sample reflectivity as a function of wavevector. The software supports a wide range of data formats from both the NG-7 and NG-1 reflectometers and single channel or multichannel, position-sensitive detectors.

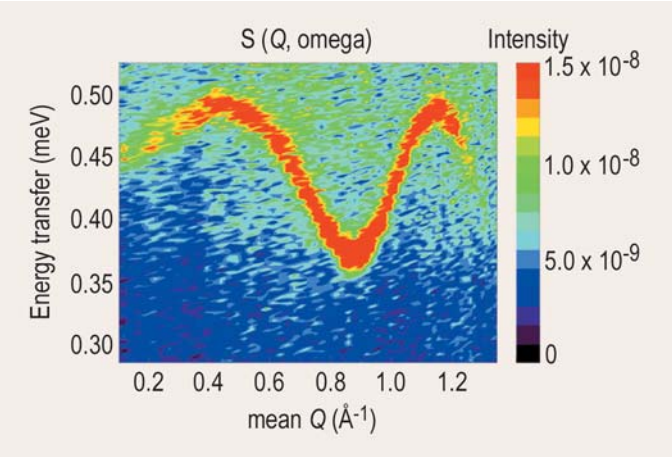

Fig. 1. An example of DAVE output: Dispersion curve of a magnetic excitation as measured using the Disk Chopper Spectrometer.

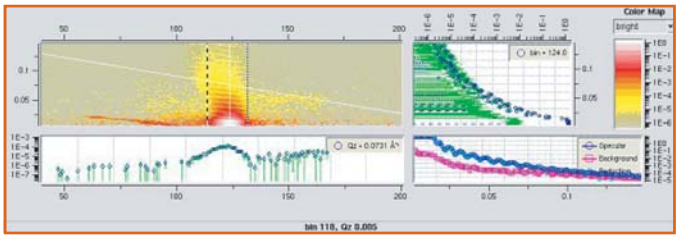

Fig. 2. Graphical interface image of neutron reflectivity data obtained using a position sensitive detector with corresponding slices of constant wavevector.

A new graphical interface has also been developed for the reflectivity-fitting program 'mlayer' [1]. This program allows users to model and fit scattering length density profiles to measured reflectivity data. The new interface for this program provides a wide set of graphical tools for adjusting and refining model parameters, controlling the fit, and constraining the model profile. A similar graphical interface has also been developed for the program that treats polarized neutron reflectivity data. Further information on these tools is available at the website: www.ncnr.nist.gov/programs/reflectometry/software.

New Monochromator Drum Shields

This year the NCNR ordered two new monochromator drum shields for the new BT-7 neutron triple axis spectrometer and for the BT-4 filter analyzer instrument. Fabrication and testing of one of these drum shields has been completed and delivery of both is planned for Dec. 2002.

Monochromator drum shields are a key component in crystal spectrometers, forming a thick, moving shield that surrounds the intensely illuminated monochromator and allowing the diffracted beam to be directed at a variety of

take-off angles towards the sample. The design of the new drum shields is based on a concept originally developed for the Advanced Neutron Source project at Oak Ridge National Laboratory which uses pairs of counter-opening shield wedges to allow the large diameter neutron beams to enter the drum. For the NCNR drums, this design concept was adapted for the specific dimensions of the NCNR source and to optimize the manufacturability of the shield. This double wedge design uses a precision cam track to position the shield wedges around the 20 cm beam opening as the drum is rotated to various take-off angles. The drum shield is rotated using a stepper motor driven gear system. The take-off angle range is between 0° and 120° and the drum can be built into either clockwise or counter-clockwise rotating models. The NCNR will be the first neutron laboratory to implement this double-wedge design for a monochromator shield.

Sample Environment Equipment

The suite of available sample support equipment at the NCNR continues to be upgraded and enhanced. This year, the superconducting magnet system with dilution refrigeration was upgraded from the seven Tesla coils available last year to the full design field coils that provide 11.5 Tesla. This system has demonstrated a 22 mK base temperature and full magnetic field strength.

The NCNR also received a new nine Tesla horizontal field superconducting magnet with single crystal windows using a design specifically optimized for small angle scattering experiments. This system uses a split coil design and windows in either direction to allow the magnetic field to be directed parallel or perpendicular to the neutron beam axis. Extensive heat shielding extends operation of the magnet to the higher sample temperatures needed for biology or polymer physics experiments without significantly altering liquid helium consumption.

Other new equipment made available this year includes a pulse tube closed cycle refrigerator (CCR) with an operating temperature range of 3 K to 325 K, two low temperature CCRs (10 K to 325 K), one high temperature CCR (15 K to 800 K), one 50 mm helium cryostat (1.5 K to 300 K) and fifteen additional temperature controllers.

Facility Improvements

Taking advantage of the opportunity provided by an extended interruption in routine operations, the NCNR staff completed several improvements to the facility during the outage early this year. The helium gas blanketing system, which provides a continuous flow of helium gas to the first 1.5 m of neutron guide closest to the cold source, was replaced with a new gas control system. Sensors and controllers on the guide vacuum systems were replaced and upgraded during the cold source installation. A computerized supervisory and control system for the facility was expanded to include monitoring of the guide vacuum pumping system.

Fig. 3. George Baltic (center, NCNR) confirms completion of a monochromator drum with Paul Brand (left, NCNR) and Rich Porter, president of Ingersol Contract Manufacturing Company.

Several improvements were made in C100, the location of the thermal neutron instruments. These include the installation of wiring and breaker panels that are part of a new power distribution system for the thermal instruments. The new system provides each neutron station with independent panels and outlet locations at the floor level adjacent to the experimental work area. A new catwalk system was also designed for accessing the face of the biological shield above the thermal instruments. This will be a significant safety and performance improvement for maintenance activities in this area. A prototype for a perimeter shield was also accepted this year. The perimeter shields surround the thermal neutron spectrometers and separate the operating area of the spectrometers from other work areas on the floor.

In the Guide Hall, the concrete floor was repainted. The original surface was badly worn and needed replacement. A three-color design was adopted to help differentiate work areas, walkways, and fire protection equipment.

References

[1] J.F. Ankner and C.F. Majkrzak, SPIE **178**, 260 (1992).

Publications[1]

Abdurashitov, J. N., Gavrin, V. N., Girin, S. V., Gorbachev, V. V., Gurkina, P. P., Ibragimova, T. V., Kalikhov, A. V., Khairnasov, N. G., Knodel, T. V., Mirmov, I. N., Shikhin, A. A., Veretenkin, E. P., Vermul, V. M., Yants, V. E., Zatsepin, G. T., Bowles, T. J., Teasdale, W. A., Nico, J. S., Cleveland, B. T., Elliott, S. R., Wilkerson, J. F., "Measurement of the Solar Neutrino Capture Rate by the Russian American Gallium Solar Neutrino Experiment During One-Half of the 22-Year Solar Cycle Activity," Jour. Exp. Th. Phys., in press.

Abdurashitov, J. N., Gavrin, V. N., Kalikhov, A.V., Matushko, V. L., Shikhin, A. A., Yants, V. E., Zaborskaia, O. S., Adams, J. M., Nico, J. S., Thompson, A. K., "A High Resolution Low Background Fast Neutron Spectrometer," Nucl. Instrum. Meth. A **476** (1-2), 318 (2002).

Allen, A. J., Long, G. G., Boukari, H., Ilavsky, J., Kulkarni, A., Sampath, S., Herman, H., Goland, A. N., "Microstructural Characterization Studies to Relate the Properties of Thermal Spray Coating to Feedstock and Spray Conditions," Surf. Coat. Techn. **146**, 544 (2001).

Amos, T. G., Huang, Q., Lynn, J. W., He, T., Cava, R. J., "Carbon Concentration Dependence of the Superconductivity Transition Temperature and Structure of MgC_xNi_3," Solid State Commun. **121** (2-3), 73 (2002).

Anderson, C. R., Andersen, K. H., Stirling, W. G., Sokol, P. E., Dimeo, R. M., "Dynamics of Superfluid ^{4}He Confined in Xerogel Glass," Phys. Rev. B **65,** 174509-174519 (2002).

Argyriou, D. N., Lynn, J. W., Osborn, R., Campbell, B., Mitchell, J. F., Ruett, U., Bordallo, H. N., Wildes, A., Ling, C. D., "Glass Transition in the Polaron Dynamics of CMR Manganites," Phys. Rev. Lett. **89**, 036401 (2002).

Arsenov, A. A., Bebenin, N. G., Gaviko, V. S., Adams, C. P., Lynn, J. W., Mashkautsan, V. V., Mukovskii, M., Shulyatev, D. A., Ustinov, V. V., Zainullina, R. I., "Absence of Polaron Conductivity in $La_{0.8}Ba_{0.2}MnO_3$," Phys. Status Solidi A **189** (3), 673 (2002).

Bagci, V. K., Gulseren, O., Yildirim, T., Gedik, Z., Ciraci, S., "Metal Nanoring and Tube Formation on Carbon Nanotubes," Phys. Rev. B **66,** 045409 (2002).

Baklanov, M. R., Kondoh, E., Lin, E. K., Gidley, D. W., Lee, H.-J., Mogilnikov, K. P., Sun, J. N., "Comparative Study of Porous SOG Films with Different Non-Destructive Instrumentation," in *Proceedings of the National Interconnect Technology Conference*, in press.

Bao, W., Aeppli, G., Christianson, A. D., Fisk, Z., Hundley, M. F., Larderda, A. H., Lynn, J. W., Pagliuso, P. G., Sarrao, J. L., Thompson, J. D., "Magnetic Properties of Heavy Fermion Superconductors $CeRhIn_5$ and $CeRhIn_8$," in *Proceedings of Physical Phenomena at High Magnetic Fields-IV* (World Scientific, Singapore, 2002), p. 350.

Bao, W., Aeppli, G., Lynn, J. W., Pagliuso, P. G., Sarrao, J. L., Hundley, M. F., Thompson, J. D., Fisk, Z., "Anisotropic Three-Dimensional Magnetic Fluctuations in Heavy Fermion $CeRhIn_5$," Phys. Rev. Lett. **65**, 100505 (2002).

Bao, W., Christianson, A. D., Pagliuso, P. G., Sarrao, J. L., Thompson, J. D., Lacerda, A. H., Lynn, J. W., "Effect of La-Doping on Magnetic Structure in Heavy Fermion $CeRhIn_5$," Physica B **312**, 120 (2002).

Bao, W., Trevino, S. F., Lynn, J. W., Pagliuso, P. G., Sarrao, J. L., Thompson, J. D., "Effect of Pressure on Magnetic Structure in Heavy Fermion $CeRhIn_5$," Appl. Phys. A, in press.

Bauer, B. J., Byrd, H. M., Guttman, C. M., "Small Angle Neutron Scattering Measurements of Synthetic Polymer Dispersions in Matrix-Assisted Laser Desorption/Ionization Matrixes," Rapid Commun. Mass. Spectrom. **16** (15), 1494 (2002).

Bauer, B. J., Guttman, C. M., Liu, D. W., Blair, W. R., "Tri-alpha-naphthylbenzene as a Crystalline or Glassy Matrix for Matrix-assisted Laser Desorption/Ionization: a Model System for the Study of Effects of Dispersion of Polymer Samples at a Molecular Level," Rapid Commun. Mass. SP **16** (12), 1192 (2002).

Becker, D. A., Mackey, E. A., "Analytical Intercomparison on NIST Renewal Pine Needles SRM 1575a," Trans. Am. Nucl. Soc., in press.

Becker, P. R., Mackey, E. A., Demiralp, R., Epstein, M. S., Donais, M. K., Goessler, W. A., Porter, B. J., Wise, S. A., "Heavy Metals and Other Trace Elements Measured in Tissues of Marine Mammals Archived by the Alaska Marine Mammal Tissue Archival Project from the Bering Sea and Cook Inlet, Alaska," in *Proceedings of The AMAP Heavy Metals Workshop,* in press.

Bianco-Peled, H., Dori, Y., Satija, S., Schneider, J., Sung, L., Tirrell, M., "Structural Study of Langmuir Monolayers Containing Lipidated Poly (Ethylene Glycol) and Peptides," Langmuir **17** (22), 6931 (2001).

Biggs, S., Walker, L. M., Kline, S. R., "The Formation of an Irreversibly Adsorbed and Organised Micelle Layer at the Solid-Liquid Interface," Science, in press.

Bishop, R. L., Blackman, M. J., "Instrumental Neutron Activation Analysis of Archaeological Ceramics: Scale and Interpretation," Acc. Chem. Res., in press.

Blackman, J. C., Raman, S., Dickens, J. K., Lindstrom, R. M., Paul, R. L., Lynn, J. E., "Thermal-Neutron Capture by Pb-208," Phys. Rev. C **65** (4), 045801 (2002).

Blackman, M. J., Redford, S., "Northern Syrian Luster and Fruitware: Petrographic and Chemical Implications for Productions and Distribution," Antiquity, in press.

[1] Publications are counted over a 1-year period. This year we inaugurate a policy of counting publications up through July 31, 2002. Hence, there is overlap with publications reported for 2001 that were counted through October 31, 2001.

Bliesner, R., Uma, S., Yokochi, A., Sleight, A. W., "Structure of $NaBi_3V_2O_{10}$ and Implications for Ionic Conductivity," Chem. Mater. **13** (11), 3825, 2001.

Bordallo, H. N., Chapon, L. C., Cook., J. C., Copley, J. R. D., Goremychkin, E., Kern, S., Lee, S.–H., Yildirim, T., Manson, J. L., "Spin Excitations in 3D Molecular Magnets Probed by Neutron Scattering," Appl. Phys. A, in press.

Borgoul, P., Kidwell, C. B., Ondov, J. M., "System for Precise Control of Volumetric Flow Rate During Sampling with a Cascade Impactor. Aerosol. Sci. Technol. **36**, 397 (2002).

Bossev, D. P., Kline, S. R., Israelachvili, J. N., Paulaitis, M. E., "Pressure-Induced Freezing of the Hydrophobic Core Leads to a $L_1 \rightarrow H_1$ Phase Transition for $C_{12}E_5$ Micelles in D_2O," Langmuir **17** (25), 7728 (2001).

Bossev, D. P., Ferdinand, S., Paulaitis, M. E., "Effect of Pressure on Microstructure in Water-in-Oil and Oil–in-Water Microemulsions for $C_{12}E_5$ n-Octane/D_20 Mixtures," Langmuir, in press.

Branford, W., Green, M. A., Neumann, D. A., "Structure and Ferromagnetism in Mn^{4+} Spinels: $AM_{0.5}Mn_{1.5}O_4$ (A = Li, Cu; M = Ni, Mg)," Chem. Mater. **14**, 1649 (2002).

Broholm, C., Aeppli, G., Chen, Y., Dender, D. C., Enderle, M., Hammar, P. R., Honda, Z., Katsumata, K., Landee, C. P., Oshikawa, M., Regnault, L. P., Reich, D. H., Shapiro, S. M., Sieling, M., Stone, M. B., Turnbull, M. M., Zaliznyak, I., and Zheludev, A., "Magnetized States of Quantum Spin Chains," in High Magnetic Fields – Applications in Condensed Matter Physics and Spectroscopy, (edited by C. Berthier, L.P. Levy, G. Martinez, Springer Verlag 2002), p. 211.

Brown, C. M., Manson, J. L., "Solid State Ligand Dynamics in Interpreting Mn[N(CN)2]2(pyrazine): A Neutron Spectroscopy Study," J. Amer. Chem. Soc. **124**, 12600 (2002).

Bu, Z., Chowdhuri, Z., Callaway, D. J. E., "Coexistence of Fluctuating Secondary Structure and Long-Range Tertiary Interaction in Highly Denatured Alpha-Lactalbumin – A Neutron Scattering Study," Protein Sci., in press.

Bu, Z., Cook, J., Callaway, D. J. E., "Dynamics Regimes and Correlated Structural Dynamics in Native and Denatured Alpha-Lactalbumin," J. Mol. Biol. **312,** 865 (2001).

Burghardt, W. R., Krishnan, K., Bates, F. S., Lodge, T. P., "Linear Viscoelasticity of a Polymeric Bicontinuous Microemulsion," Macromol. **35**, 4210 (2002).

Butler, P. D., Porcar, L., Warr, G. G., Hamilton, W. A., comment on "Evidence of a Sponge-to-Lamellar Phase Transition Under Shear by X-Ray Scattering Experiments in Couette Cell," Phys. Rev. Lett. **85**, 059601 (2002).

Caliskan, G., Kisliuk, A., Tsai, A. M., Soles, C. L., Sokolov, A. P., "Influence of Solvent on Dynamics and Stability of a Protein," J. Non-Cryst. Solids **307**, 887 (2002).

Campbell, B. J., Billinge, S. J. L., Lynn, J. W., Osborn, J. W., Osborn, R., Sinha, S. K., "The Structure of Jahn-Teller Polarons in the Colossal Magnetoresistive Manganites," in *Proceedings From Semiconductors to Proteins: Beyond the Average Structure,* edited by Billinge, S. J. L., and Thorpe, M. F., (Kluwer, Academic/Plenum, New York, 2002) p. 183.

Campbell, B. J., Osborn, R., Argyriou, D. N., Vasiliu-Doloc, L., Mitchell, J. F., Sinha, S. K., Ruett, L. U., Islam, Z., Lynn, J. W., "Structure of Nanoscale Polaron Correlations in a Colossal Magnetoresistive Manganite," Phys. Rev. B **65** (1), 014427 (2002).

Cappelletti, R. L., Clutter, L. K., edited by, "MSEL, FY2001 Programs and Accomplishments," NISTIR 6798, (2001).

Cappelletti, R. L., Clutter, L. K., edited by, "NCNR 2001 Accomplishments an Opportunities," NIST SP 977, (2002).

Carpenter, J. M., Iverson, E. B., Mildner, D. F. R., "Time Focusing of Pulsed-Source Crystal Analyzer Spectrometers II Practical Expressions," Nucl. Instrum. & Methods **483** (3), 784 (2002).

Chen, W. C., Bailey, C., Borchers, J. A., Gentile, T. R., Hussey, D. H., Majkrzak, C. F., O'Donovan, K. V., Remmes, N., Snow, W. M., Thompson, A. K., "Polarized ^{3}He Analysers for Neutron Reflectometry," Physica B, in press.

Chen, W. C., Beuser, B. J., "Small-Angle Neutron Scattering Measurements of Deuteride (Hydride) Formation and Decomposition in Single-Crystal Pd," Phys. Rev. B **65**, 014102 (2001).

Chen, W.-R., Chen, S.-H., Mallamace, F., "Small-Angle Neutron Scattering Study of the Temperature-Dependent Attractive Interaction in Dense L64 Copolymer Micellar Solutions and its Relation to Kinetic Glass Transition," Phys. Rev. E **66,** 021403 (2002).

Chen, Y. Y., Lodge, T. P., Bates, F. S., "Influence of Long-Chain Branching on the Miscibility of Poly(ethylene-r-ethylethylene) Blends with Different Microstructure," J. Polym. Sci. **40**, 466 (2002).

Chen-Mayer, H. H., Lamaze, G. P., Coakley, K. J., Satija, S. K., "Two Aspects of Thin Film Analysis: Boron Profile and Scattering Length Density Profile," Nuc. Inst. Meth. B., in press.

Chen-Mayer, H. H., Lamaze, G. P., Mildner, D. F. R., Zeissler, R., Gibson, W. M., "Neutron Imaging and Prompt Gamma Activation Analysis Using a Monolithic Capillary Neutron Lens," in *Proceedings of the 3rd International Congress on Analytic Sciences, Analytical Science*, (ICAS 2001, Tokyo, Japan, August 2001) p. 629.

Chen-Mayer, H. H., Mildner, D. F. R., Lamaze, G. P., Lindstrom, R. M., "Imaging of Neutron Incoherent Scattering from Hydrogen in Metals," J. Appl. Phys. **91** (6), 3669 (2002).

Choi, S. M., Chen, S. H., Sottmann, T., Strey, R., "The Existence of Three Length Scales and Their Relation to the Interfacial Curvatures in Bicontinuous Microemulsions," Physica A **304**, 85 (2002).

Chong, K. P., Sung, L., VanLandingham, M. R., "Solid Micromechanics: Research and Challenges," in *Proceedings of the 13th Micromechanics Europe (MME 2002) Workshop*, (Sinaia, Romania, Oct. 6-8, 2002), in press.

Ciraolo, M. F, Hanson, J. C., Toby, B. H., Grey, C. P., "Combined X-Ray and Neutron Powder Refinement and NMR Study of Hydrochlorofluorocarbon HCFC-124a (CF_2HCF_2Cl) Binding on NaX," J. Phys. Chem. B **105** (49), 12330 (2001).

Clarke, W. B., Guscott, R., Downing, R. G., Lindstrom, R. M., "Endogenous Lithium and Boron Red Cell to Plasma Ratios: Normal Subjects Versus Bipolar Patients Not on Lithium Therapy," Bipolar Disorders, in press.

Clarke, W. B., Guscott, R., Lindstrom, R. M., "Binding of Lithium and Boron to Human Plasma Proteins II: Results for a Bipolar Not on Lithium Therapy," Biol. Trace Element Res., in press.

Coakley, K. J., Chen-Mayer, H. H., Lamaze, G. P., Simons, D. S., Thompson, P. E., "Calibration of a Stopping Power Model for Silicon Based on Analysis of Neutron Depth Profiling and Secondary Ion Mass Spectrometry Measurements," J. Nucl. Instrum. & Meth. B **192** (4), 349 (2002).

Coakley, K. J., Yang, G. L., "Estimation of the Neutron Lifetime: Comparison of Methods Which Account for Background," Phys. Rev. C **65** (6), 064612 (2002).

Colle, R., Zimmerman, B. E., "A Dual-Compensated Cryogenic Microcalorimeter for Radioactivity Standardizations," Appl. Radiat. Isotopes **56** (1-2), 223 (2002).

Copley, J. R. D., "NIST Recommended Practice Guide; The Fundamentals of Neutron Powder Diffraction," NIST SP 960-2, (2001).

Crawford, M. K., Harlow, R. L., Marshall, W., Li, Z., Cao, G., Lindstrom, R. L., Huang, Q., Lynn, J. W., "Structure and Magnetism of Single Crystal $Sr_4Ru_3O_{10}$: A Ferromagnetic Triple-Layer Ruthenate," Phys. Rev. B **65**, 214412 (2002).

DeWall, J., Dimeo, R. M., Sokol, P. E., "Slow Diffusion of Molecular Hydrogen in Zeolite 13X," J. Low Temp. Phys., in press.

Deyhim, A., Zhou, J., Schwartz, F., Krueger, S., Gregurick, S., "Small Angle Neutron Scattering Studies of PNA & DNA Systems," Biophys. J. **82** (1), 622 (2002).

Dimeo, R. M., Chowdhuri, Z., Meyer, A., Gehring, P. M., Neumann, D. A., "The NIST High-Flux Backscattering Spectrometer," Appl. Phys. A, in press.

Dimeo, R. M., Neumann, D. A., Glanville, Y., Minor, D. B., "Pore Size Dependence of Rotational Tunneling in Confined Methyl Iodide," Phys. Rev. B **66**, 104201 (2002).

Douglas, J. F., Kent, M. S., Satija, S. K., Karim, A., "Polymer Brushes: Structure and Dynamics," Encyclopedia of Materials: Science and Technology, 7218, (2001).

Downing, R. G., Iyengar, G. V., "Methodological Issues in the Analytical Determination of Boron," Environ. Health Perspect., in press.

Dubsky, J., Matejicek, J., Prask, H. J., Gnäupel-Herold, T., "Residual and Applied Stresses in Plasma Sprayed Cr_2O_3 Coatings," Mater. Sci. Forum **404**, 419 (2002).

Dubsky, J., Prask, H. J., Matejicek, J., Gnäupel-Herold, T., "Stresses in Plasma Sprayed Cr_2O_3 Coatings Measured by Neutron Diffraction," in *Proceedings of the International Conference on Neutron Scattering* (Munich, Germany, September 2001), in press.

Dullo, A. R., Ruddy, F. H., Seidel, J. G., Adams, J. M., Nico, J. S., Gilliam, D. M., "The Neutron Response of Miniature Silicon Carbide Semiconductor Detectors," Nucl. Instrum. Meth. A., in press.

Dyar, D., Wiedenbeck, M., Robertson, D., Cross, L. R., Delaney, J. S., Ferguson, K., Francis, C. A., Grew, E. S., Guidotti, C. V., Hervig, R. L., Hughes, J. M., Husler, J., Leeman, W., McGuire, A. V., Rhede, D., Rothe, H., Paul, R. L., Richards, I., Yates, M., "Reference Minerals for Microanalysis of Light Elements," Geostandards Newsletter **25** (2-3), 441 (2001).

Eid, K., Portner, D., Borchers, J. A., Loloee, R., Tsoi, M., O'Donovan, K. V., Pratt, W. P., Bass, J., "Mean-Free Path Effects in CPP Magnetoresistance of Magnetic Multilayers," Phys. Rev. B **65** (5), 054424 (2002).

Elliot, J., Meuse, V., Silin, V., Krueger, S., Woodward, J. T., Petralli-Mallow, T. P., Plant, A. L., "Biomedical Membranes on Metal Supports: Opportunities and Challenges," in *Proceedings of the Biomolecular Films: Design, Function, and Application*, edited by J. Rusling (New York, Marcel Dekker, Inc.), in press.

Faraone, A., Chen, S.-H., Fratini, E., Baglioni, P., Liu, L., Brown, C. M., "Rotational Dynamics of Hydration Water in Dicalcium Silicate by Quasi-Elastic Neutron Scattering," Phys. Rev. E **65** (4), 040507 (2002).

Farrow, R. F. C., Marks, R. F., Toney, M. F., Hannibal, K., David, S., Kellock, A., Borchers, J. A., O'Donovan, K. V., Smith, D. J., "Spontaneous Chemical Ordering and Exchange Bias in Epitaxial $Mn_{0.52}Pd_{0.48}$/Fe (001) Bilayers Prepared at Room Temperature," Appl. Phys. Lett. **80** (5), 808 (2002).

FitzGerald, S. A., Thomas, J. J., Neumann, D. A., Livingston, R. A., "A Neutron Scattering Study of the Role of Diffusion in the Hydration of Tricalcium Silicate," Cement and Concrete Res. **32** (3), 409 (2002).

Fitzsimmons, M. R., Leighton, C., Nogues, J., Hoffmann, A., Liu, K., Majkrzak, C. F., Dura, J. A., Groves, J. R., Springer, R. W., Arendt, P. N., Leiner, V., Lauter, H., Schuller, I. K., "Influence of In-Plane Crystalline Quality of an Antiferromagnet on Perpendicular Exchange Coupling and Exchange Bias," Phys. Rev. B **65** (13), 8 (2002).

Fratini, E., Chen, S.-H., Baglioni, P., Cook, J., Copley, J., "Dynamic Scaling of Quasi-Elastic Neutron Scattering Spectra From Interfacial Water," Phys. Rev. E **65** (1), 010201 (2001).

Fujita, M., Yamada, K., Hiraka, H., Gehring, P. M., Lee, S.-H., Wakimoto, S., Shirane, G., "Static Magnetic Correlations Near the Insulating-Superconducting Phase Boundary in $La_{2-x}Sr_xCuO_4$," Phys. Rev. B **65** (6), 064505 (2002).

Fultz, B., Witham, C. K., Udovic, T. J., "Distributions of Hydrogen and Strains in $LaNi_5$ and $LaNi_{4.75}Sn_{0.25}$," J. Alloys Compnds. **335** (1-2), 165 (2002).

Garvey, C. J., Parker, I. H., Simon, G. P., Whittaker, A. K., Knott, R. B., "An Experimental Study by NMR and SANS of the Ambient Hydration of Paper," in *Proceedings of the 12th Fundamental Research Symposium* (Pulp and Paper Fundamental Research Society, Oxford, 2001), p. 359.

Gehring, P. M., Wakimoto, S., Ye, Z.-G., Shirane, G., "Ferroelectric Dynamics in the Perovskite Relaxor PMN," in *AIP Conference Proceedings* **626**, 89 (2002).

Gehring, P. M., Wakimoto, S., Ye, Z.-G., Shirane, G., "Soft Mode Dynamics Above and Below the Burns Temperature in the Relaxor $Pb(Mg_{1/3}Nb_{2/3})O_3$," Phys. Rev. Lett., **87** (27), 277601 (2001).

Geissler, E., Hecht, A. M., "Treatment of Incoherent Signal Subtraction," in *Proceedings of the Frontiers in SAXS and SANS, ESRF-ILL-CEA Workshop* (Grenoble, France, February 12-13, 1999), edited by Deme B., Diat O., Narayanan T., Zemb T., Report No. ILL99DE3002, (2002).

Geissler, E., Hecht, A. M., Rochas, C., Horkay, F., Bley, F., Livet, F., "Structure and Dynamics of Silica-Filled Polymers by SANS and Coherent SAXS Scattering Methods and Polymers," *in Proceedings of the 20th Discussion Conference on Scattering Methods for the Investigation of Polymers,* (July 9-12, 2001, Prague, Czech Republic), in press.

Geissler, E., Horkay, F., Hecht, A. M., Deschamps, P., "Neutron Scattering From Elastomer Gels," Kautschuk, Gummi, and Kunstoffe **54**, 446 (2001).

Gentile, T. R., "Overview of Polarized Neutron Sources," in *Proceedings of the Ninth International Workshop on Polarized Sources and Targets* (Nashville, Indiana, USA, Sept. 30 – Oct. 4, 2001, edited by V.P. Derenchuk and B. von Przewoski, World Scientific, Singapore, 2001), p. 233.

Gentile, T. R., Rich, D. R., Thompson, A. K., Snow, W. M., Jones, G. L., "Compressing Polarized ^{3}He Gas with a Modified Diaphragm Pump," J. Res. Natl. Inst. Stand. Technol. **106**, 709-729 (2001).

Gibson, W. M., Chen-Mayer, H. H., Mildner, D. F. R., Prask, H. J., Schultz, A. J., Youngman, R., Gnäupel-Herold, T., Miller, M. E., Vitt, R., "Polycapillary Optics Based Neutron Focusing for Small Sample Neutron Crystallography," Advances In x-ray Analysis **45**, in *Proceedings of the 50th Denver X-Ray Conference* (July 2001, Denver, CO), in press.

Gibson, W. M., Schultz, A. J., Chen-Mayer, H. H., Mildner, D. F. R., Gnäupel-Herold, T., Miller, M. E., Prask, H. J., Vitt, R., Youngman, R., Carpenter, J. M., "Polycapillary Focusing Optic for Small Sample Neutron Crystallography," J. Appl. Cryst, in press.

Giebultowicz, T. M., Kepa, H., Blinowski, J., Kacman, P., "Neutron Diffraction and Reflectivity Studies of Interlayer Correlations in Magnetic Semiconductor Superlattices," Physics E **10** (1-3), 411 (2001).

Gilliam, D. M., Thompson, A. K., Nico J. S., "A Neutron Sensor For Detection of Nuclear Materials In Transport," in *Proceedings of URSSRA Workshop* (15-April 17, 2002, Washington, DC), in press.

Gilra, N., Cohen C., Briber, R. M., Bauer, B. J., Hedden, R., Panagiotopoulos, A. Z., "A SANS Study of the Conformational Behavior of Linear Chains in Compressed and Uncompressed End-Linked Elastomers," Macromol. **34** (22), 7773 (2001).

Glagolenko, I. Y., Carney, K. P., Kern, S., Goremychkin, E. A., Udovic, T. J., Copley, J. R. D., Cook, J. C., "Quantitative Analysis of UH_3 in U Metal and UO_2 Matrices by Neutron Vibrational Spectroscopy," Appl. Phys. A, in press.

Gnäeupel-Herold, T. T., "Single Crystal Elastic Constants From Powder Measurements," in *Proceedings of Accuracy in Powder Diffraction. III* (NIST Special Publication), in press.

Gnäeupel-Herold, T. T., Prask, H. J., Biancaniello, F. S., "Residual Stresses and Elastic Constants on Thermal Deposits," in *Proceedings of Recent Advances in Experimental Mechanics,* in press.

Granado, E., Huang, Q., Lynn, J. W., Gopalakrishnan, J., Greene, R. L., Ramesha, K., "Mesoscopic Phase Separation and Spin-Orbital Ordering in the Double Perovskite Ca_2FeReO_6," Phys. Rev. B, in press.

Granado, E., Martinho, H., Sercheli, M. S., Pagliuso, P. G., Jackson, D. D., Torelli, M., Lynn, J. W., Rettori, C., Fisk, Z., Oseroff, S. B., "Unconventional Metallic Magnetism in $LaCrSb_3$," Phys. Rev. Lett. **89** (10), 107204 (2002).

Greenberg, C. C., Teale, D. M., Foster, M. D., Turner, C. M., Corona-Galvan, S., Cloutet, E., Quirk, R. P., Majkrzak, C. F., Demaree, D., "Surface Segregation in Blends of Linear and Regularly Star Branched Polystyrene," Macromol., in press.

Greenberg, R. R., "A Practical Approach for Evaluating the Uncertainties of Instrumental Neutron Activation Analysis Measurements," Trans. Am. Nucl. Soc., in press.

Grey, I. E., Roth, R. S., Mumme, W. G., Planes, J., Bendersky, L., Li, C., Chenavas, J., "Characterization of New 5M and 7M Polytypes of Niobia-Doped $Ca_2Ta_2O_7$," J. Solid. Sate. Chem. **161** (2), 274 (2001).

Grull, H., Esker, A. R., Satija, S. K., Han, C. C., "Polymer Transport Across Isotope-Selective Interdiffusion Barriers," Europhys. Lett. **57** (4), 533 (2002).

Gu, X., Raghavan, D., Ho, D. L., Sung, M. R., VanLandingham, M. R., Nguyen, T., "Nanocharacterization of Surface and Interfaces of Different Epoxy Networks," in *Proceedings of the MRS Fall 2001 Meeting*, edited by Frank, C. W., in press.

Gu, X., Sung, L., Ho, D. L., Michaels, C. A., Nguyen, D., Jean, Y. C. Nguyen, T., "Surface and Interface Properties of PVDF/Acrylic Copolymer Blends Before and After UV Exposure," in *Proceedings of the 80th Annual Meeting Technical Program* (Oct. 30-Nov.1, New Orleans, LA, 2002), in press.

Gulseren, O., Cohen, R. E., "High Pressure Thermoelasticity of Body-Centered Cubic Tantalum," Phys. Rev. Lett. **65** (6), 064103 (2002).

Gulseren, O., Yildirim, T., Ciraci, S., "A Systematic *ab-initio* Study of Curvature Effects in Carbon Nanotubes," Phys. Rev. **65** (15), 153405 (2002).

Gulseren, O., Yildirim, T., Ciraci, S., Kilic, C., "First-Principles Study of the Electronic Structure of Carbon Nanotubes: Variable and Reversible Band Gap Engineering," Phys. Rev. B, in press.

Hammouda, B., Ho, D., Kline, S., "Neutron Scattering from Poly(ethylene oxide) / Water Gels," Macromol., in press.

Hamilton, W. A., Porcar, L., Butler, P. D., Warr, G. G., "Local Membrane Ordering of Sponge Phases at a Solid-Solution Interface," J. Chem. Phys. **116** (19), 8533 (2002).

Hanley, H. J. M., Muzny, C. D., Ho, D. L., Glinka, C. L., Manias, E., "A SANS Study of Organoclay Dispersions," Int. J. Thermophys. **22** (5), 1435, 2001.

Haseyama, T., Asahi, K., Bowman, J. D., Delheij, P. P. J., Funahashi, H., Ishimoto, S., Jones, G., Masaike, A., Masuda, Y., Matsuda, Y., Morimoto, K., Muto, S., Penttila, S. I., Pomeroy, V. R., Sakai, K., Sharapov, E. I., Smith, D. A., Yuan, V. W., "Measurement of Parity-Nonconserving Rotation of Neutron Spin in the 0.734-eV p-Wave Resonance of La-139," Phys. Lett. B **534** (1-4), 39 (2002).

Hassan, P. A., Raghavan, S. R., Kaler, E., "Microstructural Changes in SDS Micelles Induced by Hydrotropic Salt," Langmuir **18** (7), 2543 (2002).

Hauer, B., Hempelman, R., Udovic, T. J., Rush, J. J., Kocklemann, W., Jansen, E., Scafer, W., Richter, D. "Neutron Scattering Studies on the Vibrational Excitations and the Structure of Ordered Niobium Hydrides: The β and χ Phases," Phys. Rev. B, in press.

Hayashi, M., Hashimoto, T., Weber, M., Gruell, H., Esker, A., Han, C. C., Satija, S. K., "Transient Interface Instability in Bilayer Polymer Films as Observed by Neutron Reflectivity Studies," Macromol., in press.

Hecht, A. M., Horkay, F., Geissler, E., "Structure of Polymer Solutions Containing Fumed Silica," Phys. Rev. E. **64** (4), 402 (2001).

Heuser B. J., Chen, W. C., "Small-Angle Neutron Scattering Measurements of Deuteride (Hydride) Formation and Decomposition in Single-Crystal Pd," Phys. Rev. B **65** (1), 01402 (2002).

Hirota, K., Ye, Z.-G., Wakimoto, S., Gehring, P. M., Shirane, G., "Neutron Diffuse Scattering from Polar Nanoregions in the Relaxor $Pb(Mg_{1/3}Nb_{2/3})O_3$," Phys. Rev. B **65** (10), 104105 (2002).

Hjörvarsson, B., Andersson, G., Dura, J. A., Udovic, T. J., Isberg, P., Majkrzak, C. F., "Temperature Dependence of the Magnetic Interlayer Ordering in $Fe_3/V_{14}H_x$ (001) Superlattices," Phys. Rev. B, in press.

Ho, D. L., Hammouda, B., Kline, S. R., "Clustering of Poly(ethylene oxide) in Solution Revisited," Nature, in press.

Ho, D. L., Tsao, C. S., Chen, C. S., Yang, W. C., Yang, G., Chen, S., Han, C. C., "Self Assembled Single Molecule Crystals," Science, in press.

Hoffman, A., Fitzsimmons, M. R., Dura, J. A., Majkrzak, C. F., "Investigating Magnetic Proximity Effects in NiO/Pd with Polarized Neutron Reflectometry," Phys. Rev. B **65** (2), 24428 (2002).

Hoffmann, A., Yashar, P. C., Nogues, J., Liu, K., Majkrzak, C. F., Dura, J. A., Fritzsche, H., Schuller, I. K., "Influence of Interfacial Disorder and Temperature on Magnetization Reversal in Exchange-Coupled Bilayers," Phys. Rev. B **64** (10), 104415 (2001).

Horkay, F., Basser, P. J., Hecht, A. M., Geissler, E., "Calcium-Induced Volume Transition in Polyacrylate Hydrogels Swollen in Physiological Salt Solutions," Macrolmol. **2**, 207 (2002).

Horkay, F., Basser, P. J., Hecht, A. M., Geissler, E., "SANS from Strongly Charged Polyacrylate Hydrogels in Physiological Salt Solutions," Poly. Preprints, (223rd ACS National Meeting, Orlando, FL, April 7-11, 2002) **43** (1), 369 (2002).

Horkay, F., McKenna, G. B., Geissler, E., "Nanostructures in Swollen Polymer Networks," in *Proceedings of the Polymer Networks 98, 14th Polymer Networks, Group Conference* (Trondheim, Norway, June 28-July 1, 1998), The Wiley Polymer Networks Group Review, in press.

Horkay, F., McKenna, G. B., Geissler, E., "Structure and Thermodynamic Behavior of Polymeric Gels," ANTEC 2001 Proceedings (SPE/ANTEC 2001, Technomic Pub. Co., Inc., Lancaster, PA) **2**, 186 (2001).

Horkay, F., Uriarte, R. J., Hecht, A. M., Geissler, E., "Neutron Scattering Investigations on Gels," Polym. Preprints (222nd ACS National Meeting, Chicago, IL, August 26-30, 2001, Polymer Preprints) **43**, 268 (2001).

Huang, Q., He, T., Regan, K. A., Rogado, N., Hayward, M., Haas, M. K., Inumaru, K., Cava, R. J., "Temperature Dependence of the Structural Parameters of the Non-Oxide Perovskite Superconductor $MgCNi_3$," Physica C **363,** 215 (2001).

Huffman, P. R., "Ultracold Neutrons," in McGraw-Hill Yearbook of Science and Technology, The McGraw-Hill Publishing Co., New York **394** (2002).

Huffman, P. R., Thompson, A. K., Wietfeldt, F. E., Yang, G. L., Alvine, K. J., Brome, C. R., Dzhosyuk, S. N., Mattoni, C. E. H., Michniak, R. A., McKinsey, D. N., Yang, L., Doyle, J. M., Golub, R., Habicht, K., Koch, J., Lamoreaux, S. K., Coakley, K. J., Leite, M. L. G., Maia, L., Rodrigues, A. C. M., Zanotto, E. D., "Magnetic Trapping of Ultracold Neutrons: Prospects for an Improved Measurement of the Neutron Lifetime," in Fundamental Physics with Pulsed Neutron Beams, World Scientific Publishing Co. Pte. Ltd. **156** (2001).

Huffman, P. R., "An Experiment to Search for Parity-Conserving Time Reversal Invariance Using Epithermal Neutrons From the Spallation Neutron Source," in *Proceedings of the Workshop on Astrophysics, Symmetries, and Applied Physics at Spallation Neutron Sources*, in press.

Jeng, U., Lin, T. L., Liu, W. J., Tsao, C. S., Canteenwala, T., Chiang, L. Y., Sung, L. P., Han, C. C., "SANS and SAXS Study on Aqueous Mixtures of Fullerene-Based Star Ionomers and Sodium Dodecyl Sulfate," Physica A **304** (1-2), 191 (2002).

Kang, H. J., Pengcheng, D., Mandrus, D., Jin, R., Mook, H. A., Adroja, D. T., Bennington, S. M., Lee, S.-H., Lynn, J. W., "Doping Evolution of the Phonon Density of States and Electron-Lattice Interaction in $Nd_{2-x}Ce_xCuO_{4+\delta}$," Phys. Rev. B **66** (6), 064506 (2002).

Karlsson, E. B., Abdul-Redah, T., Udovic, T. J., Hjörvarsson, B., Chatzidimitriou-Dreismann, C. A., "Short-Lived Proton Entanglement in Yttrium Hydrides," Appl. Phys. A, in press.

Kent, M., "A Quantitative Study of Tethered Chains in Various Solution Conditions Using Langmuir Diblock Copolymer Monolayers," Rapid Commun. **21**, 243 (2000).

Kent, M. S., Yim, H., Sasaki, D. Y., Majewski, J., Smith, G. S., Shin, K., Satija, S., Ocko, B. M., "Segment Concentration Profile of Myoglobin Adsorbed to Metal Ion Chelating Lipid Monolayers at the Air-Water Interface by Neutron Reflection," Langmuir **18** (9), 3754 (2002).

Kepa, H., Kutner-Pielaszek, J., Blinowski, J., Twardowski, A., Majkrzak, C. F., Story, T., Kacman, P., Galazka, R. R., Ha, K., Swagten, H. J. M., De Jonge, W. J. M., Sipatov, A. Y., Volobuev, V., Giebultowicz, T. M., "Antiferromagnetic Interlayer Coupling in Ferromagnetic Semiconductor EuS/PbS(001) Superlattices," Europhysics Letters **56** (1), 54 (2001).

Kepa, H., Kutner-Pielaszek, J., Twardowski, A., Majkrzak, C. F., Sadowsh, J., Story, T., Giebultowicz, T. M., "Ferromagnetism of GaMnAs Studied by Polarized Neutron Reflectometry," Phys. Rev. E **64** (12), 121302 (2001).

Kepa, H., Kutner-Pielaszek, J., Twardowski, A., Majkrzak, C. F., Story, T., Sadowski, J., Giebultowicz, T. M., "Polarized Neutron Reflectometry Studies of GaMnAs/GaAs Superlattices," Applied Physics A, in press.

Kepa, H., Kutner-Pielaszek, J., Twardowski, A., Sipatov, A. Y., Majkrzak, C. F., Story, T., Galazka, R. R., Giebultowicz, T. M., "Interlayer Correlations in Ferromagnetic Semiconductor Superlattices EuS/PbS," J. Magn. Magn. Mater. **226**, 1795 (2001).

Khalifah, P., Ho, D. M., Huang, Q., Cava, R. J., "The Structure and Properties of Beta-La_3RuO_7: A New Structure Type with Isolated RuO_6 Octahedra," J. Solid State Chem. **165** (2), 359 (2002).

Khalifah, P., Osborn, R., Huang, Q., Zandergen, H. W., Jin, R., Liu, Y., Mandrus, D., Cava, R. J. "Orbital Ordering Transition in $La_4Ru_2O_{10}$," Science **297**, 2237 (2002).

Khalyavin, D. D., Troyanchuk, I. O., Kasper, Huang, Q., Lynn, J. W., Szymczak, H., "Magnetic Structure of $TbBaCo_2O_{5.4}$ Perovskite," J. Mater. Research **17** (4), 838 (2002).

Khaykovich, B., Lee, Y. S., Erwin, R. W., Lee, S.-H., Wakimoto, S., Thomas, K. J., Kastner, M. A., Birgeneau, R. J., "Enhancement of Long-Range Magnetic Order by Magnetic Field in Superconducting La_2CuO_{4+y}," Phys. Rev. B **66** (1), 014528 (2002).

Kim, E., Suh, H. R., Kim, H., Char, K., Hong, J., Lee, S. H., Satija, S. K., Ivkov, R., "Neutron Reflectivity From the Monolayer of SANS Random Copolymer," Mol. Cryst. Liq. Cryst. **371**, 211 (2002).

Kim, H., Huang, Q. Z., Lynn, J. W., Kauzlarich, S. M., "Neutron Diffraction Study of the Ternary Metal Zintl Compound $Ca_{14}MnSb_{11}$," J. Solid. State. Chem., in press.

Kim, Y. J., Wakimoto, S., Shapiro, S. M., Gehring, P. M., Ramirez, A. P., "Neutron Scattering Study of Antiferromagnetic Order in $CaCu_3Ti_4O_{12}$," Solid State Commun. **121** (11), 625 (2002).

Kline, S. R., Choi, S. M., Rosov, N., "Neutron Spin Echo Spectroscopy Studies of Polymerized Micelles," in *Proceedings Abstr. Pap. Am. Chem. Soc.* **222**, 53-PMSE, Part 2, 2001.

Koga, T., Shin, K., Zhang, Y., Seo, Y.-S., Rafailovich, M. H., Sokolov, J., Chu, B., Satija, S. K., "Polymer Thin Films in Supercritical CO_2," in *Proceedings of the ASR-2000*, J. Phys. Soc. Japan., in press.

Kondoh, E., Baklanov, M. R., Lin, E. K., Gidley, D. W., Nakashima, A., "Comparative Study of Pore Size of Low-Dielectric-Constant Porous Spin-on-Glass Films with Different Ways of Non-Destructive Instrumentation," Japan. J. Appl. Phys. **40**, L323 (2001).

Koubi, L., Tarek, M., Bandyopadhyay, S., Klein, M. L., "Membrane Structural Perturbations Caused by Anesthetics and Non-Immobilizers: A Molecular Dynamics Investigation," Biophys. J. **81** 3339 (2001).

Koubi, L., Tarek, M., Bandyopadhyay, S., Klein, M. L., Scharf, D., "Effects of the Non-Immobilizer Hexafluroethane on the Model Membrane Dimyristoylphosphatidylcholine," Anesthesiology **96** (4), 848 (2002).

Koo, T.-Y., Gehring, P. M., Shirane, G., Kiryukhin, V., Lee, S.-G., Cheong, S.-W., "Anomalous Transverse Acoustic Phonon Broadening in the Relaxor Ferroelectric $Pb(Mg_{1/3}Nb_{2/3})_{0.8}Ti_{0.2}O_3$," Phys. Rev. B **65** (14), 144113 (2002).

Krishnan, K., Chapman, B., Bates, F. S., Lodge, T. P., Almdal, K., Burghardt, W. R., "Effects of Shear Flow on a Polymeric Bicontinuous Microemulsions: Equilibrium and Steady State Behavior," J. Rheol. **46** (2), 529 (2002).

Krishnamoorti, R., Graessley, W. W., Zirkel, A., Richter, D., Hadjichristidis, N., Fetters, L. J., Lohse, D. J., "Melt-State Polymer Chain Dimensions as a Function of Temperature," J. Polymer Physics: Part B **40,** 1768 (2002).

Krishnamoorti, R., Silva, A. S., Mitchell, C. A., "Effect of Silicate Layer Anisotropy on Cylindrical and Spherical Microdomain Ordering in Block Copolymer Nanocomposites," J. Chem. Phys. **115** (15), 7175 (2001).

Kucklick, J. R., Becker, P. R., Struntz, W. D. J., Mackey, E. A., Porter, B. J., Schantz, M. M., Oflaz, R. D., Epstein, M. S., Wise, S. A., Rowles, T. K., McFee, W. E., Stolen, M. K., "Persistent Organchlorine Pollutants and Elements Determined in Tissues of Rough-Toothed Dolphins (Steno Bredanensis) Banked from a Mass Stranding Event," NISTIR 6857 (2002).

Kucklick, J. R., Christopher, S. J., Becker, P. R., Pugh, R. S., Porter, B. J., Schantz, M. M., Mackey, E. A., Wise, S. A., Rowles, T. K., "Description and Results of the 2000 NIST/NOAA Interlaboratory Comparison Exercise Program for Organic Contaminants and Trace Elements in Marine Mammal Tissues," NISTIR 6849 (2002).

Kwan, K. S., Nakatani, A. I., Ivkov, R., Papanek, P., "Silica Surface Treatment Effects on the Dynamics of Poly(dimethyl siloxane) by Time-Of-Flight Neutron Spectroscopy," Polymer Preprints **42** (1), 2001.

Lai, C. H., Ming, T., Erwin, R., Borchers, J. A., "Exchange Anisotropy Between Single Twin Domain NiO and NiFe," J. Appl. Phys. **91** (10), 7751 (2002).

La-Orauttapong, D., Noheda, B., Ye, Z.-G., Gehring, P. M., Toulouse, J., Cox, D. E., Shirane, G., "Phase Diagram of the Relaxor Ferroelectric $(1-x)Pb(Zn_{1/3}Nb_{2/3})O_{3-x}PbTiO_3$," Phys. Rev. B **65** (14), 144101 (2002).

Lee, H. J., Lin, E. K., Wang, H., Wu, W.-L., Chen, W., Moyer, E. S., "Structural Comparison of Hydrogen Silsesquioxane Based Porous Low-k Thin Films Prepared with Varying Process Conditions," Chem. Mater. **14** (4), 1845 (2002).

Lee, J. H., Balsara, N. P., Krishnamoorti, R., Jeon, H. S., Hammouda, B., "Designing Balanced Surfactants for Mixtures of Immiscible Polymers," Macromol. **34** (19), 6557, (2001).

Lee, S.-H., Broholm, C., Ratcliff, W., Gasparovic, G., Huang, Q., Kim, T.H., Cheong, S.-W., "Emergent Excitations in a Geometrically Frustrated Magnet," Nature **418**, 856 (2002).

Lee, S.-H., Ratcliff, W., Broholm, C., Kim, T. H., Huang, Q., Cheong, S. W., "Neutron Scattering Study of Neel to Spin Freezing Transition Versus Dilution in Geometrically Frustrated $ZnCr_{2-2x}Ga_{2x}O_4$," Phys. Rev. B, in press.

Lee, S.-H., Tranquada, J. M., Yamada, K., Buttrey, D. J., Li, Q., Cheong, S.-W., "Freezing of a Stripe Liquid," Phys. Rev. Lett. **88** (12), 126401 (2002).

Lefebvre, A. A., Lee, J. H., Balsara, N. P., Hammouda, B., "Critical Length and Time Scales During the Initial Stages of Nucleation in Polymer Blends," J. Chem. Phys. **116** (12), 4777 (2002).

Lefebvre, A. A., Lee, J. H., Balsara, N. P., Hammouda, B., "Neutron Scattering From Pressurized Polyolefin Blends Near the Limits of Mestastability," Macromol. **33** (21), 7977 (2000).

Leighton, C., Fitzsimmons, M. R., Hoffmann, A., Dura, J. A., Majkrzak, C. F., Lund, M. S., Schuller, I. K., "Thickness Dependent Coercive Mechanisms in Exchange Biased Bilayers," Phys. Rev. B **65** (6), 061103, 2002

Lenhart, J. L., Wu, W.-L., "Deviations in the Thermal Properties of Ultrathin Polymer Network Level," Macromol. **35** (13), 5145 (2002).

Levin, I., Amos, T. G., Nino, J. C., Vanderah, T. A., Reaney, I. M., Randall, C. A., Lanagan, M. T., "Crystal Structure of the Compound $Bi_2Zn_{2/3}Nb_{4/3}O_7$," J. Mater. Res. **17** (6), 1406 (2002).

Li, J., Yokochi, A., Sleight, A. W., Amos, T.G., "Strong Negative Thermal Expansion along the O-Cu-O Linkage $CuScO_2$," Chem. Mat. **14** (6), 2602 (2002).

Lin, E. K., Lee, H. J., Lynn, G. W., Wu, W. L., O'Neill, M. L., "Structural Characterization of a Porous Low-Dielectric-Constant Thin Film with a Non-Uniform Depth Profile," Appl. Phys. Lett. **81** (4), 607 (2002).

Lin, Y., Smith, T. W., Alexandridis, P., "Adsorption of a Rake-Tyoe Siloxane Surfactant onto Carbon Black Nanoparticles Dispersed in Aqueous Media," Langmuir **18**, 6147 (2002).

Lin, E. K., Soles, C. L., Goldfarb, D. L., Trinque, B. C., Burns, S. D., Jones, R. L., Lenhart, J. L., Angelopoulos, M., Willson, C. G., Satija, S. K., Wu, W.-L., "Direct Measurement of the Reaction Front in Chemically Amplified Photoresists," Science **297**, 372 (2002).

Lin, E. K., Wu, W.-L., Lin, Q. H., Angelopoulos, M., "Feature-Shape and Line-Edge Roughness Measurement of Deep Sub-Micron Lithographic Structures Using Small-Angle Neutron Scattering," in *Proceedings of the SPIE 26th Annual International Conference on Microlithography* **4344**, 414 (2001).

Lindstrom, R. M., and Greenberg, R. R., "Accuracy and Uncertainty in Radiochemical Measurements: Learning from Errors in Nuclear Analytical Chemistry," J. Nucl. Radiochem. Sci., 2, R1-4 (2001).

Lipson, D. A., Roberts, D. A., Hansen-Flaschen, J., Gentile, T., Jones, G., Thompson, A., Dimitrov, I. E., Palevsky, H. I., Leigh, J. S., Schnall, M., Rizi, R. R., "Pulmonary Ventilation and Perfusion Scanning Using Hyperpolarized Helium-3 MRI and Arterial Spin Tagging in Healthy Normal Subjects and in Pulmonary Embolism and Orthotopic Lung Transplant Patients," Magn. Reson. Med. **47**, 1073 (2002).

Long, S. E., Kelly, W. R., "Determination of Mercury in Coal by Isotope Dilution Cold-Vapor Generation Inductively Coupled Plasma Mass Spectrometry," Anal. Chem. **74** (7), 1477 (2002).

Lynn, J. W., Borchers, J. A., Huang, Q., Santoro, A., Erwin, R. W., "Magnetic Structure Determinations at NBS/NIST," J. Res. Natl. Inst. Stand. Technol. **106** (6), 953 (2001).

Lynn, J. W., Dadmun, M. D., Wu, W. L., Lin, E. K., Wallace, W. E., "Neutron Reflectivity Studies of the Interface Between a Small Molecule Liquid Crystal, and a Polymer," Liq. Cryst. **29** (4), 551 (2002).

Lynn, J. W., "Review of Neutron Interferometry: Lessons in Experimental Quantum Mechanics," by Rauch, H., Werner, S. A., Physics Today **55**, 56 (2002).

Majkrzak, C. F., Berk, N. F., "Advances in Specular Neutron Reflectometry," J. Appl. Phys. A, in press.

Manson, J. L., Bordallo, H. N., Lynn, J. W., Huang, Q., Feyerherm, R., Loose, A., Chapon, L., Argyriou, N., "Magnetic Ordering and Spin Excitations in $Mn(dca)_2(pyz)$ [dca = $N(CN)^-_2$; pyz = pyrazine], Appl. Phys. A, in press.

Mansour, F., Dimeo, R. M., Peemoeller, H., "High Resolution Inelastic Neutron Scattering From Water in Mesoporous Silica," Physical Review E **66**, 041307 (2002).

Maranzano, B. J., Wagner, N. J., "The Effects of Interparticle Interactions and Particle Size on Reversible Shear Thickening: Hard-Sphere Colloidal Dispersions," J. Rheol. **45** (5), 1205 (2001).

Martinho, H., Granado, E., Moreno, N. O., Garcia, A., Toniani, I., Rettori, C., Neumeier, J. J., Oseroff, S. B., "Strong Charge Carrier Effect on the Magnetic Coupling of La-Doped $CaMnO_3$," Physica B, in press.

Martter, T. D., Foster, M. D., Yoo, T., Xu, S., Lizzaraga, G., Quirk, R. P., Butler, P. D., "Determination of the Thermodynamics Interaction Parameter for Blends of Star and Linear Polybutadience," Macromol., in press.

Matejicek, J., Brand, P. C., Drews, A. R., Krause, A., Lowe-Ma, C., "Residual Stresses in Cold-Coiled Helical Compression Springs for Automotive Suspensions Measured by Neutron Diffraction," Metall. Mater. Trans. A, in press.

McKelvey C. A., Kaler, E. W., "Characterization of Nanostructured Hollow Polymer Spheres with Small-Angle Neutron Scattering (SANS)," J. Colloid Inter. Sci. **245** (1), 68 (2002).

McKinley, J. P., Zeissler, C. J., Zachara, J. M., Serne, R. J., Lindstrom, R. M., Schaef, H. T., Orr, R. D., "Distribution and Retention of 137Cs in Sediments at the Hanford Site, Washington," Environ. Sci. Technol. **35,** 3433 (2001).

Meyer, A., Schober, H., Dingwell, D. B., "Structure, Structural Relaxation and Ion Diffusion in Sodium Disilicate Metls," Europhysics Letters **59** (5), 708 (2002).

Michels, A., Weissmuller, J., Erb, U., Barker, J. G., "Measurements of a Magnetic-Field Dependent Correlation Length in Nanocrystalline Ni Using Small-Angle Neutron Scattering," Phys. Stat. Solid **189** (2), 509 (2002).

Mildner, D. F. R., Carpenter, J. M., "Time Uncertainty for Guided Long Wavelength Neutrons on a Pulsed Source," Nucl. Instrum. & Meth. **484** (1-3), 486 (2002).

Mildner, D. F. R., Chen-Mayer, H. H., Gibson, W. M., "Focusing Neutrons with Tapered Capillary Optics," J. Appl. Phys., in press.

Mildner, D. F. R., Chen-Mayer, H. H., Gibson, W. M., Gnäupel-Herold, T., Miller, M. E., Prask, H. J., Schultz, A. J., Vitt, R., Youngman, R., "A Monolithic Polycaplillary Focusing Optic for Polychromatic Neutron Diffraction Applications," Rev. Sci. Instrum. **73** (5), 1985 (2002).

Mildner, D. F. R., Chen-Mayer, H. H., Gibson, W. M., Schultz, A. J., "A Monolithic Polycapillary Focusing Optic for Polychromatic Neutron Diffraction Applications," in *Proceedings of the SPIE Conference* (July 2002, Seattle, WA), in press.

Mook, H. A., Dai, P., Hayden, S. M., Hiess, A., Lynn, J. W., Lee, S.-H., Dogan F., "Magnetic Ordering in $YBa_2Cu_3O_{6+x}$ Superconductors," Phys. Rev. B, in press.

Mukherjee, S., Cohen, R. E., Gulseren, O., "Vacancy Formation Enthalpy at High Pressure in Tantalum," Phys. Rev. B, in press.

Nair, S., Tsapatsis, M., Toby, B. H., Kuznicki, S. M., "A Study of Heat-Treatment Induced Framework Contraction in Strontium-ETS-4 by Powder Neutron Diffraction and Vibrational Spectroscopy," J. Am. Chem. Soc. **123** (51), 12781 (2001).

Nakatani, A. I., Chen, W., Schmidt, R. G., Gordon, G. V., Han, C. C., "Chain Dimensions in Polysilicate-Filled Poly (Dimethyl Siloxane)," Int. J. Thermophysics **23**, 199 (2002).

Nakatani, A. I., Chen, W., Schmidt, R. G., Gordon, G. V., Han, C. C., "Chain Dimensions in Polysilicate-Filled Poly(dimethyl siloxane)," Int. J. Thermophys. **23** (1), 199 (2002).

Nakatani, A. I., Ivkov, R., Papanek, P., Jackson, C. L., Yang, H., Nikiel, L., Gerspacher, M., Krishnamoorti, R., "The Significance of Percolation on the Dynamics of Polymer Chains Bound to Carbon Black," in *Proceedings of the Filled and Nanocomposite Polymer Materials*, edited by A. Nakatani, R. P. Hjelm, M. Gerpacher, R. Krishnamoorti, R. P., Materials Research Society Symposium Proceedings, Pittsburgh, PA) **661**, KK4.2.1 (2001).

Natali-Sora, I., Santoro, A., Huang, Q., "Oxidation States of Fe in $YBa_2Fe_3O_8$ from a Bond Valence Analysis of the Structure," J. Solid State Chem., in press.

Nico, J. S., Abdurashitov, J. N., Gavrin, V. N., Girin, S. V., Gorbachev, V. V., Ibragimova, T. V., Kalikhov, A. V., Khairnasov, N. G., Knodel, V. N., Mirmov, I. N., Shikhin, A., Verentenkin, E. P., Vermul, V. M., Yants, V. E., Zatsepin, G. T., Bowles, T. J., Teasdale, W. A., Wark, D. L., Cherry, M. L., Cleveland, B. T., Davis, R., Lande, K., Wildenhain, P. S., Elliott, S. R., Wilkerson, J. F., "Solar Neutrino Results From SAGE," in *Proceedings of the 10th International Baksan School: Particles and Cosmology*, edited by E. N. Alexeev, V. A. Matveev, K. H. S., Nirov, V. A. Rubakov, (Institute for Nuclear Research of the Russian Academy of Sciences, Moscow) p. 63 (2000).

Nieh, M.-P., Glinka, C. J., Krueger, S., Prosser, R. S., Katsaras, J., "A SANS Study of the Effect of Lanthanide Ions and Charged Lipids on the Morphology of Phospholipid Mixtures," Biophys. J. **82** (5), 2487 (2002).

Nieh, M.-P., Kumar, S., Ho, D., Briber, R. , "Neutron Scattering of Polymer Conformations in Energetic Neutral Pores of the Vycor," Macromol. **35**, 6384 (2002).

Norman, B. R., Iyengar, G. V., "Further Applications of Pre-Irradiation Combustion and Neutron Activation Analysis Technique for the Determination of Iodine in Food and Environmental Reference Materials: Merits and Demerits," Fresen. J. Anal. Chem., in press.

O'Donovan, K. V., Borchers, J. A., Majkrzak, C. F., Hellwig, O., Fullerton, E. E., "Extracting Buried Twists with Polarized Neutron Reflectometry," Appl. Phys. Lett. A, in press.

O'Donovan, K. V., Borchers, J. A., Majkrzak, C. F., Hellwig, O., Fullerton, E. E., "Pinpointing Chiral Structures Using Front/Back Polarized Neutron Reflectivity," Phys. Rev. Lett. **88** (6), 067201 (2002).

Olson, D. H., Toby, B. H., Reisner, B. A., "Neutron Diffraction Study of Protons in Four Lanthanum Exchanged X and LSX Zeolites," in *Proceedings of the 13th International Zeolite Conference,* Montpellier, France, edited by Galarneau, A. Elsevier), **135** (2001).

Papanek, P., Fischer, J. E., Murthy, N. S., "Low-Frequency Amide Modes in Different Hydrogen-Bonded Forms of Nylon-6 Studied by Inelastic Neutron Scattering and Density-Functional Calculations," Macromol. **35** (10), 4175 (2002).

Park, S., Gies, H., Toby, B. H., Parise, J. B., "Characterization of a New Microporous Lithozinocosilicate with ANA Topology," Chem. Mater. **14** (7), 3187 (2002).

Pate, B. D., Choi, S. M., Werner-Zwanziger, U., Baxter, D. V., Zaleski, J. M., Chisholm, M. H., "Structure and Magnetic Alignment of Metalloporphyrazine Columnar Aggregates in their Mesophases and Crystalline Phases," Chem. Mater. **14** (5), 1930 (2002).

Paul, R. L., "Development of a Procedure for Measuring Nitrogen by Cold Neutron Prompt Gamma-Ray Activation Analysis," Analyst **126**, 217 (2001).

Paul, R. L., "Development of a Procedure for Measuring Nitrogen by Cold Neutron Prompt Gamma-Ray Activation Analysis," Analyst **126**, 217 (2001).

Paul, R. L., "Nondestructive Measurement of Hydrogen and Other Elements by Cold Neutron Capture Prompt Gamma-Ray Activation Analysis," Geostandards Newsletter **34** (3), 15 (2002).

Payne, A. C., Sprauve, A., Olmstead, M. M., Kauzlarich, S. M., Chan, J. Y., Reisner, B. A., Lynn, J. W., "Synthesis, Magnetic, and Electronic Properties of Single Crystals of $EuMn_2P_2$," J. Solid State Chem. **163** (2), 498 (2002).

Perahia D., Traiphol, R., Bunz, U. H., "From Single Molecules to Aggregates to Gels in Dilute Solution: Self-Organization of Nanoscale Rodlike Molecules," J. Chem. Phys. **117** (4), 1827 (2002).

Perez-Salas, U., Briber, R. M., Rafailovich, M. H., Sokolov, J., "Interfacial Fracture Toughness Between Glassy Polymer Networks," J. of Polym. Sci. Part B: Poly. Phys., in press.

Perez-Salas, U., Nasser, L., Briber, R. M., Hamilton, W. A., Rafailovich, M. H., Sokolov, J., "Polystyrene Network Interdiffusion," Macromol., **35** (17), 6638 (2002).

Petrash, S., Cregger, T., Zhao, B., Pokidysheva, E., Foster, M. D., Brittain, W. J., Sevastinov, V., Majkrzak, C. F., "Changes in Protein Adsorption on Self-Assembled Monolayers with Monolayer Order: Comparison of Human Serum Albumin and Human Gamma Globulin," Langmuir **17** (24), 7645 (2001).

Pivovar, A. M., Ward, M. D., Brown, C. M., Neumann, D. A., "Probing Vibrational Dynamics of Hydrogen-Bonded Inclusion Compounds with Inelastic Neutron Scattering and *ab-initio* Calculation," J. Phys. Chem. **106** (19), 4916 (2002).

Pochan, D. J., Lin, E. K., Wu, W.-L., "Surface Directed Crystallization and Autophobic in Semicrystalline Polymer Thin Films," Phys. Rev. Lett., in press.

Pochan, D. J., Pakstis, L., Nowak, A. P., Deming, T. J., "Self-Assembled Polypeptide Hydrogels; Morphology and Cytotoxicity," Biomacromol., in press.

Pochan, D. J., Pakstis, L., Ozbas, B., Nowak, A. P., Deming, T. J., "SANS and Cryo-TEM Study of Self-Assembled Diblock Copolypeptide Hydrogels with Rich Nano-Through Microscale Morphology," Macromol. **35** (14), 5358 (2002).

Popovici, M., Stoica, A., Hubbard, C., Spooner, S., Prask, H., Gnäupel-Herold, T., Gehring, P., Erwin, R., "Multi-Wafer Focusing Neutron Monochromators and Applications," in *Proceedings of the SPIE Optical Science and Technology* (edited by Wood, J. L., Anderson, I. S.) **4509**, 21 (2001).

Porcar, L., Hamilton, W. A., Butler, P. D., Warr, G. G., "A New Vapor Barrier Couette Shear Cell, for Small Angle Neutron Scattering Measurements," Rev. Sci. Instrum. **73** (6), 2345 (2002).

Porcar, L., Hamilton, W. A., Butler, P. D., Warr, G.G., "Scaling of Shear-Induced Transformations in Membrane Phases," Phys. Rev. Lett., in press.

Prask, H. J., Brand, P. C., Gnäupel-Herold, T., Hicho, G. E., "Determination of Residual Stresses Using Neutron Diffraction: Tank-Car Welds and Rail Slices," in Topics on Nondestructive Evaluation Series Nondestructive Testing and Evaluation for the Railroad Industry, (edited by H. Reis and C. Barkan, ASNT, Columbus, OH, 2002), p. 199.

Prask, H. J., Gnäupel-Herold, T, Fisher, J. W., Cheng, X., Stuart, J. T., "Residual Stress Modification by Means of Ultrasonic Impact Treatment," in *Proceedings of the 2001 SEM Annual Conference & Exposition on Experimental an Applied Mechanics*, in press.

Quijada, M. A., Simpson, J. R., Drew, H. D., Lynn, J. W., Vasiliu-Doloc, L., Mukovskii, Y. M., Karabashev, S. G., "Temperature Dependence of Low-Lying Electronic Excitations of $LaMnO_3$," Phys. Rev. B **64**, 224426 (2002).

Raghavan, S. R., Edlund H., Kaler, E. W., "Cloud-Point Phenomena in Wormlike Micellar Systems Containing Cationic Surfactant and Salt," Langmuir **18** (4), 1056 (2002).

Raghavan, S. R., Fritz, G., Kaler, E. W., "Wormlike Micelles Formed by Synergistic Self-Assembly in Mixtures of Anionic and Cationic Surfactants," Langmuir **18** (10), 3797 (2002).

Ratcliff, W., Lee, S.-H., Broholm, C., Cheong, S.-W., Huang, Q., "Freezing of Spin Correlated Nanoclusters in a Geometrically Frustrated Magnet," Phys. Rev. B **65**, 220406 (2002).

Ravel, B., Raphael, M. P., Harris, V. G., Huang, Q., "EXAFS and Neutron Diffraction Study of the Heusler Alloy Co_2MnSi," Phys. Rev. B **65** (18), 184431 (2002).

Regan, T. M., Harris, D. C., Blogett, D. W., Baldwin, K. C., Miragliotta, J. A., Thomas, M. E., Linevsky, M. J., Giles, J. W., Kennedy, T. A., Fatemi, M., Black, D. R., Lagerlof, K. P. D., "Neutron Irradiation of Sapphire for Compressive Strengthening. II. Physical Properties Changes," J. Nucl. Mater. **300** (1), 47 (2002).

Rich, D. R., Bowman, J. D., Crawford, B. E., Delheij, P. P. J., Espy, M. A., Haseyama T., Jones, G., Keith, C. D., Knudson, J., Leuschner, M. B., Masaike, A., Masuda Y., Matsuda, Y., Penttila S. I., Pomeroy, V. R., Smith, D. A., Snow, W. M., Szymanski, J. J., Stephenson, S. L., Thompson, A. K., Yuan, V., "A Measurement of the Absolute Neutron Beam Polarization Produced by an Optically Pumped He-3 Neutron Spin Filter," Nucl. Instrum. Meth. A **481** (1-3), 431 (2002).

Rich, D. R., Fan, S., Gentile, T. R., Hussey, D., Jones, G. L., Neff, B., Snow, W. M., Thompson, A. K., "Polarized ^{3}He Neutron Spin Filter Development and Application at Indiana University and NIST," Physica B **305**, 203 (2001).

Rich, D. R., Gentile, T. R., Smith, T. B., Thompson, A. K., Jones, G. L., "Spin-Exchange Optical Pumping at Pressures Near 1 Bar for Neutron Spin Filters," Appl. Phys. Lett. **80** (12), 2210 (2002).

Rogado, N., Huang, Q., Lynn, J. W., Ramirez, A. P., Huse, D., Cava, R. J., "$BaNi_2V_2O_8$: A Two-Dimensional Honeycomb Antiferromagnet," Phys. Rev. B **65** (14), 144443 (2002).

Rosenkranz, S., Osborn, R., Vasiliu-Doloc, L., Lynn, J. W., Sinha, S. K., Mitchell, J. F., "Spin Correlations and Magnetoresistance in the Bilayer Manganite $La_{1.2}Sr_{1.8}Mn_2O_7$," Physica B **312**, 763 (2002).

Rush, J. J., Udovic, T. J., "Modern Neutron Methods for the Study of Hydrogen in Materials," in *Proceedings of Symposia on Fundamentals of Advanced Materials for Energy Conservation*, TMS, edited by D. Chandra, and R. Batista (2002), p. 161.

Santoro, A., "Past and Present Crystallographic Work at the NBS/NIST Reactor," J. Res. Natl. Inst. Stand. Technol. **106** (6), 921 (2001).

Sayer, E. V., Yener, A. K., Joel, E. C., Blackman, M. J., Özbal, H., "Stable Lead Isotope Studies of Black Sea Anatolian Ore Sources and Related Bronze Age and Phrygian Artifacts from Nearby Archaeological Sites Appendix: New Central Taurus Ore Data," Archaeometry, in press.

Schmidt, G., Nakatani, A. I., Butler, P. D., Han, C. C., "Small Angle Neutron Scattering from Viscoelastic Polymer-Clay Solution Under Shear," Macromol. **35** (12), 4725 (2002).

Schmidt, G., Nakatani, A. I., Han, C. C., "Rheology and Flow-Birefringence From Viscoelastic Polymer-Clay Solutions," Rheol. Acta **41** (1-2), 45 (2002).

Schwahn, D., Richter, D., Lin, M., Fetters, L. J., "Cocrystallization of a Poly(ethylene-butene) Random Copolymer with C-24 in n-Decane," Macromol. **35** (9), 3762 (2002).

Schwahn, D., Richter, D., Wright, P. J., Symon, C., Fetters, L. J., Lin, M., "Self-Assembling Behavior in Decane Solution of Potential Wax Crystal Nucleators Based on Poly(co-olefins)," Macromol. **35** (3), 861 (2002).

Serpico, J. M., Ehrenberg, S. G., Fontanella, J. J., Jiao, X., Perahia, D., McGrady, K. A., Sanders, E. H., Kellogg, G. E., Wnek, G. E., "Transport and Structural Studies of Sulfonated Styrene-Ethylene Copolymer Membranes," Macromol. **35**, 5916 (2002).

Shah, N., Green, M. A., Neumann, D. A., "Phase Stability in the $LnCa_2Mn_2O_7$ (Ln = Pr, Nd, Sm and Gd) Ruddlesden – Popper Series," J. Phys. Chem. Solids **63**, 1779 (2002).

Shapiro, S. M., Bao, W., Raymond, S., Lee, S. H., Motoya, K., "Observation of Linear Spin Wave Dispersion in Re-Entrant Spin Glass $Fe_{0.7}Al_{0.3}$," in *Proceedings ICNS 2001*, in press.

Shen, L., Stachowiak, A., Fateen, S. K., Laibinis, P. E., Hatton, T. A., "Structure of Alkanoic Acid Stabilized Magnetic Fluids. A Small-Angle Neutron and Light Scattering Analysis," Langmuir **17**, 288 (2001).

Shin, K., Koga, T., Zhang, Y., Seo, Y., Occhiogrosso, R., Rafailovich, M. H., Sokolov, J. C., Chu, B., Satija, S. K., "Anomalous Carbon Dioxide-Induced Swelling of Polymer Thin Films at Gas-Supercritical Transition," J. Am. Chem. Soc., in press.

Silas J. A., Kaler, E. W., " The Phase Behavior and Microstructure of Efficient Cationic-Nonionic Microemulsions," J. Colloid and Interface Sci. **243** (1), 248 (2001).

Silva, A. S., Mitchell, C. A., Tse, M.F., Wang, H.-C., Krishnamoorti, R., "Templating of Cylindrical and Spherical Block Copolymers Microdomains by Layered Silicates," J. Chem. Phys. **115** (15), 7166 (2001).

Simmons, A., Irvin, G. C., Agarwal, V., Bose, A., John, V. T., McPherson, G. L., Balsara, N. P., "Small Angle Neutron Scattering Study of Microstructural Transitions in a Surfactant-Based Gel Mesophase," Langmuir **18**, 624 (2002).

Sitepu, H., Prask, H. J., "Assessment of Preferred Orientation with Neutron Powder Diffraction Data," J. Appl. Crystallogr. **35**, 274 (2002).

Sitepu, H., Schmahl, W. W., Stalick, J. K., "Use of Generalized Spherical-Harmonic Model for Describing Texture in NiTi Shape Memory Alloy by Neutron Diffraction," Appl. Phys. A, in press.

Skripov, A. V., Cook, J. C., Udovic, T. J., Kozhanov, V. N., Hempelmann, R., "Quasielastic Neutron Scattering Studies of H Motion in Laves-Phase Compounds," Appl. Phys. A. in press.

Slebarski, A., Maple, M. B., Freeman, E. J., Sirvent, C., Radlowska, M., Jezierski, A., Granado, E., Huang, Q.-Z., Lynn, J. W., "Strongly Correlated Electron Behavior in the Compound CeRhSn," Philos. Mag. **82** (8), 943 (2002).

Smee, S. A., Orndorff, J. D., Scharfstein, G. A., Qiu, Y., Brand, P. C., Broholm, C. L., Anand, D. K., "MACS Low Background Doubly Focusing Neutron Monochromator," Appl. Phys. A **75**, 3 (2002).

Soles, C. Douglas, J. F., Dimeo, R. M., Wu, W.-L., "The Dynamics of Confined Polycarbonate Chains with Incoherent Neutron Scattering," Polym. Mat. Sci. Eng. **85**, 81 (2001).

Soles, C. L., Douglas, J. F., Wu, W.-L., Dimeo, R. M., "Incoherent Neutron Scattering and the Dynamics of Confined Polycarbonate Films," Phys. Rev. Lett. **88** (3), 037401 (2002).

Soles, C. L., Douglas, J. F., Wu, W.-L., Peng, H., Gidley, D. W., "A Broad Perspective on the Dynamics of Highly Confined Polymer Films," in *Proceedings of the MRS Conference* **710** (2002),

Soles, C. L., Lin, E. K., Lehart, J. L., Jones, R. L., Wu, W.-L., Goldfarb, D., Angelopoulos, M., "Thin Film Confinement Effects on the Thermal Properties of Model Photoresist Polymers," J. Vac. Sci. Technol. B. **19** (6), 2690 (2001).

Stone, M. B., Chen, Y., Rittner, J., Yardimci, H., Reich, D. H., Broholm, C., Ferraris D. V., Lectka, T., "Frustrated Three-Dimensional Quantum Spin Liquid in CuHpCl," Phys. Rev. B **65** (6), 064423 (2002).

Stone, M. B., Rittner, J., Chen, Y., Yardimci, H., Reich, D. H., Broholm, C., Ferris, D. V., Lectka, T., "Cu_2(1,4-diazacycloheptane)$_2Cl_4$ is not a Spin Ladder," Phys. Rev. B, in press.

Stone, M. B., Rittner, J., Chen, Y., Yardimci, H., Reich, D. H., Broholm, C., Ferraris, D. V., Lectka, T., "Frustrated 3-Dimensional Quantum Spin Liquid in CuHpCl," Phys. Rev. B **65** (6), 064423 (2002).

Stone, M. B., Zaliznyak, I. A., Reich, D. H., Broholm, C., "Frustration Induced Quantum Disordered Phase in Two Dimensional Heisenberg Antiferromagnet Piperazinium Hexachlordicuprate," Phys. Rev. B **64**, 144405 (2001).

Streletzky, K. A., Zvinevich, Y., Wyslouzil, B. E., Strey, R., "Controlling Nucleation and Growth of Nanodroplets in Supersonic Nozzles," J. Chem. Phys. **116** (10), 4058 (2002).

Sugiyama, M., Shefelbine, T. A., Vigild, M. E., Bates, F. S., "Phase Behavior of an ABC Triblock Copolymer Blended with A and C Homopolymers," J. Phys. Chem. B **105**, 12448 (2001).

Sung, L., Karim, A., Douglas, J. F., Han, C. C., "Modification of Thin Film Phase Separation by a Surfactant," Macromol., in press.

Tande, B. M., Wagner, N. J., Mackay, M. E., Hawker, C. J., Jeong, C. J., "Viscosimetric, Hydrodynamic, and Conformational Properties of Dendrimers and Dendrons," Macromol. **34**, 8580 (2001).

Tarek, M., Tobais, D. J. "The Role of Protein-Water Hydrogen Bond Dynamics in the Protein Dynamical Transition," Phys. Rev. Lett. **88** (13), 138101 (2002).

Tarek, M., Tobias, D. J., Chen, S.–H., Klein, M. L., "Short Wavelength Collective Dynamics in Phospholipid Bilayers: A Molecular Dynamics Study," Phys. Rev. Lett. **87** (23), 238101 (2001).

Terry, J. S., Heller-Zeisler, S., Ondov, J. M., "Behavior of Three Atmospheric Tracer Materials in a Pilot-Scale Coal Combuster," J. Radio. Analyt. Nuc. Chem. **251** (2), 205 (2002).

Thomas, K. J., Lee, Y. S., Chou, F. C., Khaykovich, B., Lee, P. A., Kastner, M. A., Cava, R. J., Lynn, J. W., "Antiferromagnetism, ferromagnetism and Magnetic Phase Separation in $Bi_2Sr_2CoO_{6+\delta}$," Phys. Rev. B. **66**, 054415 (2002).

Toby, B. H., "Diffraction Analysis and Crystallographic Structure Determination," Handbook of Ceramic Engineering, edited by M. N. Rahaman, in press.

Toby, B. H., "Investigations of Zeolite Materials at the NIST Center for Neutron Research," J. Res. Natl. Inst. Stand. Technol. **106** (6), 965 (2001).

Toby, B. H., "The Classification of Powder Diffraction Data," International Tables for Crystallography, in press.

Toby, B. H., "Twenty-Five Years in Crystallography, One Person's View," Zeitschrift fur Kristallographie **87**, 374 (2002).

Trouw, F., Borodin, O., Cook, J. C., Smith, G. D., "A Quasilelastic Neutron Scattering Study of the Local Dynamics of Poly(ethylene glycol) in Aqueous Solution," J. Phys. Chem., in press.

Truong, M. T., Walker, L. M., "Quantifying the Importance of Micellar Microstructure and Electrostatic Interactions on the Shear-Induced Structural Transition of Cylindrical Micelles," Langmuir **18**, 2024 (2002).

Udovic, T. J., Karmonik, C., Huang, Q., Rush, J. J., Vennström, M., Andersson, Y., Flanagan, T. B., "Comparison of the Dynamics of Hydrogen and Deuterium Dissolved in Crystalline Pd_9Si_2 and $Pd_3P_{0.8}$," J. Alloy Compnds. **330**, 458 (2002).

Vajk, O. P., Mang, P. K., Greven, M., Gehring, P. M., Lynn, J. W., "Quantum Impurities in the Two-Dimensional Spin One-Half Heisenberg Antiferromagnet," Science **295** (5560), 1691 (2002).

Wada, N., Kamitakahara, W. A., "Quasielastic and Inelastic Neutron Scattering Studies on Intercalated Water Molecules in Zeolite LTA and FAU," Mol. Cryst. Liq. Cryst., in press.

Wagner, N. J., Butera, R., "Shear Distortion and Relaxation Dynamics of Colloidal Crystals Investigated by SANS Time Slicing," Phys. Rev. E, in press.

Wakimoto, S., Stock, C., Birgeneau, R. J., Ye, Z.-G., Chen, W., Buyers, W. J. L., Gehring, P. M., Shirane, G., "Ferroelectric Ordering in the Relaxor $Pb(Mg_{1/3}Nb_{2/3})O_3$ as Evidenced by Low-Temperature Phonon Anomalies," Phys. Rev. B **65** (17), 172105 (2002).

Wakimoto, S., Tranquada, J. M., Ono, T., Kojima, K. M., Uchida, S., Lee, S.–H., Gehring, P. M., Birgeneau, R. J., "Diagonal Static Spin Correlations in the Low Temperature Orthorhombic Pccn Phase of $La_{1.55}Nd_{0.4}Sr_{0.05}CuO_4$," Phys. Rev. B **64**, 174505 (2001).

Wang, H. Douglas, J. F., Satija, S. K., Composto, R. J., Han, C. C., "Early-Stage Compositional Segregation in Polymer Blend Films," Phys. Rev. Lett., in press.

Wang, H., Shimizu, K., Hobbie, E. K., Wang, Z. G., Meredith, G. C., Karim, A., Amis, E. J., Hsiao, B. S., Hsieh, E. T., Han, C. C., "Phase Diagram of a Nearly Isorefractive Polyolefin Blend," Macromol. **35** (3), 1072 (2002).

Welp, K. A., Co, C., Wool, R. P., "Improved Reflectivity Fitting Using SERF: Spreadsheet Environment Reflectivity Fitting," J. Neutron Res., in press.

Wesley, R., Armes, S. P., Thompson, L. J., "Block Copolymer Interactions With Surfactants," Langmuir, in press.

Wesley, R. D., Cosgrove, T., Thompson, L., Armes, S. P., Baines, F. L., "Structure of Polymer/Surfactant Complexes Formed by Poly(2-(dimethylamino)ethyl Methacrylate) and Sodium Dodecyl Sulfate," Langmuir **18**, 5704 (2002).

Williams, R. E., Rowe, J. M., "Developments in Neutron Beam Devices and an Advanced Cold Source for the NIST Research Reactor," Physica B **311** (1-2), 117 (2002).

Wiyatno, W., Pople, J. A., Gast, A. P., Waymouth, R., Fuller, G. G., "A Scattering Study of Elastomeric Polypropylene," in press.

Wong-Ng, W., Huang, Q., Levin, I., Kaduk, J. A., Dillingham, J., Huagan, T., Suh, J., Cook, L. P., "Crystal Chemistry and Phase Equilibria of Selected SrO-R_2O_3 CuO_x and Related Systems, R=Lanthanides and Yttrium," Int. J. Inorg. Mater. **3** (8), 1283 (2001).

Wong-Ng, W., Roth, R. S., Vanderah, T. A., McMurdie, M. H., "Phase Equilibria and Crystallography of Ceramic Oxides," J. Res. Natl. Inst. Stand. Technol. **106** (6), 1097 (2001).

Wu, S. Y., Yang, C. C., Li, W.-H., Lee, K. C., Lynn, J. W., Yang, H. D., "Mn Ordering and Induced Ce Ordering in $La_{0.7}(Ce_{0.5}Ca_{0.5})_{0.3}MnO_3$," J. Magn. Magn. Mater. **239** (1-3), 14 (2002).

Xu, G., Broholm, C., Reich, D. H., Adams, M. A., "Triplet Waves in Quantum Spin Liquid," Phys. Rev. Lett. **84** (19), 4465 (2000).

Yamaura, K., Huang, Q., Takayama-Muromachi, E., "Crystal Structure and Magnetism of the Linear-Chain Copper Oxides $Sr_5Pb_{3-x}BiCuO_{12}$," Phys. Rev. B **64** (18), 184428 (2001).

Yamaura, K., Huang, Q., Takayama-Muromachi, E., "Synthesis, Crystal Structure and Magnetic Properties of the Linear-Chain Cobalt Oxide $Sr_5Pb_3CoO_{12}$," J. Solid State Chem. **164** (1), 12 (2002).

Yang, C. C., Wu, S. Y., Li, W.-H., Lee, K. C., Lynn, J. W., Wu, C.-G., "Magnetic Ordering of Fe in NCH_5-Intercalculated Iron Phosphate $Fe(OH)PO_4$," Solid State Communications, in press.

Yang, G. Y., Briber, R. M., Huang, E., Rice, P. M., Volksen, W., Miller, R. D., "Morphological Development in Nanoporous PMSSQ Films," Chem. Mater., in press.

Yang, G. Y., Briber, R. M., Huang, E., Rice, P. M., Volksen, W., Miller, R. D., "Morphology of Nanoporous PMSSQ Films," Appl. Phys. Lett., in press.

Yang, S., Mirau, P., Pai, C. S., Nalamasu, O., Reichmanis, E., Lin, E. K., Lee, H. J. Gidley, D., Frieze, W., Dull, T., Sun, J., Yee, A. F., "Design of Nanoporous Ultra Low-Dielectric Constant Organosilicates by Self-Assembly," in *Proceedings of the ACS National Meeting 2001, Polymeric Materials: Science and Engineering* **84**, 287 (2001).

Yang, S., Mirau, P., Pai, C. S., Nalamasu, O., Reichmanis, E., Pail, J. C., Obeng, Y. S., Seputro, J., Lin, E. K., Lee, H. J., Sun, J., Gidley, D. W., "Nanoporous Ultra Low-Dielectric Constant Organosilicates Templated by Triblock Copolymers," Chem. Mat. **14** (1), 369 (2002).

Yang, S., Mirau, P., Pai, C. S., Nalamasu, O., Reichmanis, E., Lin, E. K., Lee, H. J. Gidley, D. W., Sun, J., "Molecular Templating of Nanoporous Ultra Low-Dielectric-Constant (~1.5) Organosilicates by Tailoring the Microphase Separations of Triblock Copolymers," Chem. Mat. **13**, 2762 (2001).

Yildirim, T., Gulseren, O., "A Simple Theory of 40K Superconductivity in MgB_2; First Principles Calculations of T_c, its Dependence in Boron Mass and Pressure," J. Phys. Chem. Solids, in press.

Yildirim, T., Gulseren, O., "First-Principles Zone-Center Theory of Superconductivity in MgB_2," Physica A, in press.

Young, S. K., Trevino, S. F., Beck Tan, N. C., "Small Angle Neutron Scattering Investigation of Structural Changes in Nafion Membranes Induced by Swelling with Various Solvents," J. Polym. Sci. Part B: Polym. Phys. **40** (4), 387 (2002).

Young, S. K., Trevino, S. F., Beck Tan, N. C., Paul, R. L., "Utilization of Prompt Gamma Neutron Activation Analysis in the Evaluation of Various Counterion Nafion Membranes," J. Polym. Sci. Part B: Polym. Phys. **220**, 134 (2000).

Yurekli, K., Krishnamoorti, R., "Dynamics of Block Copolymer Micelles," Macrmol. **35**, 4075 (2002).

Zaliznyak, I. A., Tranquada, J. M., Erwin, R., Moritomo, Y., "Spin-entropy-Driven Melting of the Charge Order in $La_{1.5}Sr_{0.5}CoO_4$," Phys. Rev. B **64** (19), 195117 (2001).

Zeitler, T. R., Toby, B. H., "Parallel Processing for Rietveld Refinement," J. Appl. Crystallogr. **35**, 191 (2002).

Zhang, Y., Ge, S., Tang, B., Rafailovich, M. H., Sokolov, J., Peiffer, D., Li, Z., Lin, M., Dias, J. A., McElrath, K. O., Nguyen, D., Satija, S., Schwarz, S. A., "Interfacial Properties of Brominated Isobutylene-co-p-Methylstyrene and Butadiene Polymers," in *Proceedings of the American Chemical Society 154th Rubber Conference*, in press.

Zheludev, A., Honda, Z., Chen, Y., Broholm, C. L., Katsumata, K., Shapiro, S. M., "Quasielastic Neutron Scattering in the High-field Phase of a Haldane Antiferromagnet," Phys. Rev. Lett., **88** (7), 077206 (2002).

Zheludev, A., Kenzelmann, M., Raymond, S., Masuda, T., Uchinokura, K., Lee, S. H., "Spin Dynamics in the Quasi-One-Dimensional S=1/2 Antiferromagnet $BaCu_2Si_2O_7$," Phys. Rev. B **65** (1), 014402 (2002).

Zheludev, A., Maslov, S., Zaliznyak, I., Regnault, L. P., Masuda, T., Uchinokura, K., Erwin, R. W., Shirane, G., "Experimental Evidence for Shekhtman-Entin-Wohlman-Aharony (SEA) Interactions in $Ba_2CuGe_2O_7$," Phys. Rev. B, in press.

Zhou, C., Hobbie, E. K., Bauer, B. J., Han, C. C., "Equilibrium Structure of Hydrogen-Bonded Polymer Blends," J. Polym. Sci. Part B: Poly. Phys., in press.

Zimmerman, M. V., "X-Ray Scattering Studies of Orbital and Charge Ordering in $Pr_{1-x}Ca_xMnO_3$," Phys. Rev. B, in press.

Instruments and Contacts

High resolution powder diffractometer (BT-1)
B. H. Toby, (301) 975-4297, brian.toby@nist.gov
C. Jones, (301) 975-4507, camille@nist.gov
Q. Huang, (301) 975-6164, qing.huang@nist.gov
J. K. Stalick, (301) 975-6223, judy.stalick@nist.gov

DARTS, Residual stress and texture diffractometer (BT-8)
H. J. Prask, (301) 975-6226, hank@nist.gov
T. Gnaeupel-Herold, (301) 975-5380, thomas.gnaeupel-herold@nist.gov

30-m SANS instrument (NG-7)
C. J. Glinka, (301) 975-6242, cglinka@nist.gov
B. S. Greenwald, (301) 975-5795, bsgreen@nist.gov
L. Porcar, (301) 975-5049, lionel.porcar@nist.gov

30-m SANS instrument (NG-3) (NIST/NSF-CHRNS)
B. Hammouda, (301) 975-3961, hammouda@nist.gov
S. R. Kline, (301) 975-6243, steven.kline@nist.gov
D. Ho, (301) 975-6422, derek.ho@nist.gov
T. K. Misra, (301) 975-6650, tmisra@nist.gov

8-m SANS instrument (NG-1)
D. Ho, (301) 975-6422, derek.ho@nist.gov
C. J. Glinka, (301) 975-6242, cglinka@nist.gov
J. G. Barker, (301) 975-6732, john.barker@nist.gov

USANS, Perfect crystal SANS (BT-5) (NIST/NSF-CHRNS)
J. G. Barker, (301) 975-6732, john.barker@nist.gov
M. H. Kim, (301) 975-6469, kimmh@nist.gov
C. J. Glinka, (301) 975-6242, cglinka@nist.gov

Cold neutron reflectometer-vertical sample-polarized beam option (NG-1)
C. F. Majkrzak, (301) 975-5251, cmajkrzak@nist.gov
J. A. Dura, (301) 975-6251, jdura@nist.gov

Cold neutron reflectometer-horizontal sample (NG-7)
S. K. Satija, (301) 975-5250, satija@nist.gov
Y.-S. Seo, (301) 973-5391, young-soo.seo@nist.gov

Triple-axis polarized-beam spectrometer (BT-2)
J. W. Lynn, (301) 975-6246, jeff.lynn@nist.gov

Triple-axis fixed incident energy spectrometer (BT-7)
J. W. Lynn, (301) 975-6246, jeff.lynn@nist.gov

Triple-axis spectrometer (BT-9)
R. W. Erwin, (301) 975-6245, rerwin@nist.gov
P. M. Gehring, (301) 975-3946, pgehring@nist.gov

SPINS, Spin-polarized triple-axis spectrometer (NG-5) (NIST/NSF-CHRNS)
S. Park, (301) 975-8369, sungil.park@nist.gov
S.-H. Lee, (301) 975-4257, seung-hun.lee@nist.gov
P. M. Gehring, (301) 975-3946, pgehring@nist.gov

FANS, Filter-analyzer neutron spectrometer (BT-4)
T. J. Udovic, (301) 975-6241, udovic@nist.gov
C. M. Brown, (301) 975-5134, craig.brown@nist.gov
J. Leaõ, (301) 975-8867, jleao@nist.gov
D. A. Neumann, (301) 975-5252, dan@nist.gov

FCS, Fermi-chopper time-of-flight spectrometer (NG-6)
C. M. Brown, (301) 975-5134, craig.brown@nist.gov
T. J. Udovic, (301) 975-6241, udovic@nist.gov

DCS, Disk-chopper time-of-flight spectrometer (NG-4) (NIST/NSF-CHRNS)
J. R. D. Copley, (301) 975-5133, jcopley@nist.gov
I. Peral, (301) 975-6235, inma@nist.gov

HFBS, High-flux backscattering spectrometer (NG-2) (NIST/NSF-CHRNS)
R. M. Dimeo, (301) 975-8135, robert.dimeo@nist.gov
Z. Chowdhuri, (301) 975-4404, zema.chowdhuri@nist.gov
D. A. Neumann, (301) 975-5252, dan@nist.gov

NSE, Neutron spin echo spectrometer (NG-5) (NIST/NSF-CHRNS)
N. S. Rosov, (301) 975-5254, nrosov@nist.gov
D. Bossev, (301) 975-4662, dbossev@nist.gov

Prompt-gamma neutron activation analysis (NG-7)
R. M. Lindstrom, (301) 975-6281, dick.lindstrom@nist.gov
R. L. Paul, (301) 975-6287, rpaul@nist.gov

Other activation analysis facilities
R. R. Greenberg, (301) 975-6285, rgreenberg@nist.gov

Cold neutron depth profiling (NG-0)
G. Lamaze, (301) 975-6202, lamaze@nist.gov

Instrument development station (NG-0)
D. F. R. Mildner, (301) 975-6366, mildner@nist.gov
H. H. Chen, (301) 975-3782, chenmayer@nist.gov

Neutron interferometer (NG-7)
M. Arif, (301) 975-6303, muhammad.arif@nist.gov
D. Jacobson, (301) 975-6207, jacobson@nist.gov

Fundamental neutron physics station (NG-6)
M. S. Dewey, (301) 975-4843, mdewey@nist.gov

Theory and modelling
N. F. Berk, (301) 975-6224, nfb@nist.gov
T. Yildirim, (301) 975-6228, taner@nist.gov

Sample environment
D. C. Dender, (301) 975-6225, dender@nist.gov


MSEL